March 1997 • NREL/SR-520-21882

Very High Efficiency Photovoltaic Cells Based on Fully Organic Multiple Quantum Wells

Final Report

S.R. Forrest
Center for Photonics and Optoelectronic Materials,. Department of Electrical Engineering, Princeton University

National Renewable Energy Laboratory
1617 Cole Boulevard
Golden, Colorado 80401-3393
A national laboratory of
the U.S. Department of Energy
Managed by Midwest Research Institute
for the U.S. Department of Energy
under Contract No. DE-AC36-83CH10093

NREL/SR-520-21882 • UC Category: 1260 • DE97000063

Very High Efficiency Photovoltaic Cells Based on Fully Organic Multiple Quantum Wells

Final Report

S.R. Forrest
Center for Photonics and Optoelectronic Materials, Department of Electrical Engineering, Princeton University

NREL technical monitor: R. McConnell

National Renewable Energy Laboratory
1617 Cole Boulevard
Golden, Colorado 80401-3393
A national laboratory of
the U.S. Department of Energy
Managed by Midwest Research Institute
for the U.S. Department of Energy
under Contract No. DE-AC36-83CH10093

Prepared under Subcontract No. XAI-3-11167-03
March 1997

Available to DOE and DOE contractors from:
Office of Scientific and Technical Information (OSTI)
P.O. Box 62
Oak Ridge, TN 37831
Prices available by calling (423) 576-8401

Available to the public from:
National Technical Information Service (NTIS)
U.S. Department of Commerce
5285 Port Royal Road
Springfield, VA 22161
(703) 487-4650

Printed on paper containing at least 50% wastepaper, including 20% postconsumer waste

FINAL REPORT

Title:
Very High Efficiency Photovoltaic Cells Based on Fully Organic Multiple Quantum Wells

Organization:
Department of Electrical Engineering
Center for Photonics and Optoelectronic Materials (ATC/POEM)
E-QUAD J301
Princeton University
Princeton, NJ 08544

Contributors:
Stephen Forrest, Principal Investigator, Vladimir Bulović, Dr. Dmitri Garbuzov

Introduction:

The need for development of renewable energy sources has stimulated new approaches for production of efficient low-cost photovoltaic cells. Photovoltaics (PVs) based on organic materials such as molecular organics, conjugated polymers, and liquid crystals are emerging as an alternate technology to more conventional approaches based on inorganic semiconductors such as silicon and gallium arsenide. Photosensitivity of organic molecules together with their high optical absorption coefficient and compatibility with vacuum deposition, give promise for realizing large area, thin-film PV cells that can be produced at a modest cost. The demonstrated ability to deposit organic materials on flexible or shaped substrates allows for development of lightweight and conformable photovoltaics. The immense variability in the molecular composition and layer structure assures the continued improvement in the development of PV cells based on molecular organics.

Project Objectives:

The principal project objective is to demonstrate relatively high solar conversion efficiency using extremely low cost thin film technology based on crystalline organic multiple quantum well photovoltaic cells. We base our work on recent observations both in our lab and elsewhere that have indicated the quantum efficiency of organic photoconductors based on vacuum deposited thin films can be increased by at least two orders of magnitude (to at least 10%) if the organic films are grown in a highly ordered manner, and if organic multiple quantum wells are used in the absorption region. Thus, we are investigating the physical origin of this phenomenon, and are growing thin film MQW cells which demonstrate relatively high quantum efficiencies to determine the practicality of crystalline organic thin film cells for solar power applications. The

investigations are based on a unique, ultrahigh vacuum organic molecular beam deposition system in our laboratory.

Results:

It has long been recognized that organic materials provide a promising means for solar energy conversion due to the potential for very low cost manufacture of solar cells employing such materials. In particular, crystalline organic semiconductors such as the phthalocyanines (Pc's), perylenes and other relatively low atomic weight polyacenes have been regarded as having the greatest potential due to their ability to be controllably deposited via conventional vacuum techniques, their relatively high purity, and high mobilities (hence relatively low series resistance). In spite of considerable research having been pursued in investigating both organic p-n junction and Schottky barrier crystalline organic photovoltaic (PV) cells over the past 20 years, however, there has yet to be a demonstration of such a cell whose characteristics are adequate for even the most undemanding of solar conversion applications. Their poor performance can be ascribed principally to the following three causes: 1. Due to the intrinsic nature of photoconductivity in crystalline organic materials, where free electron-hole pairs are generated in a *second order* process following absorption and exciton generation, the efficiencies realized to date are very low (typically <1% to AM0 - AM2 illumination). 2. Due to the limited π-orbital overlap between adjacent molecules in an organic crystalline stack, and due to the presence of numerous defects in the crystalline order in the deposited materials, the free carrier mobilities in many organics are very low (typically $<10^{-3}$ $cm^2/V\text{-}s$). This leads to high film resistance, and hence low power conversion efficiency.

While these problems still prevent the realization of fully organic, low cost PV cells, several significant advances in the growth and processing technology of such materials have been made in our own lab, and by other researchers worldwide. These advances suggest that we are at a turning point in the technology of crystalline organic semiconductor PV cells. Indeed, recent experiments indicate that there are novel and effective means for growing nearly perfect, multiple quantum well (MQW) crystalline structures which can significantly increase the quantum efficiency and carrier lifetime in organic materials. Furthermore, materials which are grown with a high degree of crystalline perfection have enhanced π-orbital overlap, thereby decreasing bulk layer resistance. Finally, recent work in our laboratory has shown that very high stability photodetectors can be obtained using certain organic molecules based on perylene and naphthalene derivatives.

The crystal structure of PTCDA, many metal phthalocyanines (Pc's), and other related compounds consists of molecules which, when deposited under high vacuum conditions, form very extended, nearly perfect stacks. For such structures, the charge mobility (and hence the conductivity) along the stacks is high, leading to significant charge delocallization in this direction. In the case of PTCDA, the stacking axis is

perpendicular to the film plane, hence allowing for charge to be easily transported between contacts made to the top and bottom film surfaces.

In general, low η in organic semiconductors is attributed to the intrinsic nature of the photoconductivity process. That is, absorbed solar energy first results in the highly efficient generation of excitons in the film bulk (described by the process $S_o + h\nu \rightarrow S_o^*$, where S_o and S_o^* denote the molecular ground and excited states, respectively). These excitons then diffuse to an impurity site (denoted M), crystal defect or interface where they ionize into a free electron and hole pair, via $S_o^* + M \Rightarrow e + h$. Typically, exciton dissociation (prior to recombination) and charge collection are very low efficiency (<1%) processes. Although the ionization process is not fully understood, it is often attributed to exciton dissociation in the presence of the built-in electric field surrounding the crystal defect. If this dissociation occurs in an otherwise neutral region of the film, the free electron-hole pairs generated in the ionization event are still localized near the defect where they recombine without being collected in the external circuit. Hence, to significantly increase h as is the objective of our Phase I research, two conditions must be met: 1) The film must be relatively free of random defects which generate local electric fields, and 2) The exciton and free carrier diffusion lengths must be sufficiently long such that these particles can migrate to regions of the film where the built-in electric field from an adjacent junction is high enough to separate the free electron-hole pairs prior to recombination.

The work in this program has therefore been to determine the ultrahigh vacuum growth conditions, structures and materials combinations which result in the highest η for use in fully organic MQW PV cells. The investigations has been to study the dependence of η on MQW layer thickness ($\leq$10Å to 500Å) and composition grown in this system. To assess materials quality, photoconductor structures were fabricated in both the substrate-normal (using In and ITO contacts) and substrate-parallel (using interdigitated electrodes) geometries. We found that under the appropriate growth conditions, very long exciton diffusion lengths could be obtained (220 nm) due to the extended stacking of the molecules. Furthermore, substantial photoconductive efficiencies (approaching 1%) were achieved at what is apparently the lowest applied fields ever reported in organic thin films ($\sim 10^4$ V/cm). These results are strongly indicative of the high structural ordering and purity of the thin films grown in our laboratory. Indeed, the low fields necessary to achieve high carrier collection efficiency, along with the long exciton diffusion lengths are necessary preconditions to achieving high PV cell efficiencies. These experiments have shed a fundamental new light on charge generation and transport in organic thin films, and suggest that PV cells of reasonable power efficiencies can be obtained using very tightly π-stacked organic structures such as PTCDA.

Typical MQW materials combinations investigated include CuPc/PTCDA and NTCDA/PTCDA multilayers. Due to the absorption of all of these materials in the visible, good spectral coverage of solar radiation by these combinations is anticipated. Rectifying isotype heterojunctions consisting of PTCDA/CuPc or PTCBI/CuPc (PTCBI

is another perylene derivative closely related to PTCDA) can be used to create V_{bi} across the MQW stacks. We have found that the V_{bi} of these heterojunctions are 0.5 V and 0.7 V, respectively. On the other hand, rectifying p-n heterojunctions consisting of, for example, PTCDA/CuPc MQWs in contact with PBD will be attempted. In another approach, blocking contacts such as Au/PTCDA junctions can be used to form Schottky barriers which deplete the underlying MQW stack. Typically, the absorption coefficient of these organics is $>10^5$ cm^{-1} in their absorption band, implying that fully depleted MQW stacks of only a few thousand Ångstroms thickness are needed to obtain very high η. Given the very low carrier concentrations of materials such as PTCDA and PTCBI (where $N_d = 5 \times 10^{14}$ cm^{-3}), these V_{bi} are adequate to achieve such depletion region widths.

In corollary work, we have identified several organic phosphors which, when deposited directly onto Si PV cells, can increase their UV collection efficiencies by a substantial amount. The process involved film absorption in the UV and then near 100% re-emission efficiency in the green, where the Si PV cell is quite sensitive. Application of these re-emitting films can increase the AM0 efficiency of UV-enhanced PV cells by nearly 3%-5%. While similar techniques have been used for enhancing the sensitivity of CCD imaging arrays, to our knowledge, our particular technique of optimizing the film for both anti-reflection in the visible and UV regions while enhancing the UV sensitivity of PV cells is unique. We have submitted a patent application covering this work.

Beyond those issues covered above, we have accomplished the following:

1. Established growth methods for achieving high quality crystalline films of PTCDA, NTCDA and PTCBI using OMBD.
2. Established measurement procedures and constructed experimental set-up for modified Shockley-Haynes measurements.
3. Trained student in the experimental and analysis procedures to be employed in the experiment.
4. Measured carrier velocities in PTCDA bulk and MQW films
5. Measured of absorption coefficients of PTCDA and PTCBI
6. Currently measuring quantum efficiency of as-grown films and MQWs

References (1-4 attached as Appendix):

1. "Excitons in Crystalline Thin Films of 3,4,9,10 Perylenetetracarboxylic Dianhydride Studied by Photocurrent Response", V. Bulović and S. R. Forrest, *Chem. Phys. Lett., **238** 88 (1995).*

2. "Study of Locallized and Extended Excitons in Semiconductor 3,4,9,10 Perylenetetracarboxylic Dianhydride (PTCDA) I. Spectroscopic Properties of Thin Films and Solutions", V. Bulović, P. E. Burrows, S. R. Forrest, J. A. Cronin and M. E. Thompson, *Chem. Phys.,* invited, (1996).

3. "Study of Locallized and Extended Excitons in Semiconductor 3,4,9,10 Perylenetetracarboxylic Dianhydride (PTCDA) II. Photoconductivity at Low Electric Fields", V. Bulović and S. R. Forrest, *Chem. Phys.,* invited, (1996).

4. "Organic Film Deposition on Si *p-n* Junctions: Accurate Measurements of Fluorescence Internal Efficiency, and Application to Luminescence Antireflection Coatings", D.Z. Garbuzov, S.R. Forrest, A.G. Tsekoun, P.E. Burrows, V. Bulović and M.E. Thompson, *J. Appl. Phys.* **80** (8), October 15, 1996.

5. "Optoelectronics with Thin Film Organic Semiconductors", S. R. Forrest, *1995 Int'l. Semiconductor Device Research Symposium, plenary,* Charlottesville (Dec., 1995).

Excitons in Crystalline Thin Films of 3,4,9,10-Perylenetetracarboxylic Dianhydride Studied by Photocurrent Response

V. Bulović and S.R. Forrest

Advanced Technology Center for Photonics and Optoelectronic Materials

Department of Electrical Engineering and the Princeton Materials Institute

Princeton University

Princeton, NJ 08544

Abstract

We study excitons in crystalline thin films of the archetype molecular compound: 3,4,9,10-perylenetetracarboxylic dianhydride (PTCDA) by measuring the photocurrent response under small electric fields ($< 10^4$ V/cm). A previously uncharacterized exciton at a wavelength of $\lambda = 590$ nm, or at 2.10 eV above the PTCDA highest occupied molecular orbital, is identified. Lower in energy than either of the previously observed charge transfer excitons at $\lambda = 475$ nm and 555 nm in PTCDA, the $\lambda = 590$ nm exciton is speculated to be Frenkel-like. The diffusion length of this exciton is (225 ± 15) nm, compared to (88 ± 6) nm for excitons generated between 475 nm and 555 nm.

Excitons in Crystalline Thin Films of 3,4,9,10-Perylenetetracarboxylic Dianhydride Studied by Photocurrent Response

V. Bulovic and S.R. Forrest
Advanced Technology Center for Photonics and Optoelectronic Materials
Department of Electrical Engineering and the Princeton Materials Institute
Princeton University
Princeton, NJ 08544

The significance of excitons in organic molecular crystals (OMCs) is evident from their fundamental role in optical absorption and charge generation. Previous studies have identified molecular excitons as either Frenkel or charge transfer (CT) states, where a Frenkel exciton consists of an electron-hole pair located on the same molecule, whereas a CT exciton is a correlated system of an electron located on a molecule adjacent to a hole. Of the two states, the Frenkel exciton is more tightly bound and has a smaller radius.

We focus our study on examining the excitonic behavior of the archetype molecular compound: 3,4,9,10-perylenetetracarboxylic dianhydride (PTCDA). Numerous investigations regarding its very promising optoelectronic properties are evidence of the technological potential of PTCDA and other perylene derivatives. The transport properties of PTCDA are characterized by large hole mobilities (exceeding $1 cm^2/V\text{-}s$), and a total bandwidth[1] of ~0.9 eV. These properties result from the small interplanar molecular stacking distance[2] and the concomitant large π-orbital overlap of the constituent molecules. Perpendicular to the molecular stacks, the in-plane intermolecular interaction is considerably reduced, leading to large anisotropies in the dielectric constant and the hole mobility. These interesting properties have led to extensive studies for the use of PTCDA in photoconductors[3], photovoltaic cells[4], optical waveguides[5], and modulators[5]. The demonstration in several laboratories worldwide of the growth of highly ordered

crystalline thin films of PTCDA identify this OMC as an ideal system for the study of excitons[6,7].

Many properties of PTCDA excitons have previously been studied by electroabsorption[8], photoluminescence[8], and photoconduction[4]. Electroabsorption spectroscopy was used to identify the prominent absorption peak at $\lambda = 555$ nm (Fig. 1) to be a CT state. Curiously, however, Frenkel excitons in PTCDA have not previously been identified despite the large oscillator strength of such direct transitions from the ground state. The absence of a distinct absorption feature for wavelengths longer than $\lambda = 555$ nm (Fig. 1), corresponding to a tightly bound Frenkel state, has led to some question as to the nature of excitonic features previously identified for PTCDA.

Our study examines the photocurrent response of vacuum-deposited thin films of PTCDA under small electric fields ($<10^4$V/cm). By comparing the photocurrent, photovoltage and absorption spectra of PTCDA, diffusion lengths of several excitonic features are determined. Through the analysis of exciton diffusion, we identify for the first time an exciton at $\lambda = 590$ nm which we assign to a Frenkel-like state. The $\lambda = 590$ nm exciton is distinct from those generated at 555 nm and 475 nm. Its relatively weak contribution to the absorption spectrum results from its merging with the low-energy tail of the pronounced CT-peak at $\lambda = 555$ nm.

All measurements were performed on vacuum-deposited thin films of PTCDA[9], grown on 94% transparent, 10 x 20 mm^2, 15 Ω/□ ITO-coated glass slides. Prior to growth, the slides were cleaned using a process described elsewhere[10]. A 5 x 10 mm^2 contact edge strip on the ITO surface was masked prior to organic film deposition. The samples were then loaded into a vacuum chamber with a base pressure of 5×10^{-7} Torr. Film growth was preceded by cooling the substrates to less than 90 K, after which 1000 Å to 1 μm thick, pre-purified PTCDA was deposited by thermal evaporation from a baffled Mo crucible at a rate of 3-5 Å/s. Using grazing incidence x-ray[11] and in-situ reflection high energy electron diffraction[6], we have previously shown that under these growth

conditions ordered thin films consisting of extended stacks of planar PTCDA molecules may be achieved over large surface areas on a variety of substrates, including glass, graphite, and gold. On top of the organic layer, an array of 4000 Å thick In electrodes was deposited by thermal evaporation through a shadow mask. A schematic cross-section of the test device is shown in the inset of Fig. 1.

Device photoresponse was measured at room temperature and atmospheric conditions by illumination with a 1000 W tungsten-halogen lamp in conjunction with a 1.2 nm linewidth resolution monochromator. The incident photon flux varied between 5×10^{13} $cm^{-2}s^{-1}$ and 5×10^{15} $cm^{-2}s^{-1}$ depending on the wavelength of the light incident through the transparent ITO electrode. Linear photoresponse was observed at all illumination conditions used in this study. The light was chopped at 165 Hz, and detected using a current amplifier at the input of a lock-in amplifier. For photovoltage measurements made at zero bias, the sample probes were connected directly to the 100 MΩ input of the lock-in.

Typical absorption, zero voltage photocurrent, and photovoltage response spectra of a 5000Å thick PTCDA device are shown in Fig. 1. Previous studies have shown that peaks in the absorption spectra of organic molecular crystals correspond to excitonic transitions[12]. From Fig. 1 it is evident that the peaks in the absorption spectrum closely match the photoresponse. Further, there is an excellent match between the photocurrent and photovoltage response, from which we infer that there is no significant charge trapping within the thin film.

Figure 2 shows the dependence of the photocurrent spectral response on the polarity and amplitude of the applied electric field. At small fields (±100 V/cm), a photoconduction peak at $\lambda = 590$ nm appears. Further increase in the applied field (> 0.1 V/μm) results in significant differences between the spectra obtained at positive and negative voltages (as referenced to the In electrode). Positive fields > 0.1 V/μm (Fig. 2a) distort the spectral response by suppressing the photocurrent in the highly absorptive

region (425 - 565 nm), and enhancing the response at the absorption edges (most notably at 590 nm). Increasing the field above 0.4 V/μm results in a renewed increase in the photoresponse in the 425 - 565 nm region. On the other hand, for negative bias (Fig. 2b), a uniform increase in yield at all wavelengths preserves the shape of the spectral response, until at -0.4 V/μm, a flattening of the response obscures many spectral features.

Biasing the sample changes the ratio of potential drops over the two electrode/PTCDA interfaces. As the applied fields used in this study (≤ 1 V/μm) are not sufficient to ionize excitons[12] or to induce space-charge effects[13], they only serve to provide a field gradient for the electron drift across the thin film[10].

Taking into account the lower absorption coefficient at $\lambda = 590$ nm (where the absorption constant is $\alpha = 5.0 \times 10^4$ cm^{-1}) as opposed to at shorter wavelengths (e.g. at $\lambda = 475$ nm, $\alpha = 3.0 \times 10^5$ cm^{-1}), it is apparent that the spatial concentration of $\lambda = 590$nm excitons, as compared to those generated at either 475nm or 555nm, is considerably different. A model of exciton spatial concentration dependence on the absorption coefficient has previously been developed by Ghosh and Feng[14]. In their model, the organic/electrode contact readily dissociates excitons, thereby acting as an infinite charge sink. The exciton density (n) as a function of distance (z) from the ITO electrode due to diffusion, is then:

$$n(z) = \frac{\alpha N \phi}{D} \frac{1}{\beta^2 - \alpha^2} \left[\frac{\exp(\beta L) - \exp(-\alpha L)}{\exp(-\beta L) - \exp(\beta L)} \exp(-\beta z) - \frac{\exp(-\beta L) - \exp(-\alpha L)}{\exp(-\beta L) - \exp(\beta L)} \exp(\beta z) + \exp(-\alpha z) \right] \quad (1)$$

Here, ϕ is the quantum efficiency for exciton generation, and N is the incident photon flux. Also, $\beta = 1/L_D$, where L_D is the exciton diffusion length. Finally, in Eq. (1), D is the diffusivity, and L is the sample thickness. In effect, n(z) takes into account the attenuation of the light intensity across the film thickness as well as the boundary condition that all excitons dissociate or recombine at the electrodes.

As the organic/electrode interface provides a site for exciton dissociation, the photocurrent yield (η) is directly proportional to the exciton diffusion current near the electrodes at $z = 0$ or L. Assuming, for simplicity, that the PTCDA energy band bending is significant only near one of the electrodes, that the exciton generation efficiency is independent of λ, and that $L_D < L$, then from Eq. (1) the photocurrent yield due to generation at the electrode on which the light is incident ($z = 0$) can be shown to be: $\eta_{NEAR} = \eta_O [\alpha / (\alpha+\beta)]$. A plot of $1/\eta_{NEAR}$ vs. $1/\alpha$, therefore is a straight line which intersects the abscissa at a point corresponding to $1/\beta = -L_D$. Similarly, for generation at the far electrode ($z = L$), the photocurrent yield is $\eta_{FAR} = \alpha\eta_O \exp(-\alpha L) / (\beta-\alpha)$. In this case, $1 / [\eta_{FAR} \exp(\alpha L)]$ vs. $1/\alpha$ is a straight line which intersects the abscissa at $1/\beta = +L_D$.

Figure 3a is a plot of $1/[\eta_{FAR}\exp(\alpha L)]$ vs. $1/\alpha$ for the wavelength range between $\lambda =$ 595nm and 625nm, at positive voltages. All of the linear fits to the data intersect the $1/\alpha$ axis at (225 ± 15) nm, corresponding to the diffusion length of excitons generated at λ = 590nm. A straight line fit to the data indicates that, at positive voltages, photocurrent originates primarily from the dissociation of the 590nm excitons at the In (far) electrode. A further conclusion from the polarity of these data is that PTCDA is p-type, in agreement with previous observations in thin films of PTCDA, grown under similar conditions[1].

Excitons in the high absorbency region (425 - 565 nm) are expected to be generated closer to the ITO electrode. In Fig. 3b, therefore, we plot $1/\eta_{NEAR}$ vs. $1/\alpha$ for the photocurrent generated at $V < 0$. Linear fits to the data intersect the $1/\alpha$ axis, corresponding to a diffusion length of (88 ± 6) nm. This value is in good agreement with previous measurements for the diffusion length of these short wavelength PTCDA excitons[4].

The photocurrent signal at < 420 nm mimicks the voltage dependance of the 590 nm photocurrent response since the film, once more, becomes transparent at these short wavelengths. In Fig. 3c, therefore, we plot $1/[\eta_{FAR}\exp(\alpha L)]$ vs. $1/\alpha$ for the

wavelength range between λ = 380nm and 420nm, at positive voltages. Linear fits to the data yield a diffusion length of (79 ± 7) nm, in excellent agreement with the value obtained for the mid-wavelength data in Fig. 3b. This indicates that the 400 nm photocurrent signal has the same origin as the photocurrent signal generated in the high absorbancy region. Due to the smaller absorption coefficient, the 400nm signal is enhanced when bias is applied over the sample. All three of the fits in Fig. 3 indicate that the diffusion length is voltage independent. This confirms that the observed characteristics are excitonic in origin.

The dependence of L_D on wavelength indicates that the λ = 590nm peak is due to the generation of an exciton different from those generated at shorter wavelengths. The lower energy and longer diffusion length of the 590nm exciton allows for some speculation on its nature. For example, the smaller radius exciton should indeed have a longer diffusion length, as observed. Further, Frenkel excitons are more tightly bound than charge transfer excitons in molecular solids, and thus should be deeper in the band gap of PTCDA. Electroabsorption studies[8] have found that the binding energy of the CT exciton previously identified at λ = 555 nm is -(150 ± 18) meV, which implies a binding energy for the λ = 590nm exciton of -(280 ± 25) meV. As both the diffusion length of the λ = 590nm exciton is longer than any of the previously identified CT excitons, and as it exhibits the largest binding energy, we tentatively identify it as a small radius Frenkel state. Following Haskal, *et al.*[8], the exciton binding energy can be expressed as $E_{ex} \cong -q^2 / (2\, a^* \varepsilon_{eff})$, where a* is the effective radius, and ε_{eff} = 3.6 is the spatially averaged dielectric constant of PTCDA[15]. From this we obtain a* = 7.0 ± 0.8 Å, which is smaller than the molecular length, and comparable to twice the intermolecular planar stacking distance in PTCDA.

Long exciton diffusion lengths in OMCs are necessary if these materials are to be used in efficient photoconductor and photovoltaic devices: An exciton with a long L_D has a higher probability of encountering a dissociation site before recombining, which in turn

can result in a higher quantum yield in an optimized device in comparison to excitons with a smaller L_D. The exciton at $\lambda = 590$ nm might, therefore, significantly increase the efficiency of organic optoelectronic devices based on this material.

In summary, the photoresponse at small applied electric fields in crystalline organic thin films of PTCDA provides evidence for a previously uncharacterized exciton at $\lambda = 590$ nm, or 2.10 eV above the PTCDA highest occupied molecular orbital. The large binding energy of $-(280 \pm 25)$ meV and long diffusion length of (225 ± 15) nm of this exciton, as compared to that of the previously characterized, lower energy CT excitons, suggests that this long wavelength feature corresponds to a small radius Frenkel state.

Acknowledgments

The authors thank J. McHale for his growth of the PTCDA samples and P.E. Burrows for helpful discussions. We gratefully acknowledge AFOSR, NREL and the NSF MRSEC program for their generous support of this research.

Figure Captions

Figure 1 Short circuit photocurrent and open circuit photovoltage spectra of a 5000 Å PTCDA film sandwiched between the ITO and In electrodes. The PTCDA absorption (α) spectra is also shown for comparison. *Inset:* Schematic cross-section of the device under investigation.

Figure 2 Short circuit photocurrent response of a 5000 Å PTCDA film structure at (a) positive and (b) negative applied electric fields. Field polarity is referenced to the In electrode.

Figure 3 Inverse photocurrent quantum yield ($1/\eta$) at different applied fields plotted as a function of inverse absorption coefficient ($1/\alpha$). Diffusion lengths of (a) $L_D = 225 \pm 15$ nm for the 590nm peak, (b) $L_D = 88 \pm 6$ nm for peaks at 475nm and 555nm, and (c) $L_D = 79 \pm 7$ nm for the 400nm peak were determined from linear least square fits to the data.

References

[1] S.R. Forrest, M.L. Kaplan and P.H. Schmidt, *J. Appl. Phys.* ***55****, 1492 (1984).*

[2] F.F. So and S.R. Forrest, *Mol. Cryst. Liq. Cryst. Sci. Technol.* ***2****, 205 (1992).*

[3] K.-Y. Law, *Chem. Rev.* ***93****, 449 (1993).*

[4] N. Karl, A. Bauer, J. Holzäpfel, J. Marktanner, M. Möbus and F. Stölzle, *Mol. Cryst. Liq. Cryst., in press.*

[5] D.Y. Zang and S.R. Forrest, *Appl. Phys. Lett.* ***60****, 189 (1992).*

[6] S.R. Forrest, P.E. Burrows, E.I. Haskal and F.F. So, *Phys. Rev. B* ***49****, 11309 (1994).*

[7] C. Ludwig, B. Gompf, J. Petersen, R. Strohmaier and W. Eisenmenger, *Z. Phys. B* ***93****, 365 (1994).*

[8] E.I. Haskal, Z. Shen, P.E. Burrows and S.R. Forrest, *Phys. Rev. B (Feb 15, 1995).*

[9] Aldrich Chemical Company, Milwaukee, WI.

[10] V. Bulović and S.R. Forrest, submitted for publication.

[11] P. Fenter, P.E. Burrows, P. Einsenberger and S.R. Forrest, submitted for publication.

[12] M. Pope and C.E. Swenberg, Electronic Processes in Organic Crystals, Ch. 1, *Oxford University Press, New York (1982).*

[13] S.R. Forrest and F.F. So, *J. Appl. Phys.* ***64****, 399 (1988).*

[14] A.K. Ghosh and T. Feng, *J. Appl. Phys.* ***49****, 5982 (1978).*

[15] D.Y. Zang, F.F. So and S.R. Forrest, *Appl. Phys. Lett.* ***59****, 823 (1991).*

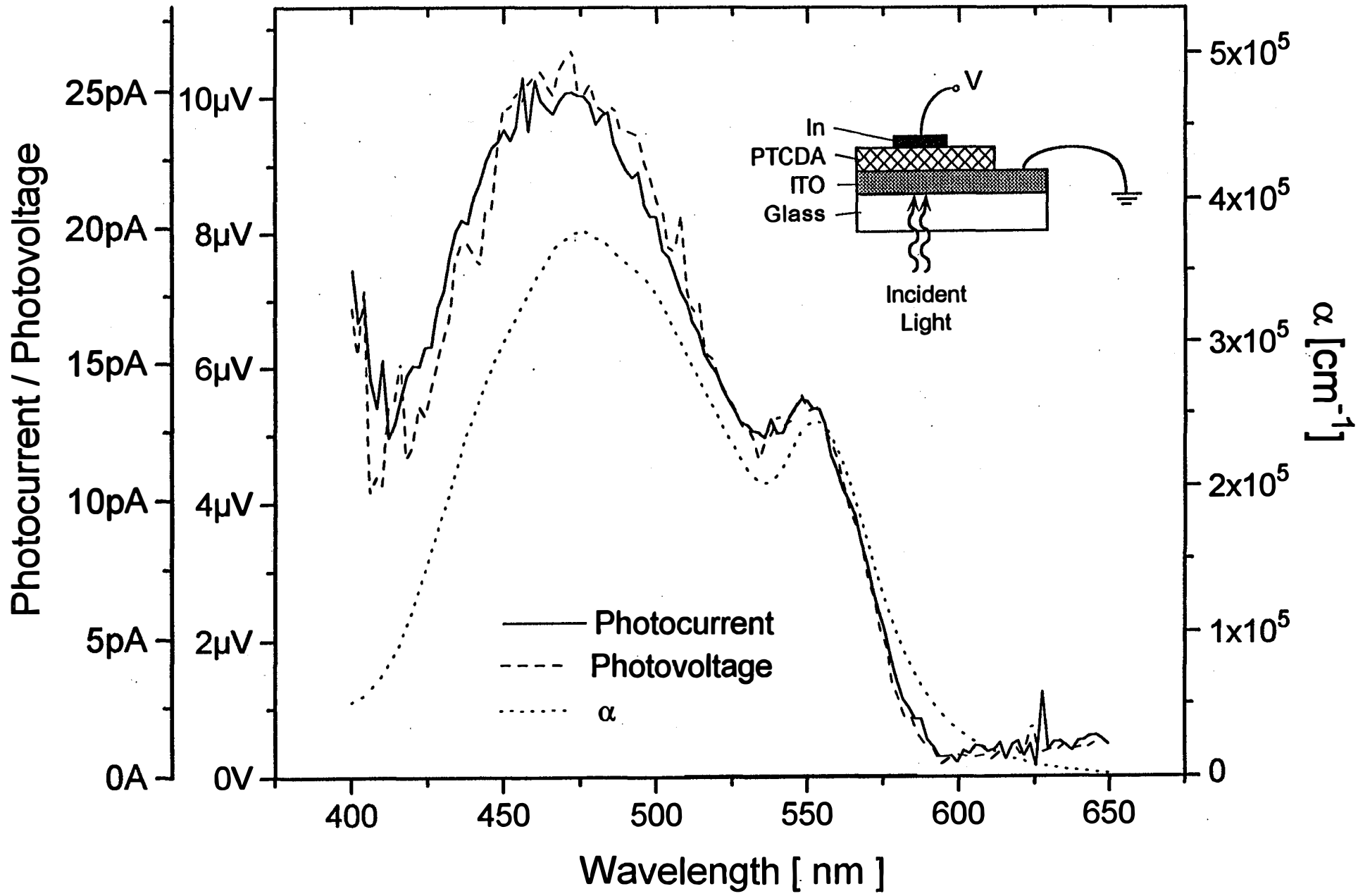
Photocurrent / Photovoltage
25pA
20pA
15pA
10pA
5pA
0A
10μV
8μV
6μV
4μV
2μV
0V
5x10^5
4x10^5
3x10^5
2x10^5
1x10^5
0
α [cm^-1]
400
450
500
550
600
650
Wavelength [nm]
Photocurrent
Photovoltage
α
V
In
PTCDA
ITO
Glass
Incident
Light

Fig. 1

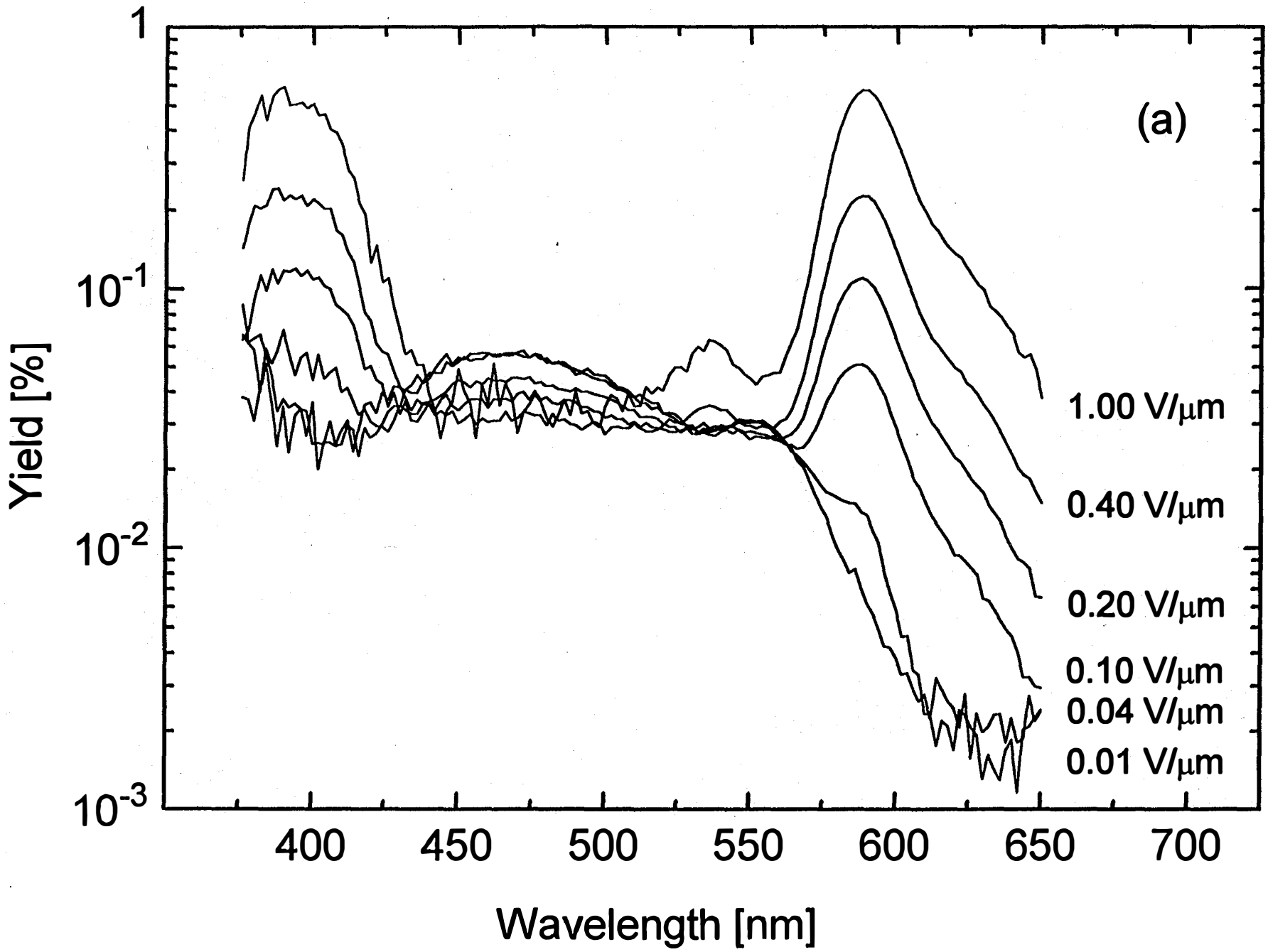
1
10^{-1}
10^{-2}
10^{-3}
Yield [%]
400
450
500
550
600
650
700
Wavelength [nm]
(a)
1.00 V/μm
0.40 V/μm
0.20 V/μm
0.10 V/μm
0.04 V/μm
0.01 V/μm

Fig. 2a

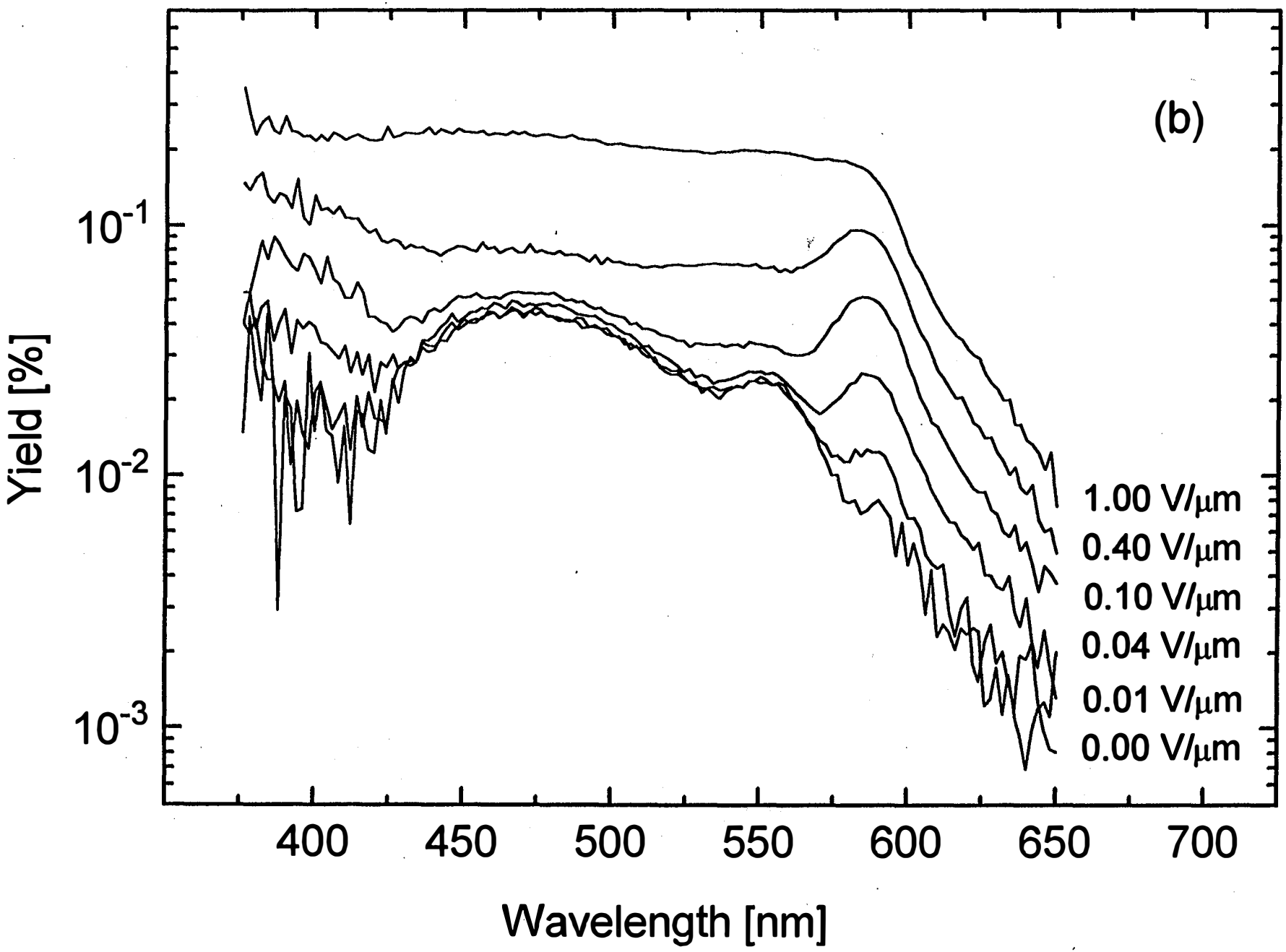
(b)
Yield [%]
10^{-1}
10^{-2}
10^{-3}
400
450
500
550
600
650
700
Wavelength [nm]
1.00 V/μm
0.40 V/μm
0.10 V/μm
0.04 V/μm
0.01 V/μm
0.00 V/μm

Fig. 2g

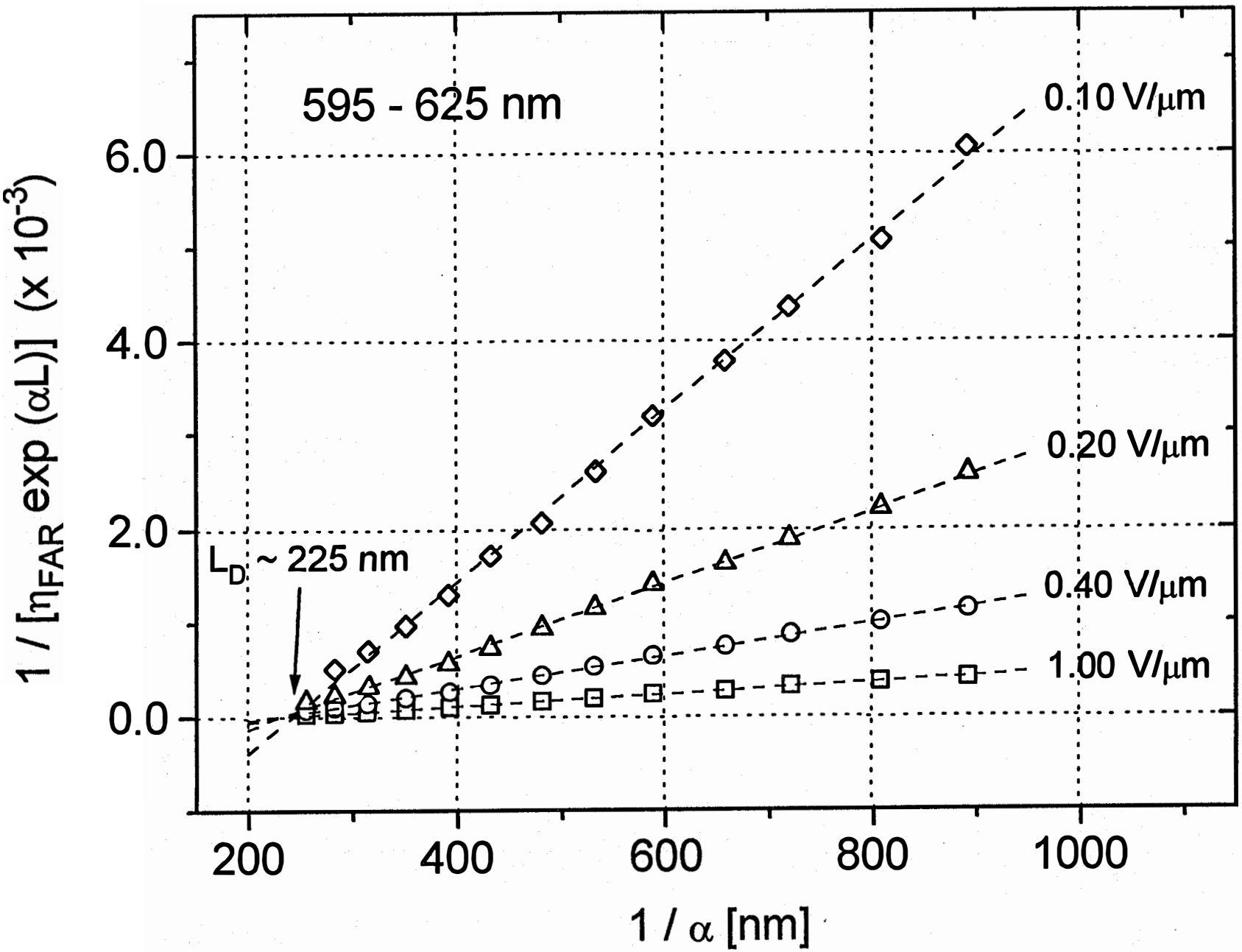
595 - 625 nm
0.10 V/μm
0.20 V/μm
0.40 V/μm
1.00 V/μm
L_D ~ 225 nm
1 / [η_FAR exp (αL)] (x 10^-3)
1 / α [nm]
6.0
4.0
2.0
0.0
200
400
600
800
1000

Fig. 2a

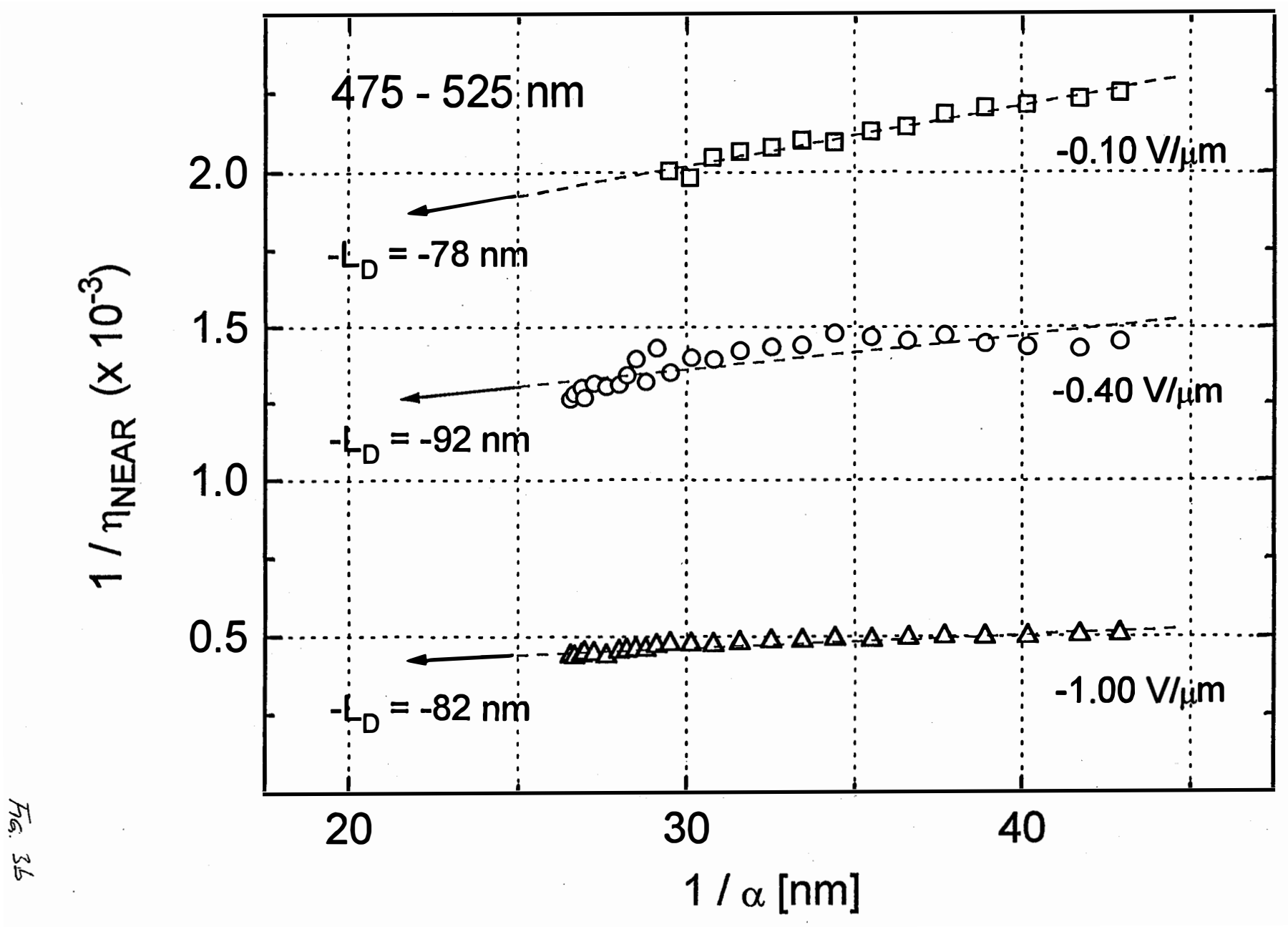
475 - 525 nm
-0.10 V/μm
-0.40 V/μm
-1.00 V/μm
-L_D = -78 nm
-L_D = -92 nm
-L_D = -82 nm
2.0
1.5
1.0
0.5
1 / η_NEAR (x 10^-3)
20
30
40
1 / α [nm]

Fig. 3b

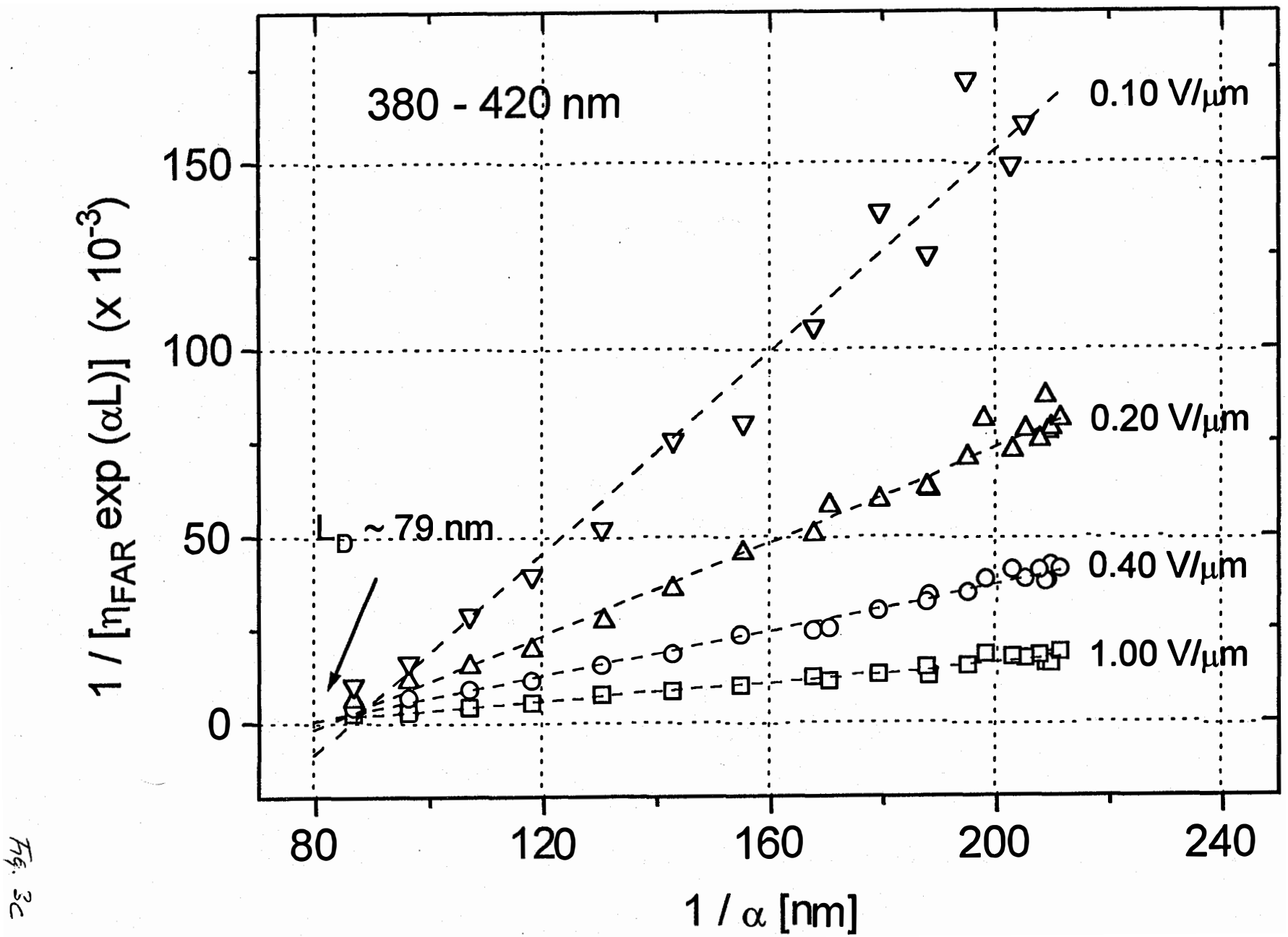
380 - 420 nm
0.10 V/μm
0.20 V/μm
0.40 V/μm
1.00 V/μm
$L_D \sim 79$ nm
$1 / [\eta_{FAR} \exp(\alpha L)]$ (x 10^{-3})
$1 / \alpha$ [nm]
150
100
50
0
80
120
160
200
240

Fig. 3c

Study of Localized and Extended Excitons in 3,4,9,10 - Perylenetetracarboxylic Dianhydride (PTCDA) I. Spectroscopic Properties of Thin Films and Solutions

V. Bulović, P. E. Burrows, S. R. Forrest
Advanced Technology Center for Photonics and Optoelectronic Materials (ATC/POEM)
Department of Electrical Engineering and the Princeton Materials Institute
Princeton University
Princeton, NJ 08544

J.A. Cronin and M. E. Thompson
Department of Chemistry
University of Southern California
Los Angeles, CA 90089

ABSTRACT

Excitonic transitions responsible for low energy absorption and fluorescence in dilute solutions and thin films of the organic molecule 3,4,9,10 - perylenetetracarboxylic dianhydride (PTCDA) have been investigated. Combining the results of concentration-dependent solution and thin film absorption and fluorescence with results on thin film exciton diffusion lengths (presented in the following paper, Paper II), we propose a comprehensive model for the low energy excitonic states in this archetype molecular crystal. We unambiguously identify an extended free charge transfer state at $E_{CT}^{F} = (2.23 \pm 0.03)$ eV which has previously been observed to exhibit effects of quantum confinement in ultrathin layers grown under ultrahigh vacuum. This state self-traps at an energy of $E_{CT}^{ST} = (2.11 \pm 0.04)$ eV due to the strong exciton-phonon coupling characteristic of this closely packed organic crystal.

Study of Localized and Extended Excitons in

3,4,9,10 - Perylenetetracarboxylic Dianhydride (PTCDA)

I. Spectroscopic Properties of Thin Films and Solutions

V. Bulović, P. E. Burrows, S. R. Forrest

Advanced Technology Center for Photonics and Optoelectronic Materials (ATC/POEM)

Department of Electrical Engineering and the Princeton Materials Institute

Princeton University

Princeton, NJ 08544

J.A. Cronin and M. E. Thompson

Department of Chemistry

University of Southern California

Los Angeles, CA 90089

I. INTRODUCTION

Recently, a considerable body of research has developed in the study of the archetype molecular compound, 3,4,9,10 - perylenetetracarboxylic dianhydride (PTCDA). The primary motivation for focusing on PTCDA are promising optical and electronic properties that stem from its regular planar π-π stacking with an unusually small intermolecular distance[1] of only 3.21 Å. The extremely close π-π stacking makes PTCDA an important "transition" material -- i.e. a material which shares many properties with conventional semiconductors (with their delocalized electronic states), and insulator-like organic molecular crystals (OMCs) (with their large absorption oscillator strengths, excitonic self-trapping, polaron-assisted conduction, etc.). As such, PTCDA is an ideal system in which to study the fundamental processes connecting both of these more conventional classes of materials. In addition, PTCDA, which presumably represents a larger class of similar OMCs, exhibits many phenomena which ultimately may prove useful in optoelectronic device applications, such as optical modulators employing the

quantum confined Stark effect,[2] and low threshold current, all-organic multiple quantum well (MQW) lasers.

It has been demonstrated that crystalline thin films of PTCDA can be grown, in vacuum, with monolayer flatness extending over macroscopic distances even in the absence of lattice-matching with the substrate.[3] The ability to control the thickness of such films to within a monolayer, coupled with a high material purity and stability, has lead to the demonstration of the first organic MQW structures where quantum confinement of extended charge-transfer (CT) exciton states was observed.[4,5] While several independent experiments, including analysis of peak absorption,[4] fluorescence energy,[5] radiative lifetime,[4] and electroabsorption,[6] as functions of film thickness have confirmed that the lowest energy state (with a peak absorption at energy E = 2.23 eV) is a spatially extended exciton, several questions as to the fundamental nature of the excitonic spectrum of PTCDA remain. For example, it has long been assumed that CT states in OMCs have a much lower oscillator strength than do Frenkel states,[7,8] and hence it is unclear why the CT absorption coefficient in PTCDA approaches that of the Frenkel exciton oscillator strength characteristic of OMCs such as anthracene or pyrene.[9] We can speculate that by analogy with inorganic semiconductors, strong CT oscillator strengths in a compound such as PTCDA are due to the small intermolecular stacking distance which encourages delocalization along the molecular stacking axis. However, to fully clarify the origin and nature of exciton states, and quantum confinement effects in ultrathin layers of PTCDA, one must obtain a clear identification of the spectroscopic features of this important material. It is the purpose of this work to provide an unambiguous picture of exciton levels in PTCDA, and to further explore the origin of the absorption peak previously assigned to a delocalized CT state.

This paper (Paper I) concerns a spectroscopic analysis of excitons in solutions and thin films of PTCDA, and is the first of a two part study. Our results provide clear assignment of the low energy spectroscopic features of PTCDA monomers and thin films. We unambiguously identify the E = 2.23 eV state observed in absorption as charge-transfer like, consistent with earlier less direct measurements of this excitonic feature. Furthermore, we find that the absorption between E = 2.3 eV and 3.0 eV is due to a

Frenkel, S_1 manifold. Self trapping, line broadening and interlevel transition processes are also studied in this work. The second part (referred to as Paper II) is an analysis of exciton transport properties obtained through a study of thin film photoconductivity.[10] This paper is organized as follows: In Sec. II we discuss thin film and solution sample preparation. Measurement results are presented in Sec. III, including the absorption and fluorescence spectra of thin films as well as colloidal solutions of varying concentration. Fluorescence lifetime measurement of solution samples and excitation spectra of thin films are also presented. Results are discussed in Sec. IV, where the initial and final states of the fluorescence and absorption transitions are identified for both thin films and solutions. Conclusions are given in Sec. V.

II. Sample Preparation

Thin films were grown by the ultrahigh vacuum process of organic molecular beam deposition using pre-purified[3] PTCDA powder source material.[11] The glass substrates for film growth were maintained at ~ 85 K to ensure uniform molecular stacking throughout the thickness of the sample.[3] Previous RHEED[3,12] and X-ray diffraction[13] studies indicate that films grown under these conditions exhibit a high degree of crystalline order.

Solution samples were prepared by dissolving pre-purified PTCDA crystalline powder in dimethylsulfoxide, $(CH_3)_2S{:}O$ (DMSO) via sonication. The solution was centrifuged for 30 minutes at 90 Krpm and then decanted to generate a saturated solution. PTCDA is found to be weakly soluble in DMSO, which implies a small solvent/molecule interaction, while limiting the most concentrated (stock) solution to only (2 ± 1) μM (as determined from absolute absorption measurements). To determine the effects of PTCDA concentration on the absorption and fluorescence spectra, this stock solution was repeatedly diluted in DMSO.

The anhydride groups in PTCDA react with water, hydrolyzing to give a carboxylic acid. The spectroscopic grade DMSO solvent used in these experiments was therefore dried prior to use. To check for residual hydrolysis in the most dilute solutions, a small amount of water (3 drops of H_2O to 2 mL of DMSO) was added to a sample of

the 2 μM solution. The red/orange-colored solution rapidly became colorless, as the absorption decreased by the factor of ten. The spectral signature of the resultant tetracarboxy derivative was extremely broad, differing significantly from the relatively narrow spectra shown in this work. This indicates that hydrolyzed PTCDA does not contribute significantly in our measurements.

A second set of solutions was prepared by dissolving pre-purified PTCDA crystalline powder in N-methylpyrrolidinone (NMP) via sonication. The saturated solution concentration was (13 ± 6) μM, indicating that PTCDA is somewhat more soluble in NMP than in DMSO. The effects of PTCDA concentration in NMP on the absorption spectrum were also studied by repeated dilution.

III. Experimental

The absorption spectrum of the 2 μM stock solution in DMSO, shown in Fig. 1a, has four clearly resolved peaks with a shoulder on the high energy side of the 2.7 eV peak. In addition, the low energy tail (defined as the energy at which the absorption is > 5% of the peak absorption) extends to $E < 1.90$ eV. This is compared to the thin film absorption spectrum (Fig. 1b) with a broad absorption feature at $E > 2.3$ eV and a distinct, narrow peak centered at $E = 2.23$ eV. Furthermore, the low energy tail is comparatively short, extending to only $E \sim 2.0$ eV.

The evolution of absorption features was studied as a function of concentration of PTCDA in DMSO (Fig 2a). Starting with a saturated 2 μM solution, each dilution step reduced the PTCDA concentration to 80% of its previous value, yielding a concentration of $[k] = 0.25$ μM after nine steps. It is evident from Fig. 2a that no energy shifts are observed for any of the four peaks on dilution. However, to accurately determine behavior of absorption transitions on concentration, each solution absorption spectrum was fit to six gaussian peaks with the parameters provided in Table 1. Each of the four high energy gaussian curves corresponds to the clearly distinct absorption peaks in this spectrum. Fitting parameters for the two lowest curves at $E = 2.23$ eV and 2.12 eV are chosen to agree with independent studies of electroabsorption[6] and photoconduction[10,14] in PTCDA thin films. Table 1 also shows the results of a similar fit to the thin film

absorption spectrum, where the two lowest energy peaks are obtained from these same previous studies.

The dependence of the E = 2.23 eV, 2.39 eV, 2.55 eV, and, 2.74 eV integrated peak areas (which are proportional to the transition oscillator strength) as a function of PTCDA concentration in DMSO are shown in Fig. 2b, while a sample fit for the spectrum of a [k] = 0.8 μM solution is shown in the inset. The plot in Fig. 2b indicates a rapid attenuation of both the E = 2.74 eV and the lowest energy peak (E = 2.23 eV) with respect to the E = 2.39 eV peak, however only the 2.23 eV peak completely attenuates at concentrations of [k] ≤ 0.25 μM. For the three higher energy peaks, the rate of decrease in absorption with decreasing PTCDA concentration is a function of energy, where the 2.39 eV peak attenuates the slowest compared to the highest energy, 2.74 eV spectral feature.

Figure 3 shows the decrease in absorption with PTCDA concentration in NMP, where the first eight dilution steps reduce the solution concentration to 75% of the previous value, while the last three steps reduce the concentration by 50% per dilution. We find that similar spectra are observed for both DMSO and NMP solutions, where in both cases the 2.23 eV peak attenuates most rapidly on dilution. The higher energy (E > 2.3 eV) absorption peaks of 13 μM NMP solution have a closer resemblance to the absorption of PTCDA thin films of the same energy range than does the 2 μM DMSO solution. As discussed below, this indicates a higher concentration of molecular aggregates in the saturated NMP colloidal solutions as compared to the saturated DMSO. Note that an additional low energy feature is observed at E = 1.85 eV in the NMP solution. This is probably the signature of a charge-transfer complex arising from NMP-PTCDA monomer interactions, not present in DMSO-PTCDA solutions.

Returning to Fig. 1, we observe that there are also significant differences between the fluorescence spectra of PTCDA solutions and thin film samples. For these spectra, a E = 2.59 eV (λ = 480 nm) Xe-arc lamp excitation source was used in the case of solutions, and E = 2.54 eV (λ = 488 nm) Ar ion laser was employed for the thin film. The solution fluorescence spectrum (Fig. 1a) has a maximum at E = 2.32 eV, with a shoulder at E = 2.18 eV. No radiation at lower energies (down to E = 1.38 eV) is

detected. As is commonly observed for many molecular systems, there is a high degree of mirror symmetry between the fluorescence and the low energy absorption spectra of the dilute solutions, suggesting that the fluorescence exhibits a classical Stokes shift from absorption. In contrast, the thin film short wavelength fluorescence is completely quenched, with the peak fluorescence centered at E = 1.70 eV, and with an additional feature at E = 1.55 eV. No significant changes in the shape of the thin film or solution fluorescence spectra was observed as the pump energy was changed from E = 2.72 eV to 2.05 eV. The fluorescence intensity scales linearly with the intensity of the excitation light (from 20 to 200 mW/cm^2) in both cases, indicating a single photon generation process.

Fig. 4a shows the decrease in fluorescence of the DMSO solution on successive dilution. Here, the fluorescence decreases uniformly at all wavelengths, and scales sub-linearly with concentration (inset Fig. 4a). An increased intermolecular interaction in the most concentrated solutions results in line broadening, which is also apparent in thin films with their broad fluorescence lines. Fig. 4b shows this effect for the normalized fluorescence spectra of [k] = 2 μM and 0.25 μM solutions. The thin film fluorescence spectrum is superimposed on the solution spectra in Fig. 4b, although it has been blue-shifted by 0.60 eV for comparison.

The room-temperature lifetime of 2 μM solution fluorescence was measured to be (4.0 ± 0.5) ns, using a 1 ns pulsed N_2 discharge source with an excitation energy of 3.32 eV, and observing the response at 2.32 eV. The fluorescence lifetime for the thin films (with thicknesses > 100 Å) was also previously measured[4] to be (10.8 ± 0.5) ns, using a sub-nanosecond Ar-laser pulse excitation at E = 2.59 eV (see Fig. 4b inset). The thin film fluorescence lifetime was found to be independent of temperature from T = 20 K to 295 K,[4] although the film spectrum broadens with increasing temperature (Fig. 5) due to increased exciton-phonon interactions. The Boltzmann redistribution of occupied phonon levels also results in a small blue shift in the fluorescence spectrum at the highest temperatures (T = 300 K).

The excitation spectrum of the luminescence peak centered at E = 1.70 eV of the 650 nm thick film is shown in Fig. 6. In this measurement, the film was excited by

monochromatic light generated from a Xe-arc lamp in conjunction with a monochromator. The fluorescence quantum efficiency was determined by comparison with a previously calibrated standard thin film sample (300 nm thick film of aluminum-tris-quinolate[15]) measured in an identical configuration. Low fluorescence efficiency (< 1%) is observed at $E > 2.2$ eV, although it peaks at ~ 20 times its short wavelength efficiency at 2.10 eV. The quantum efficiency enhancement at $E < 2.2$ eV increases with film thickness, indicating that non-radiative surface recombination for the thinnest films (~ 200 nm in our experiments) partially quenches the observed enhancement. Indeed, we might expect that the enhancement shown in Fig. 6 is also due primarily to surface recombination effects. That is, at $E < 2.2$ eV the film is nearly transparent, leading to uniform illumination (and hence exciton generation) throughout the film bulk. At higher energies, the excitons are generated within a diffusion length of the surface where they recombine, leading to a reduced radiative recombination efficiency. However, we note that the transparency at the high-energy tail ($E > 3.1$ eV) is equal to that at $E < 2.2$ eV, yet we observe no comparable enhancement in quantum efficiency. Given that the exciton diffusion length measured[10,14] at high energies ($L_D = 85$ nm) is considerably shorter than at $E < 2.1$ eV (where $L_D = 225$ nm), we would expect surface recombination enhancements at the high energy side to be even more pronounced, contrary to observation. Hence we conclude that the low energy peak in the excitation spectrum in Fig. 6 is primarily a bulk rather than a surface phenomenon.

IV. Discussion

To interpret the data of Figs. 1 to 6, in the context of considerable previous work on the spectroscopic properties of PTCDA,[4-6, 10, 14, 16, 26] we use the configuration space representations of the molecular levels shown in Fig. 7. Here, Fig. 7a corresponds to the absorption transitions, whereas in Fig. 7b the fluorescence transitions occurring after nuclear relaxation are shown.

A. Absorption

The electronic ground state of PTCDA is spin-singlet (labeled S_0 in Fig. 7). The high oscillator strength of the absorption features in Figs. 1 and 2 is therefore a signature

of spin-allowed singlet-to-singlet transitions. The distinctly different behavior of the high energy solution absorption peaks (E = 2.39 eV, 2.55 eV, 2.74 eV, 2.90 eV) as compared to the broad peak at 2.23 eV as a function of PTCDA concentration, leads us to assign these two groups of transitions to separate singlet manifolds.[17]

The equal spacing between the four high energy solution absorption peaks (c.f. Table 1) indicates that these peaks correspond to transitions to different vibronic states (ν_n) in the singlet, S_1 band, labeled $S_1[0\text{-}\nu_n]$. Using this conventional labeling scheme, the observed transitions are $S_1[0\text{-}0]$, $S_1[0\text{-}1]$, $S_1[0\text{-}2]$ and $S_1[0\text{-}3]$. Note that in the thin film, absorption energy differences between these transitions are not exactly equal, indicating some anharmonicity in the S_1 potential induced upon crystallization and subsequent exciton delocalization, or additional vibrational modes of PTCDA in the solid state. In solution, the absorption spectral shape of these S_1 transitions is not significantly influenced by the PTCDA concentration in DMSO (Fig. 2a), indicating that S_1 is Frenkel-like, i.e. the excitation is largely confined to the individual monomers. This is further supported by the shape of the monomer fluorescence (Fig. 4a) obtained via excitation into the S_1 band, which is also unaffected by the PTCDA solution concentration. As previously, we note that the fluorescence spectrum is simply a Stokes-shifted replica of the S_1 band transitions.

The situation for the solution absorption transition centered at E = 2.23 eV is considerably different than for absorption into S_1. In this case, the absorption is strongly affected by concentration, becoming vanishingly small for [k] < 0.1 μM solutions. This is expected for an aggregate state arising from the π-π orbital overlap of closely stacked PTCDA molecules, and is similar to aggregate states observed in other organic crystals such as α-perylene,[18] tetracene,[8] and C_{60}.[19] Since PTCDA is only weakly soluble in DMSO, small particles with three-dimensional crystalline properties (e.g. extended charge-transfer states) form a suspension in solution. As the colloidal solution is diluted, the concentration of aggregate particles is reduced to the extent that, at the lowest concentrations, their contribution to the absorption spectrum is negligible. This leads to the observed attenuation of this "3D" peak at low PTCDA concentrations in both DMSO and NMP (Fig. 2a and Fig. 3).

Note that in Fig. 2a there are no peak shifts as the solution concentration (and hence the monomer-to-aggregate ratio) is varied. In particular, we do not observe a systematic shift of the lowest energy S_1 peak toward the peak at 2.23 eV as [k] increases. Such a shift, if observed, would suggest that these features arise from excitons in the same manifold (e.g. due to Davydov splitting of the S_1 state). In addition, when the aggregate concentration is very small in the most dilute solution, the peak at 2.23 eV is undetectable, from which we infer this peak is associated only with aggregate formation and is non-Frenkel-like in nature, i.e. it is not associated with the lowest observed monomer band, S_1.

Thus, we assign the 2.23 eV absorption feature to a charge-transfer (CT) exciton of the extended PTCDA structure. The lower energy of the 2.23 eV peak as compared to the S_1 state is also consistent with this picture, where CT states are generally found at energies lower than the corresponding maxima of the monomer spectrum.[9,20] This assignment of the 2.23 eV peak as a CT state is fully consistent with previous experiments including MQW absorption,[4] electroabsorption,[6] and fluorescence lifetime[4] studies, where it was found to have a radius of $a \approx 12$ Å along the PTCDA stacking direction. Since the intermolecular stacking distance is only 3.21 Å, we conclude that there is a considerable charge transfer associated with this aggregate state.

We note that the CT line is considerably broadened for solutions as compared with thin films. This is due to the limited, but nevertheless finite interaction of the colloidal particles with the solution coupled with the extended excitonic wavefunction, giving rise, for example, to surface effects. An additional source of broadening is the existence of a distribution of aggregate sizes in the colloidal solution.

B. Solution Fluorescence

Since monomers are the dominant species in the most dilute solutions, and since the fluorescence spectrum does not significantly change with concentration, the solution fluorescence in Fig. 1a is attributed to direct monomer transitions from S_1 to S_0 (see Fig. 7b). In contrast, the thin film fluorescence spectrum peaks at 0.60 eV lower energy than does the monomer fluorescence (Fig 1b). We note that the fluorescence quantum

efficiency of the thin films is significantly lower than that of solutions due to phonon-enhanced fluorescence quenching. Therefore, despite a finite (but small) aggregate concentration in PTCDA solutions, we do not observe the low energy aggregate peak in the solution fluorescence spectrum. The S_1 absorption lines of aggregates and thin films are broader than for monomers due to the increased coupling of phonon modes with electronic transitions in solids. With an increase in PTCDA concentration, we thus observe a small broadening of S_1 absorption lines in DMSO, as indicated in Table 1.

We can quantify the relative concentration of aggregated and solvated molecules in our solutions by analyzing the sub-linear dependence of the integrated fluorescence intensity as a function of concentration (Fig. 4a inset). By assuming that the fluorescence data in the inset of Fig 4a is linear in the monomer concentration, $[k^m]$ (which corresponds to a constant monomer quantum efficiency, η^m, with dilution), then the *deviation* of the data from a straight line intercepting the origin and the point at $[k] = [k^m] = 0.25\ \mu M$, is a result of a small concentration of aggregated molecules, $[k^a]$, i.e. $[k^a] = [k] - [k^m]$. Thus, by subtracting the actual intensity values from this simple linear fit, we can calculate both $[k^m]$ and $[k^a]$. Figure 8 is a plot of $[k^m]$ and $[k^a]$ vs. $[k]$. Numerical fits to the data using $[k^{m,a}] \propto [k]^r$, where r is the rate of rise, are also plotted in Fig. 8. Note that the rate of rise of the aggregate absorption peak (labeled CT [0-ST], where ST denotes "self-trapped," in Fig. 2b) is $r = 1.75 \pm 0.02$, which is in good agreement with the rate of rise of $[k^a]$ obtained from fluorescence data in Fig. 8. Therefore, the assumption of constant η^m is consistent with both the observed solution absorption and fluorescence intensities.

An alternative explanation for the apparent decrease in η^m in Fig. 4a has previously been attributed to the increase of inter-molecular collisions.[21] However, typical concentrations at which collisional effects have been observed are $\sim 10^3$ times larger than in our experiments. Therefore, it is unlikely that the small probability for molecular collisions is responsible for the decrease in the quantum efficiency of monomer fluorescence in Fig. 4a.

We note that the change in the relative oscillator strength of the vibrational states of the S_1 manifold is also due to the increase in aggregate-to-monomer ratio with increasing [k]. As plotted in Fig. 2b, the rate of rise (r) of individual S_1 vibrational lines increases from S_1[0-0] to S_1[0-1] to S_1[0-2]. This is due to configurational shifts in the condensed state of PTCDA which change the overlap of the S_0 ground state wave function with the S_1 vibronic levels, thereby favoring the higher ν_n transitions.[5] This effect is clearly evident in thin films where the oscillator strength of S_1[0-2] is more than three times greater than that of S_1[0-0] (see Table 1). Therefore, with increasing solution concentration where the aggregate contribution becomes more important, the oscillator strengths of the higher vibrational levels are expected to increase faster than that of lower vibrational levels, as observed.

C. Thin Film Fluorescence

The thin film fluorescence line shape does not change as the excitation energy is varied between 2.72 eV (corresponding to excitation directly into S_1) and 2.05 eV (with excitation into the CT state), although the peak energy is red-shifted by 0.60 eV from its value for solutions. This indicates that in solid PTCDA, S_1 and CT are in equilibrium at room temperature, and that relaxation into either the CT state or another state even lower in energy, occurs prior to fluorescence. Since the fluorescence quantum efficiency in the excitation spectrum peaks at 2.10 eV which corresponds to the low energy tail of CT, the CT state is likely the initial level in the fluorescence process, and there are non-radiative losses in the $S_1 \rightarrow$ CT transitions.

The low fluorescence quantum efficiency for $E > 2.2$ eV (see Fig. 6) also indicates that a significant fraction of S_1 excitons undergoes non-radiative recombination. These observations lead us to speculate that most S_1 excitons undergo either $S_1 \rightarrow S_0$ internal conversion that is fast enough to effectively compete with fluorescence, or intersystem-crossing into a non-radiative triplet state, T_1, which is typically lower in energy than S_1. In Fig. 9 we schematically indicate the various transitions possible between the lowest energy states found for PTCDA thin films in this work. Both internal conversion and the spin-forbidden $T_1 \rightarrow S_0$ non-radiative transition can account for the low quantum

efficiency of PTCDA, similar to observations for a number of organic dyes.[21] That is, since CT transitions are radiative, we conclude that S_1 relaxation via non-radiative $S_1 \rightarrow S_0$ or $S_1 \rightarrow T_1$ is favored over $S_1 \rightarrow$ CT. This can also be deduced from the difference in the diffusion lengths for excitons generated by absorption into the S_1 and CT states.[10, 14] For excitons generated by direct absorption into CT, the diffusion length is $L_D = 225$ nm, compared with $L_D = 85$ nm for absorption directly into S_1. Thus, the larger fraction of S_1 excitons that undergo relaxation into S_0 or T_1 determine the apparent S_1 state diffusion length, while the smaller fraction that relaxes into CT are responsible for the observed low efficiency fluorescence.

D. Self-Trapping

In molecular crystals such as pyrene[22] and perylene,[23] strong exciton-phonon coupling results in the formation of self-trapped excitons. These states are lower in energy than the corresponding free excitons and can be solely responsible for the observed fluorescence. We therefore examine self-trapping in PTCDA by analyzing the low energy thin-film-absorption tail of the CT state. Due to strong exciton-phonon coupling,[5] self-trapping is very likely. The implications regarding exciton transport will be discussed further in Paper II.

It was previously shown[24] that the criterion for self-trapping in three dimensional solids is that the exciton-phonon coupling constant, g, must exceed a critical value:

$$g_c = 1 - (2n)^{-1} = 0.75 \qquad (1)$$

where n is the number of nearest neighbor sites in the crystal structure (n = 2 in PTCDA). We can estimate g for PTCDA by analyzing the low-energy tail of the exciton absorption line peaked at $E_0 = 2.23$ eV using the Urbach absorption rule:[25]

$$\alpha(E) = \alpha_0 \exp\left(-\sigma \frac{E_0 - E}{kT}\right) \qquad (2)$$

Here, α is the absorption constant, k is the Boltzmann constant, T is the temperature, and $\alpha = \alpha_0$ at $E = E_0$. From Eq. (2), a plot of $\ln(\alpha/\alpha_0)$ vs. E should yield a straight line with slope: σ / kT. From this we can find σ_0 (the value of σ as $T \rightarrow \infty$), via:

$$\sigma = \sigma_0 \frac{2kT}{\hbar\omega_p} \tanh\left(\frac{\hbar\omega_p}{2kT}\right) \qquad (3)$$

where $\hbar$ is the Planck's constant divided by 2π, and $\omega_p = 1065\ cm^{-1}$ is the dominant phonon frequency associated with the phenyl ring breathing mode.[5,26] Finally, g, is obtained using:

$$g = 1.5/\sigma_0 \qquad (4)$$

where the factor, 1.5, is called the "steepness index" obtained through numerical simulations[24] for 3-D lattice structures. Figure 10 is a plot of $\ln(\alpha/\alpha_0)$ vs. E of the low energy absorption tail of the CT state. The slope of the straight line fit to the data yields $\sigma/kT = (16 \pm 1)\ eV^{-1}$, which from Eq. (3) and (4) gives $g = 1.4 \pm 0.2$ at T = 300 K. Since $g > g_c$, self-trapping of the CT excitons appears likely in PTCDA aggregates and thin films.

Finally, using g we can estimate the self-trapping energy (ΔE_{ST}) of the CT state via:

$$g = \frac{\Delta E_{ST} + B}{B} \qquad (5)$$

Here $2B$ is the bandwidth of the CT state, which we estimate to be the energy difference between the free CT (or CT [0-F]), (2.23 ± 0.03) eV and S_1 [0-0], (2.38 ± 0.03) eV absorption transitions, or $2B = (0.15 \pm 0.05)$ eV. This yields a small self-trapping energy of $\Delta E_{ST} = (0.04 \pm 0.02)$ eV. The self-trapped energy of the CT exciton is therefore (2.19 ± 0.05) eV, which is in reasonable agreement with (2.11 ± 0.04) eV obtained through numerical fits to the absorption spectrum shown in the inset of Fig. 10. Furthermore, the self-trapped exciton is expected to be broader, and have a lower transition probability than the corresponding free exciton.[27] Both of these conditions are satisfied for the data in the inset of Fig. 10 and Table 1, where absorption transitions from S_0 to free and self-trapped CT states are indicated. Note also that this self trapping energy is consistent with photoconductivity measurements[14] given in Paper II.

Previous measurements of the fluorescence lifetime dependence on temperature[4] give us information on the energy barrier between CT^F and CT^{ST}. Recall that the radiative lifetime and spectral line shape of fluorescence obtained by photoexcitation into

the thin film S_1 band is temperature independent from 20 K to 295 K. This suggests that in the solid state, the $S_1 \rightarrow$ CT transition is not thermally dependent, and further that the potential barrier for CT^F to CT^{ST} transitions is comparable to or less than the thermal energy at 20 K, or ~ 2 meV.

It is less clear if the S_1 exciton is self-trapped. Since Frenkel excitons such as S_1 are small, they are not subject to long-range lattice interactions. Hence, it is not expected that they exhibit self-trapping, as do more polar, large diameter CT states.[9] From the small Stokes shift (< 0.1 eV) between the solution peak absorption and fluorescence spectra (Fig. 1a), we conclude that it is likely that de-excitation occurs directly from the free S_1 state into S_0. This conclusion is supported by the solution fluorescence lifetime of (4.0 ± 0.5) ns, which is comparable to the 5 ns decay time of perylene monomers.[28] For the self-trapped state of α-perylene, on the other hand, a much longer fluorescence decay time (~ 120 ns) was measured[23] at room temperature. Analogously in PTCDA, the thin film fluorescence lifetime for excitation into S_1 is about three times longer, (10.8 ± 0.5) ns, than that of the solution fluorescence. The short lifetime of solution luminescence implies a lack of significant self-trapping for S_1.

V. CONCLUSION

Using the absorption and fluorescence spectra of PTCDA thin films and solutions, we have studied the low energy excitonic transitions of this interesting molecular crystal. We identified a Frenkel S_1 state with a readily observable phonon structure in the absorption spectra at E > 2.3 eV, and find that the feature at E_{CT}^F = (2.23 ± 0.03) eV is a free charge-transfer exciton. Evolution of the CT peak with an increase in the colloidal solution concentration unambiguously identifies this state as due to PTCDA aggregates. These data are consistent with previous electroabsorption and multiple quantum well absorption shift measurements which suggested the existence of extended (with radius $a \approx 12$ Å) CT excitons in PTCDA thin films. Through the analysis of the strong exciton-phonon coupling in PTCDA, we also identified a weakly self-trapped CT state in the low energy tail of the absorption spectrum. Numerical analysis, supported by the

PTCDA excitation spectrum, provide an estimate of the energy of this self-trapped state as (2.11 ± 0.04) eV above S_0.

ACKNOWLEDGMENTS

We would like to thank D.Z. Garbuzov, Y. Hirose, Z. Shen, and R.B. Taylor for helpful discussions. We are grateful to AFOSR and NSF (MRSEC) for their partial support of this project.

TABLES

Table 1 Numerical fit to the absorption spectra of PTCDA thin films, and 2 μM and 0.25 μM solutions of PTCDA in DMSO. Each spectrum was fit to six gaussian shapes corresponding to six transitions identified in the text and noted in the left-most column. For each gaussian curve, the peak energy (E_0), energy difference of the neighboring energy peaks (ΔE), the full width at half maximum (FWHM), and the integrated area below the curve (f) normalized to the area of S_1 [0-0], are indicated.

	Thin Film				**2 μM Solution**				**0.25 μM Solution**			
Transition	E_0 [eV]	ΔE [eV]	FWHM [eV]	f [a.u.]	E_0 [eV]	ΔE [eV]	FWHM [eV]	f [a.u.]	E_0 [eV]	ΔE [eV]	FWHM [eV]	f [a.u.]
CT [0-ST]	2.11		0.17	0.46	2.12		0.36	1.10	2.16		0.50	0.63
CT [0-F]	2.23		0.14	2.03	2.20		0.16	0.73	2.20		0.16	0.06
S_1 [0-0]	2.38	> 0.11	0.14	1.00	2.39	> 0.16	0.10	1.00	2.39	> 0.17	0.09	1.00
S_1 [0-1]	2.49	> 0.17	0.21	2.86	2.55	> 0.19	0.16	1.58	2.56	> 0.17	0.13	1.03
S_1 [0-2]	2.66	> 0.19	0.23	3.20	2.74	> 0.16	0.16	0.94	2.73	> 0.17	0.12	0.39
S_1 [0-3]	2.85		0.26	3.31	2.90		0.13	0.22	2.90		0.23	0.41

FIGURE CAPTIONS

Figure 1 Absorption (solid line) and fluorescence (dashed line) spectra of (a) 2 μM solution of PTCDA in DMSO, and (b) 1000 Å thick PTCDA film. The energy position for each absorption and fluorescence transition is identified.

Figure 2 (a) Absorption spectrum of PTCDA in DMSO solution as a function of PTCDA concentration. Each dilution step reduces PTCDA concentration to 80% of the starting solution. (b) Relative oscillator transition strength (proportional to the integrated area) of E = 2.20 eV, E = 2.39 eV, E = 2.55 eV, and E = 2.74 eV solution absorption peaks as a function of PTCDA in DMSO concentration. The slopes refer to the linear fits (straight lines) to the data. The plot was normalized to the oscillator strength of the S_1 [0-0] transition at a concentration of 2 μM. *Inset:* Sample numerical fit to the 0.80 μM solution absorption spectrum.

Figure 3 Absorption spectrum of PTCDA in NMP solution as a function of PTCDA concentration.

Figure 4 (a) Fluorescence spectrum of a PTCDA in DMSO solution as a function of PTCDA concentration [k]. Each dilution step reduces PTCDA concentration to 80% of the starting solution. *Inset:* Dependence of the integrated fluorescence intensity on [k] (b) Fluorescence for 2 μM and 0.25 μM solutions, as well as for thin films. The energy of thin film fluorescence has been increased by 0.60 eV to allow for superposition with the solution spectra. *Inset:* Temporal response of PTCDA solution and thin film (reprinted from Ref. 4) fluorescence response to E = 2.59 eV.

Figure 5 Dependence of 200 nm thick PTCDA film fluorescence on temperature (from Refs. 5, 16).

Figure 6 Excitation fluorescence spectrum of a 650 nm thick PTCDA film sample.

Figure 7 (a) Absorption and (b) fluorescence configuration space diagrams along with direct transitions proposed for PTCDA.

Figure 8 Dependence of monomer concentration, $[k^m]$, and aggregate concentration, $[k^a]$, on the total concentration of PTCDA in DMSO, [k], as calculated using data in the inset of Fig. 3a. Numerical fits of the form $[k^{m,a}] \propto [k]^r$ are indicated by dashed lines.

Figure 9 Proposed transitions between the lowest lying thin film PTCDA energy levels. The straight and wavy lines indicate single-step, and multi-step non-radiative transitions, respectively.

Figure 10 Low energy thin film absorption spectrum of PTCDA. The straight line fit (solid line) yields the empirical slope coefficient $\sigma / kT = (16 \pm 1)\ eV^{-1}$. *Inset:* Absorption spectrum of a 400 Å thick PTCDA film (solid line). Absorption components, noted in Table 1, are indicated by dashed lines. CT [0-ST], CT [0-F], and the sum of $S_0 \rightarrow S_1$ transitions are identified. The sum of these fits is given by the solid line, and is found to agree well with the observed total spectrum (open dots).

REFERENCES

[1] F.F. So and S.R Forrest, *Mol. Cryst. Liq. Cryst. Sci. Technol. - Sec. B* ***2****, 205 (1992).*

[2] Z. Shen and S.R. Forrest, *Phys. Rev.* ***B 48****, 17584 (1993).*

[3] S.R. Forrest, P.E. Burrows, E.I. Haskal, F.F. So, *Phys. Rev.* ***B 49****, 11309 (1994).*

[4] F.F. So and S.R. Forrest, *Phys. Rev. Lett.* ***66****, 2649 (1991).*

[5] E.I. Haskal, Y. Zhang, P.E. Burrows and S.R. Forrest, *Chem. Phys. Lett.* ***219****, 325 (1994);* E.I. Haskal, Z. Shen, P.E. Burrows and S.R. Forrest, *Phys. Rev.* ***B 51****, 4449 (1995).*

[6] Z. Shen, P.E. Burrows, S.R. Forrest, M. Ziari, W.H. Steier, *Chem. Phys. Lett.* ***236****, 129 (1995).*

[7] J.J. Ewing and D.R. Kearns, *J. Chem. Phys.* ***44****, 3139 (1966).*

[8] L. Sebastian, G. Weiser, and H. Bässler, *Chem. Phys.* ***61****, 125 (1981).*

[9] M. Pope and C.E. Swenberg, Electronic Processes in Organic Crystals, *Oxford University Press, Oxford (1982).*

[10] V. Bulović and S.R. Forrest, *Chem. Phys.*, Paper II, following this paper.

[11] PTCDA obtained from Aldrich Chemical Co., Inc., Milwaukee, WI 53201.

[12] E.I. Haskal, F.F. So, P.E. Burrows, S.R. Forrest, *Appl. Phys. Lett.* ***60****, 3223 (1992).*

[13] P. Fenter, P.E. Burrows, P. Eisenberger, S.R. Forrest, *J. Crystal Growth* ***152****, 65 (1995).*

[14] V. Bulović and S.R. Forrest, *Chem. Phys. Lett.* ***238****, 88 (1995).*

[15] D.Z. Garbuzov, V. Bulović, P.E. Burrows and S.R. Forrest, *Chem. Phys. Lett.* ***249****, 433 (1996).*

[16] F.F. So, Doctoral Dissertation, *University of Southern California, May 1991.*

[17] This assignment is consistent with the Lyons model. See, for example, E.A. Silinish, Organic Molecular Crystals, Chapter 1, *Springer-Verlag, Berlin (1980).*

[18] J. Tanaka, *Bull. Chem. Soc. Jpn.* ***36****, 1237 (1963).*

[19] M.K. Kelly, P. Etchegoin, D. Fuchs, W. Krätschmer, K. Fostiropoulos, *Phys. Rev.* ***B 46****, 4963 (1992).*

[20] F. Gutmann and L.E. Lyons, Organic Semiconductors, *Robert E. Krieger Publishing Co., Malabar, Florida (1981).*

[21] F.P. Schäfer, "Principles of Dye Laser Operation" in Dye Lasers, Ed.: F.P. Schäfer, *Springer-Verlag, Berlin (1973).*

[22] A. Matsui and H. Nishimura, *J. Phys. Soc. Jpn.* ***49****, 657 (1980).*

[23] H. Nishimura, T. Yamaoka, K. Mizuno, M. Iemura, and A. Matsui, *J. Phys. Soc. Jpn.* ***53****, 3999 (1984).*

[24] M. Schreiber and Y. Toyozawa, *J. Phys. Soc. Jpn.* ***51****, 1544 (1982).*

[25] K.S. Song and R.T Williams, Self-Trapped Excitons, *Springer-Verlag, Berlin (1993).*

[26] K. Akers, R. Aroca, A.-M. Hor, R.O. Loutfy, *J. Phys. Chem.* ***91****, 2954 (1987).*

[27] E.I. Rashba, "Self-Trapping of Excitons," in Excitons, Ed. E.I. Rashba and M.D. Sturge, *North Holland Publishing Co., Amsterdam (1982).*

[28] N. Mataga, Y. Torihashi, and Y. Ota, *Chem. Phys. Lett.* ***1****, 385 (1967).*

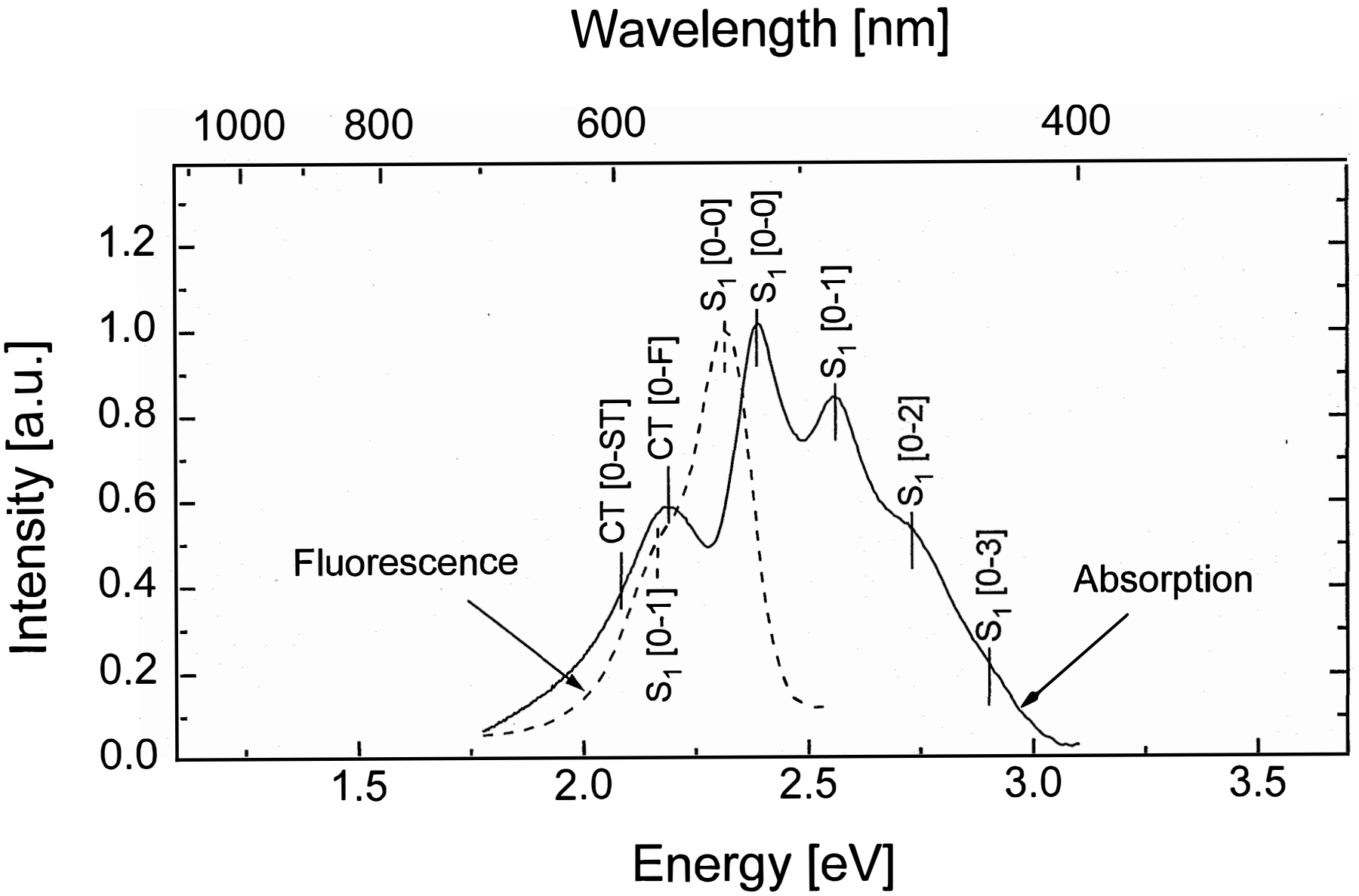
Wavelength [nm]
1000
800
600
400
Intensity [a.u.]
1.2
1.0
0.8
0.6
0.4
0.2
0.0
1.5
2.0
2.5
3.0
3.5
Energy [eV]
Fluorescence
Absorption
CT [0-ST]
CT [0-F]
S1 [0-1]
S1 [0-0]
S1 [0-0]
S1 [0-1]
S1 [0-2]
S1 [0-3]

Fig. 1a

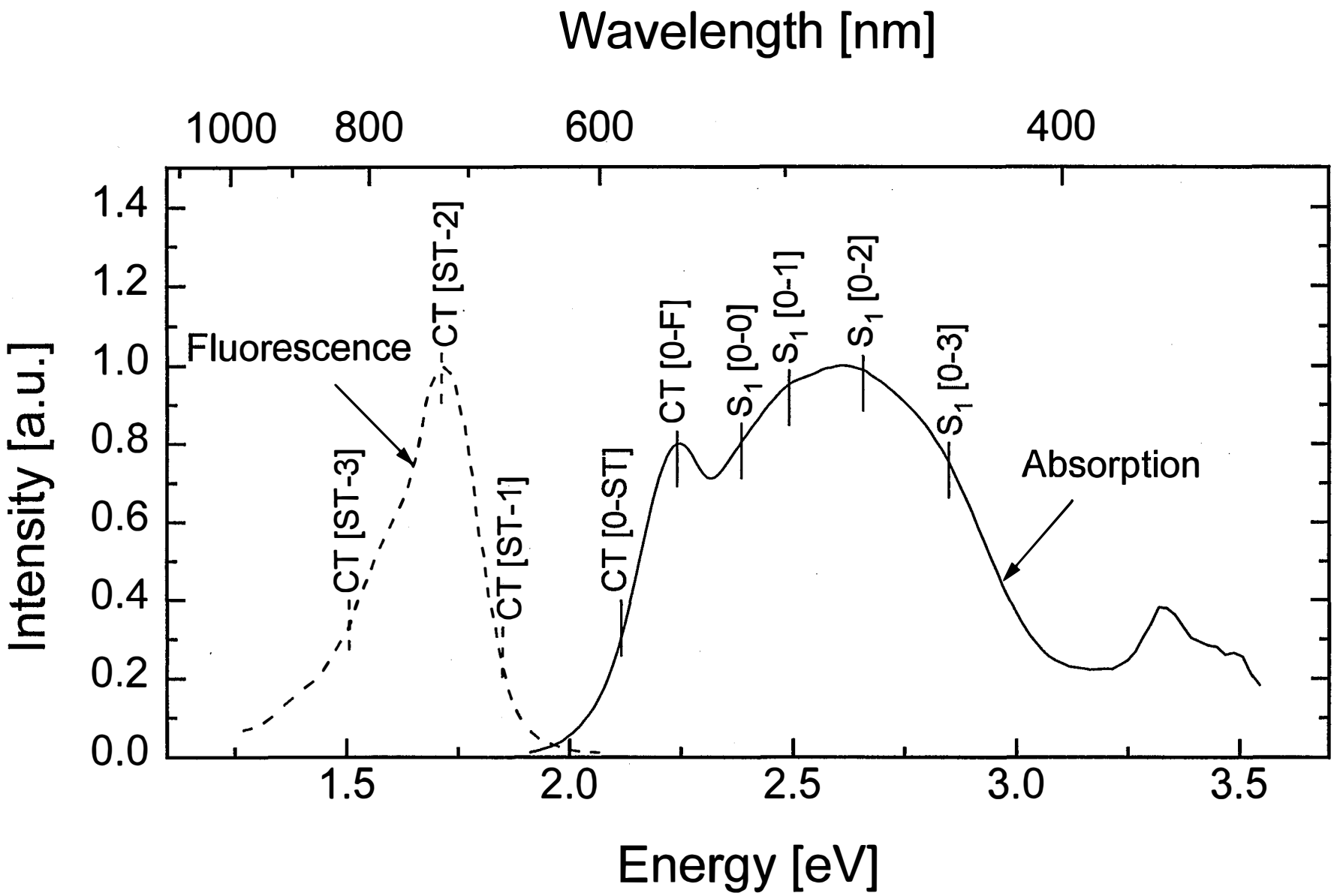
Wavelength [nm]
1000
800
600
400
Intensity [a.u.]
1.4
1.2
1.0
0.8
0.6
0.4
0.2
0.0
Fluorescence
CT [ST-3]
CT [ST-2]
CT [ST-1]
CT [0-ST]
CT [0-F]
S1 [0-0]
S1 [0-1]
S1 [0-2]
S1 [0-3]
Absorption
1.5
2.0
2.5
3.0
3.5
Energy [eV]

Fig. 16

Fig. 2a

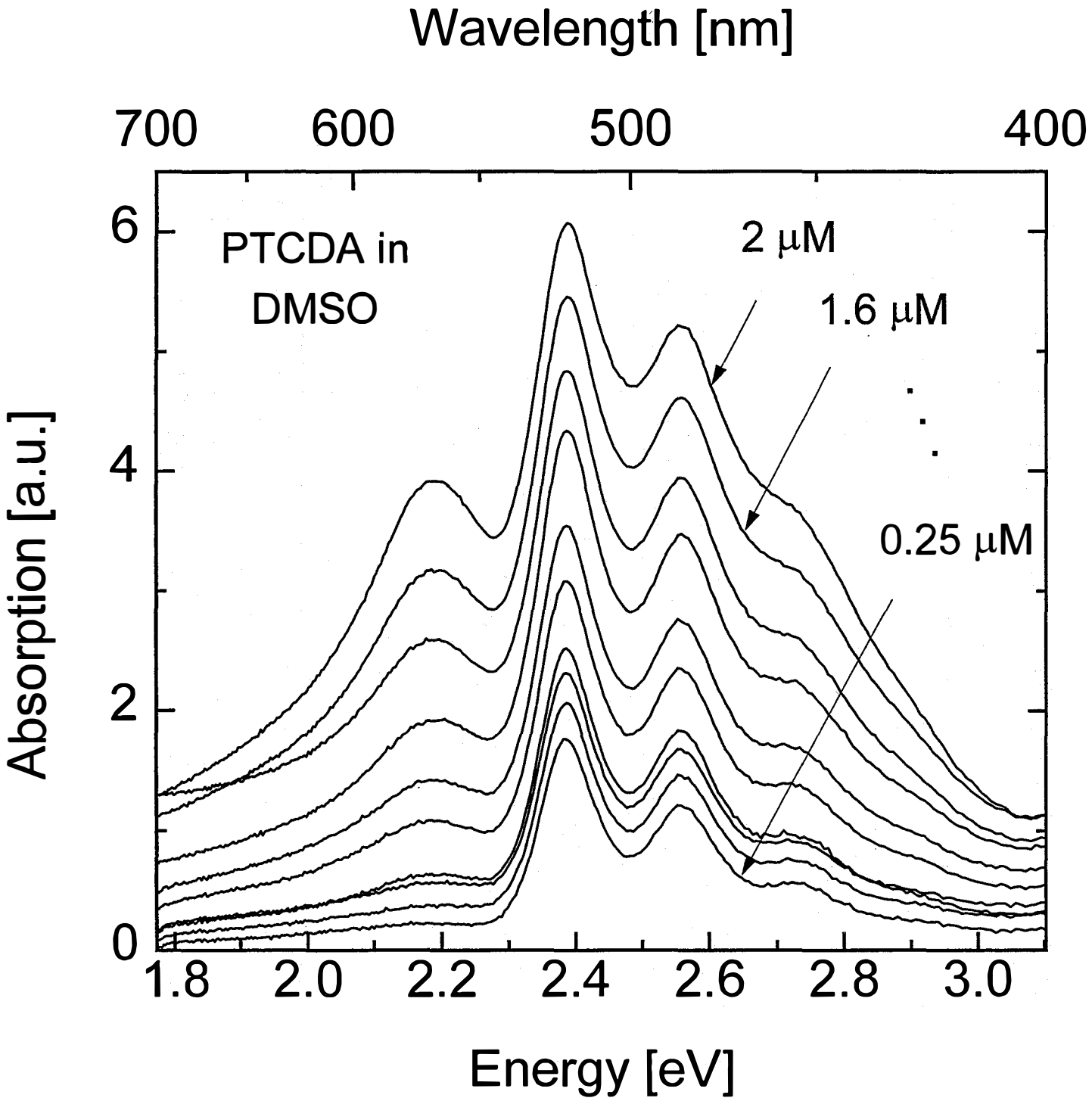
Wavelength [nm]
700
600
500
400
PTCDA in
DMSO
2 μM
1.6 μM
0.25 μM
Absorption [a.u.]
0
2
4
6
1.8
2.0
2.2
2.4
2.6
2.8
3.0
Energy [eV]

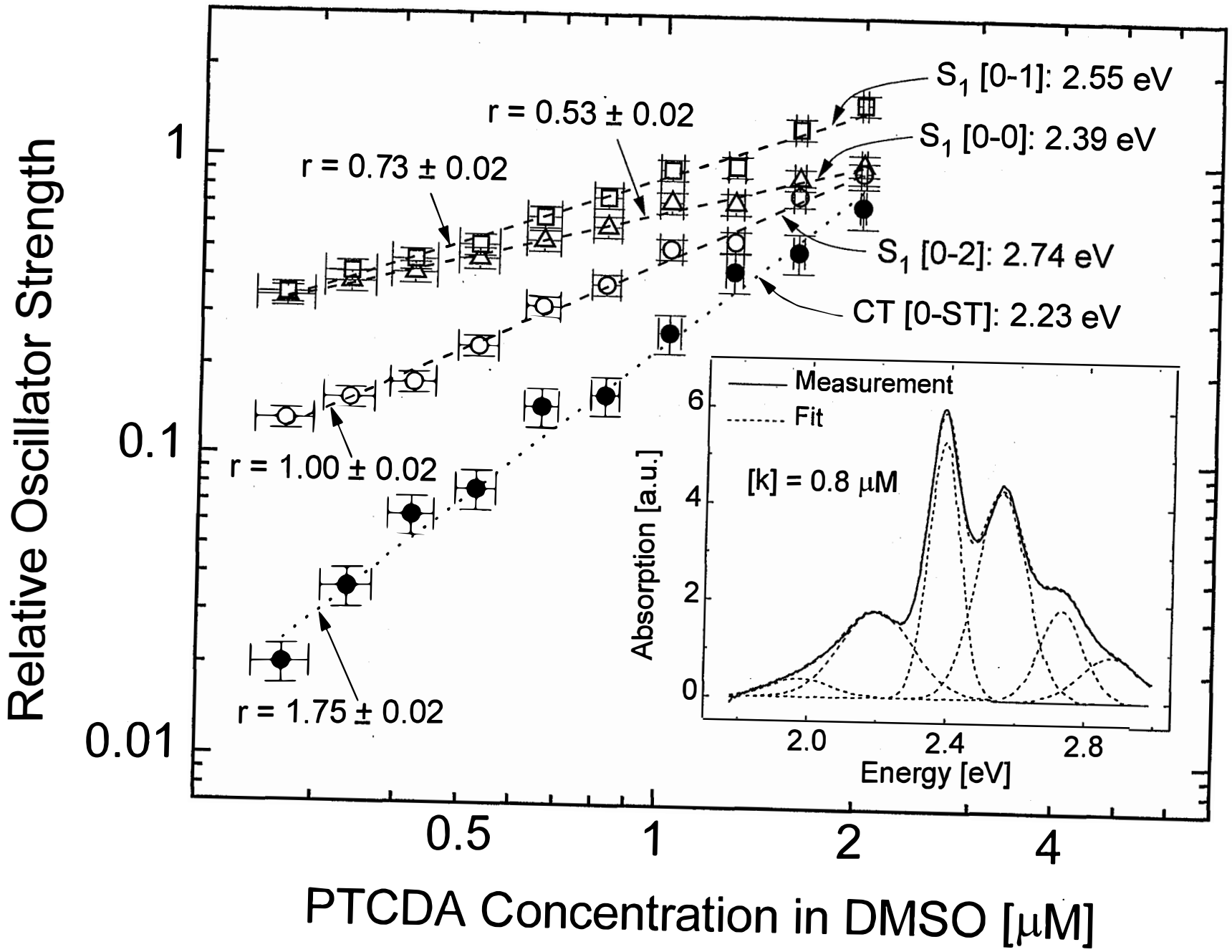
Relative Oscillator Strength
1
0.1
0.01
0.5
1
2
4
PTCDA Concentration in DMSO [μM]
r = 0.53 ± 0.02
r = 0.73 ± 0.02
r = 1.00 ± 0.02
r = 1.75 ± 0.02
S1 [0-1]: 2.55 eV
S1 [0-0]: 2.39 eV
S1 [0-2]: 2.74 eV
CT [0-ST]: 2.23 eV
Measurement
Fit
[k] = 0.8 μM
Absorption [a.u.]
0
2
4
6
2.0
2.4
2.8
Energy [eV]

Fig. 26

Fig. 3

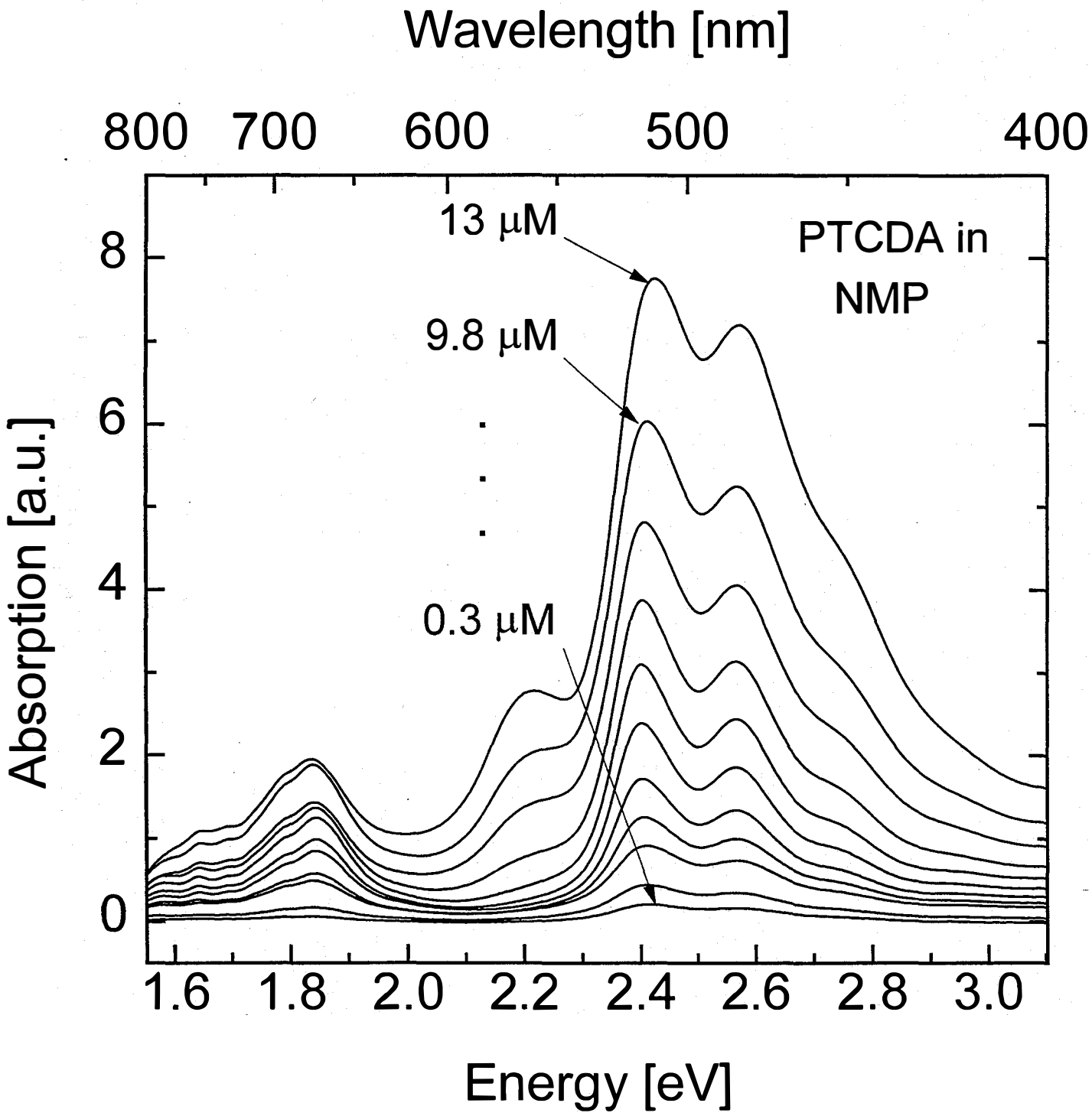
Wavelength [nm]
800
700
600
500
400
13 μM
9.8 μM
0.3 μM
PTCDA in
NMP
Absorption [a.u.]
0
2
4
6
8
1.6
1.8
2.0
2.2
2.4
2.6
2.8
3.0
Energy [eV]

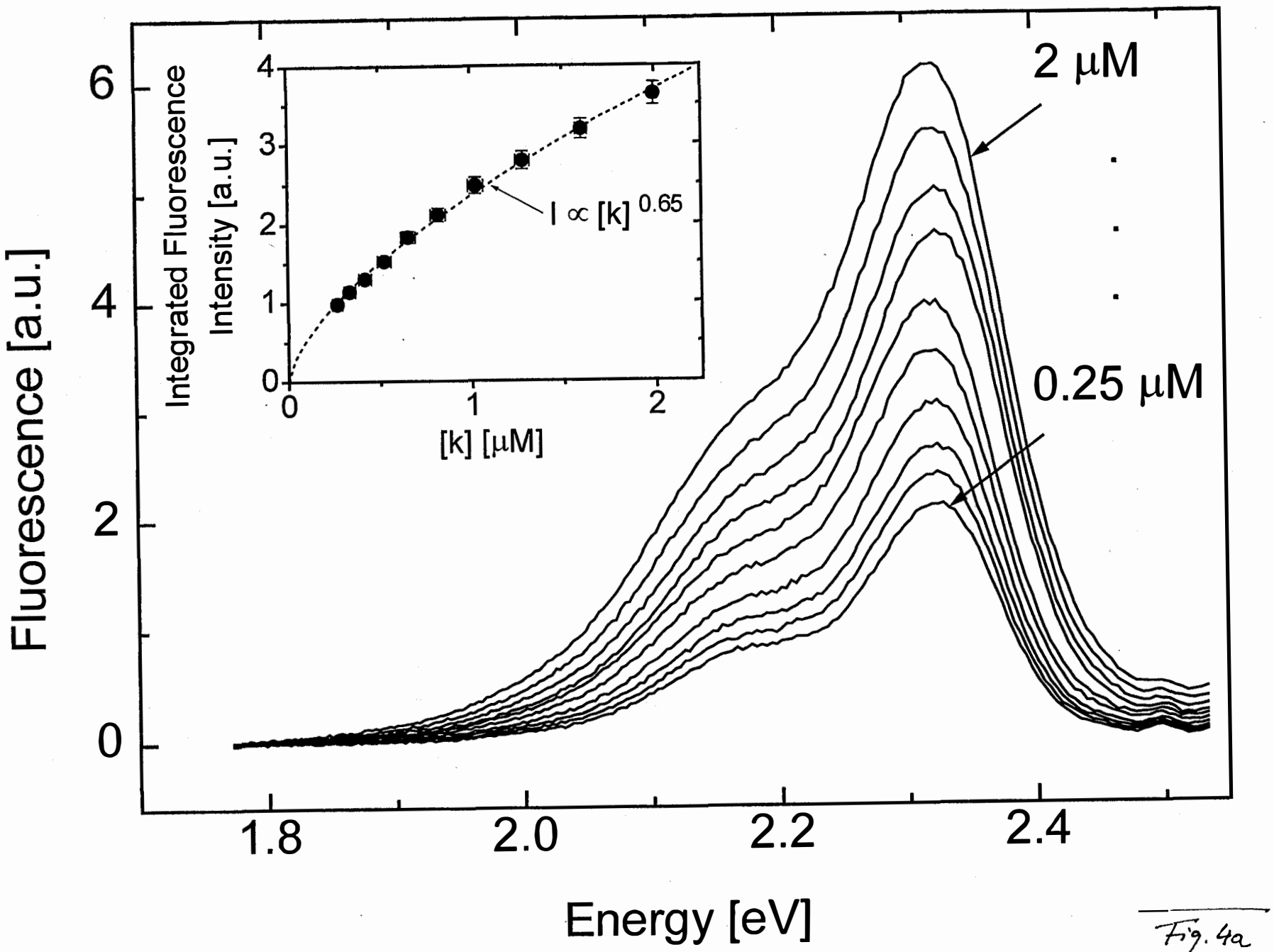
Fluorescence [a.u.]
Energy [eV]
2 μM
0.25 μM
Integrated Fluorescence Intensity [a.u.]
[k] [μM]
I ∝ [k] 0.65

Fig. 4a

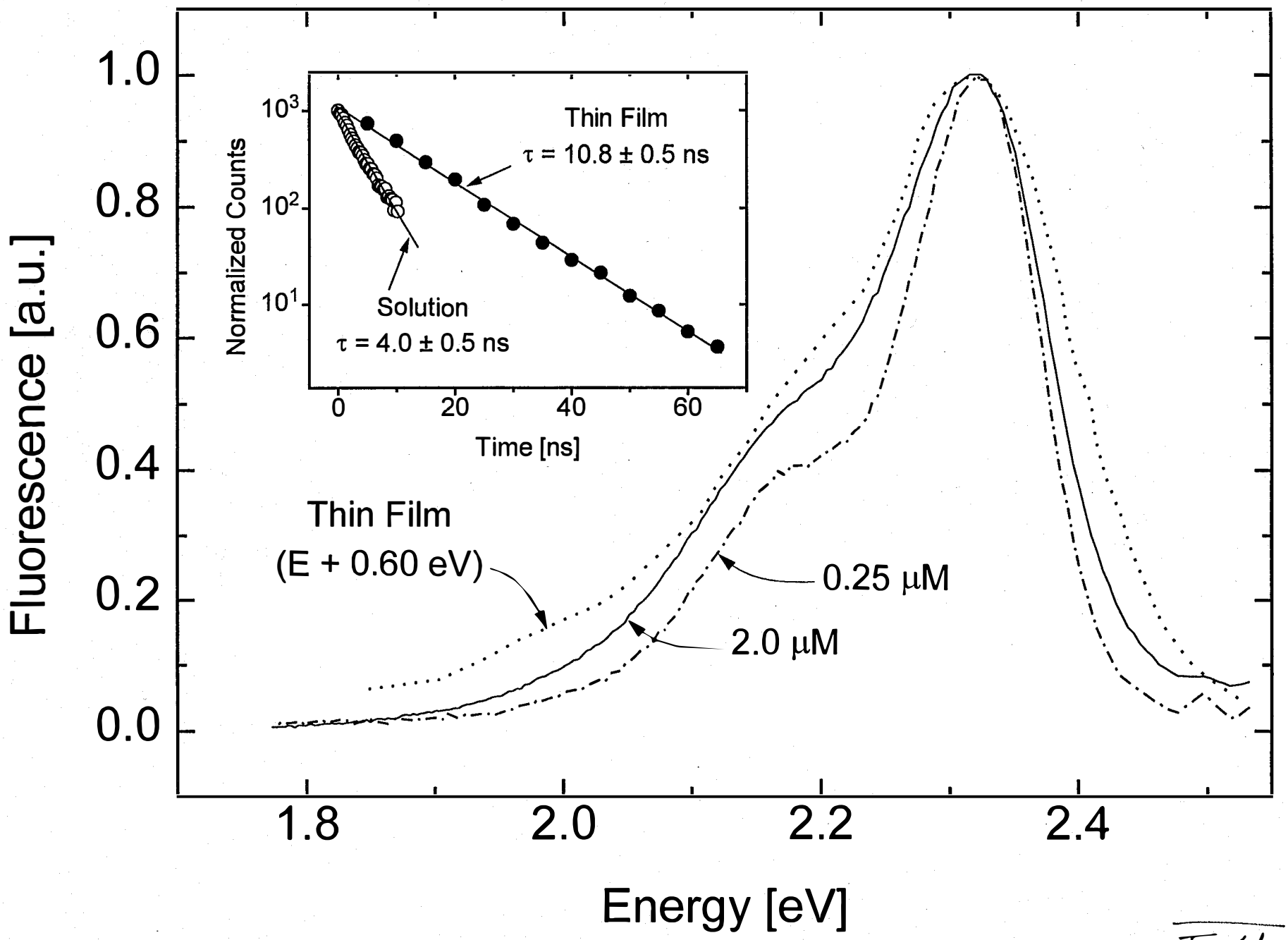
Fluorescence [a.u.]
1.0
0.8
0.6
0.4
0.2
0.0
1.8
2.0
2.2
2.4
Energy [eV]
Thin Film
(E + 0.60 eV)
0.25 μM
2.0 μM
Normalized Counts
10^3
10^2
10^1
Thin Film
τ = 10.8 ± 0.5 ns
Solution
τ = 4.0 ± 0.5 ns
0
20
40
60
Time [ns]

Fig. 4b

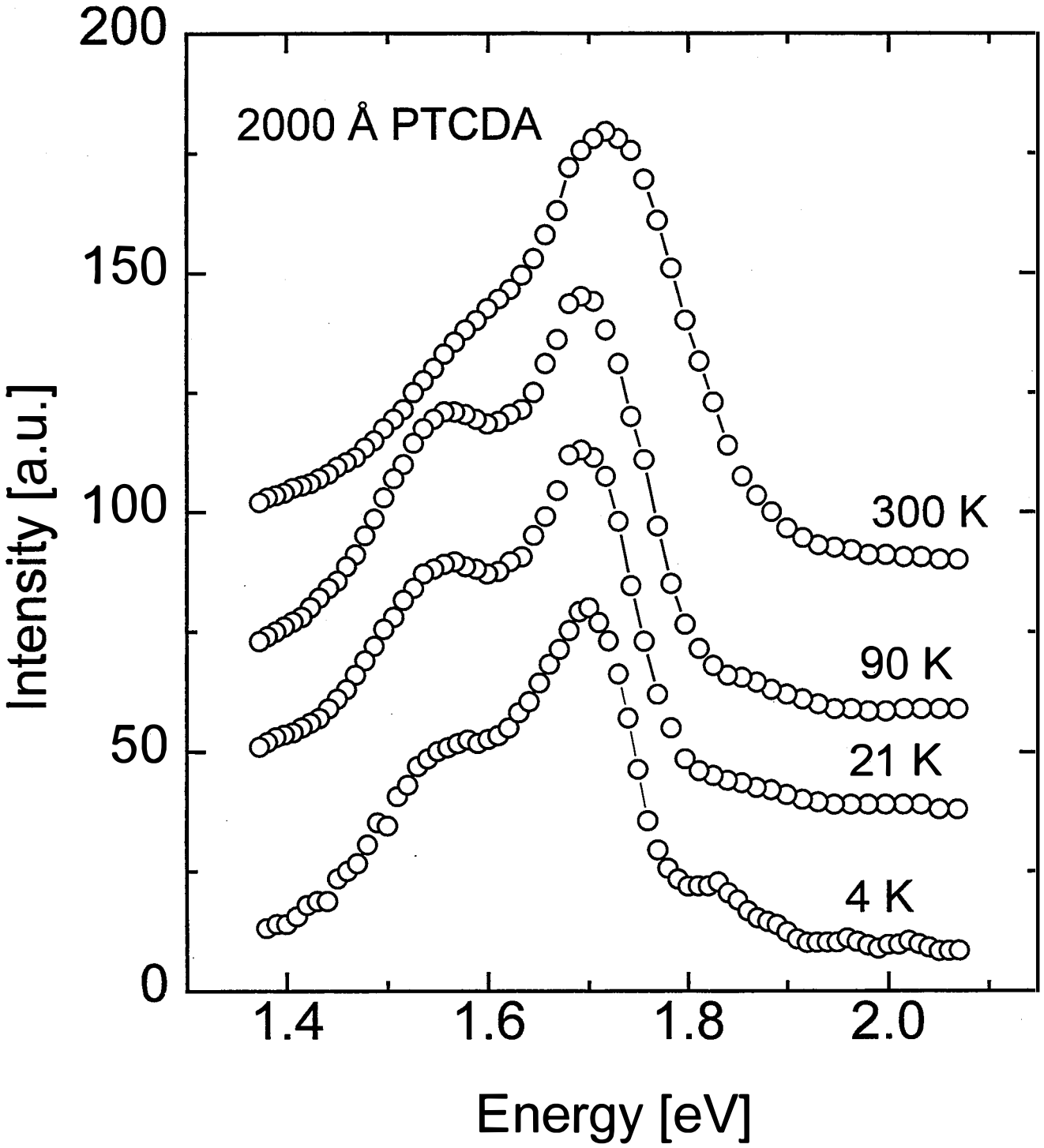
2000 Å PTCDA
300 K
90 K
21 K
4 K
Intensity [a.u.]
Energy [eV]
0
50
100
150
200
1.4
1.6
1.8
2.0

Fig. 5

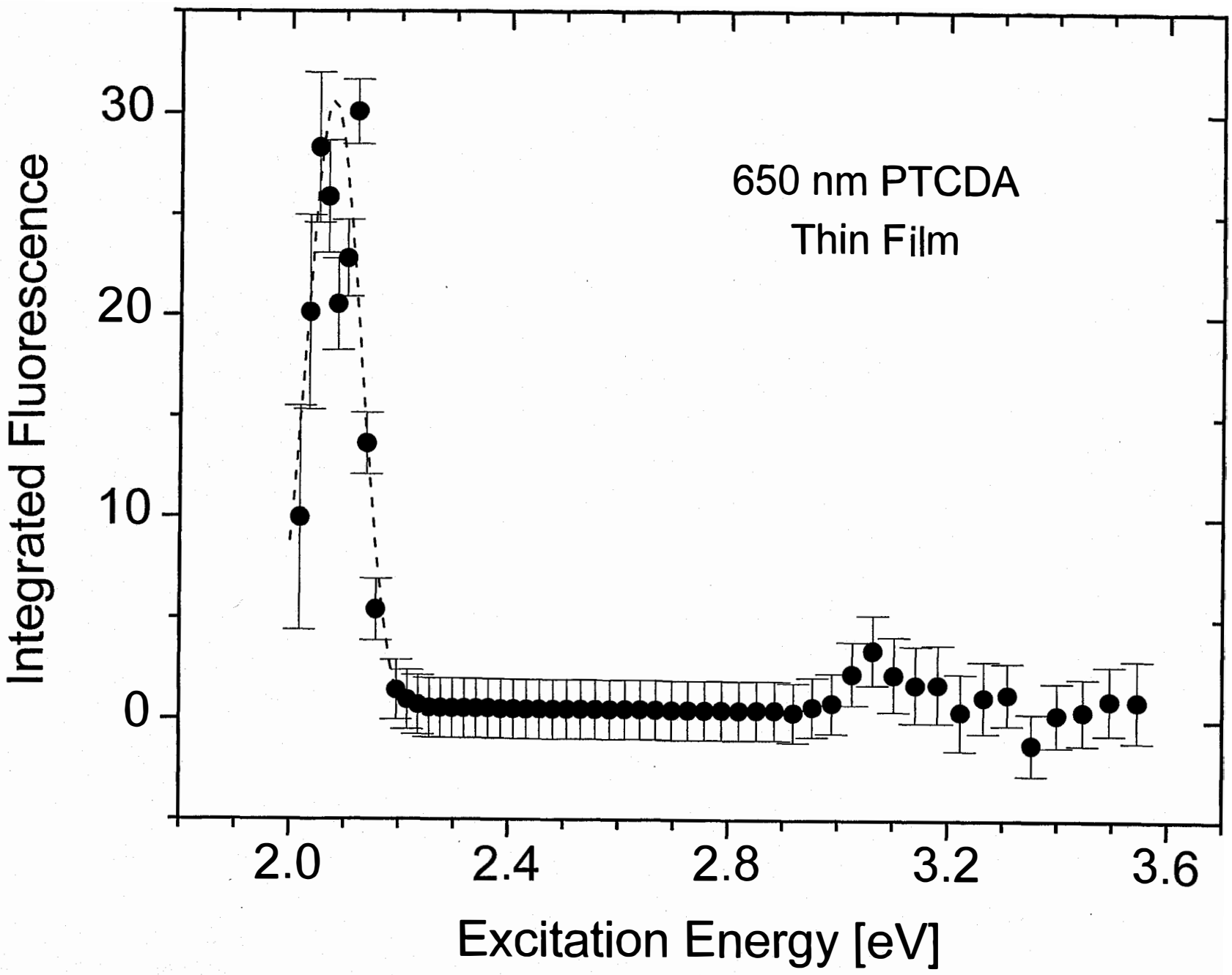
650 nm PTCDA
Thin Film
Integrated Fluorescence
Excitation Energy [eV]
30
20
10
0
2.0
2.4
2.8
3.2
3.6

Fig 6

(a)

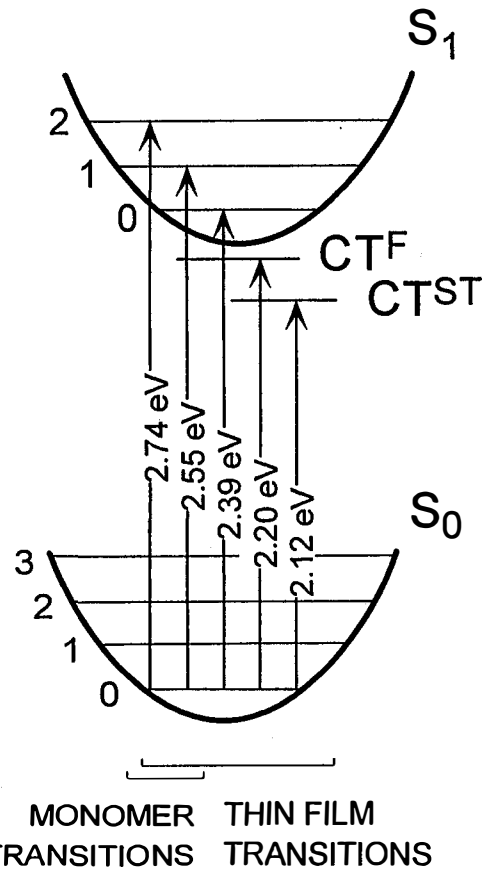
S1
2
1
0
CTF
CTST
2.74 eV
2.55 eV
2.39 eV
2.20 eV
2.12 eV
S0
3
2
1
0
MONOMER TRANSITIONS
THIN FILM TRANSITIONS

(b)

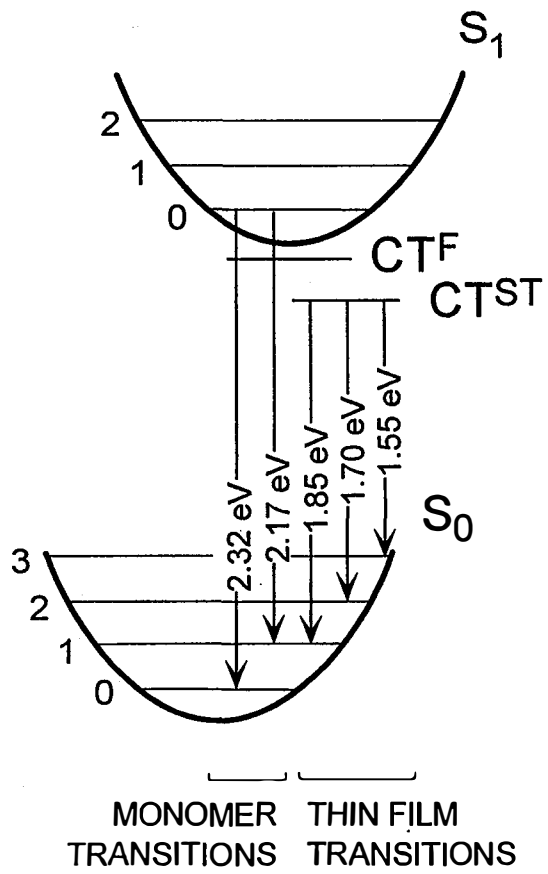
S1
2
1
0
CTF
CTST
2.32 eV
2.17 eV
1.85 eV
1.70 eV
1.55 eV
S0
3
2
1
0
MONOMER TRANSITIONS
THIN FILM TRANSITIONS

Fig. 7

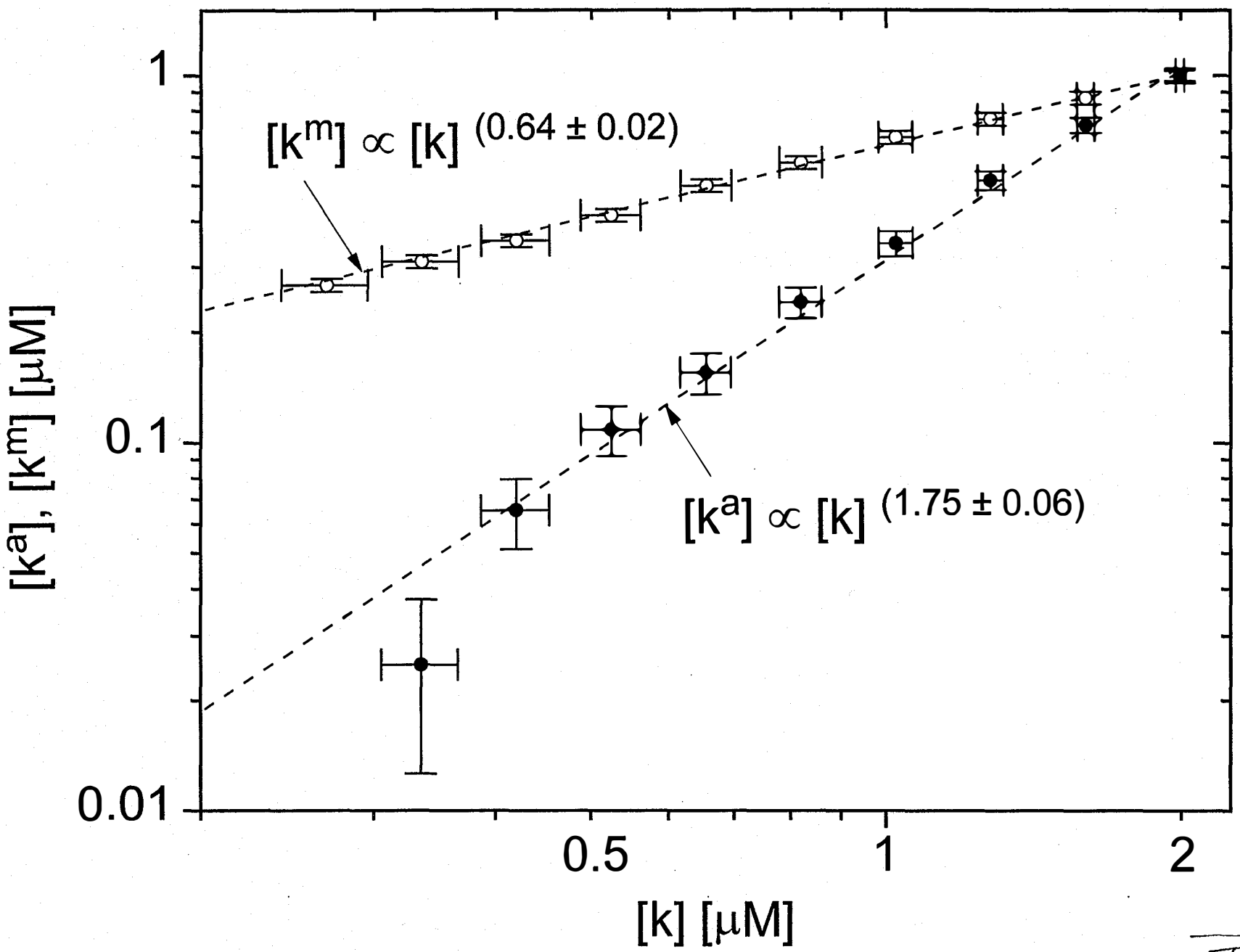

Fig. 8

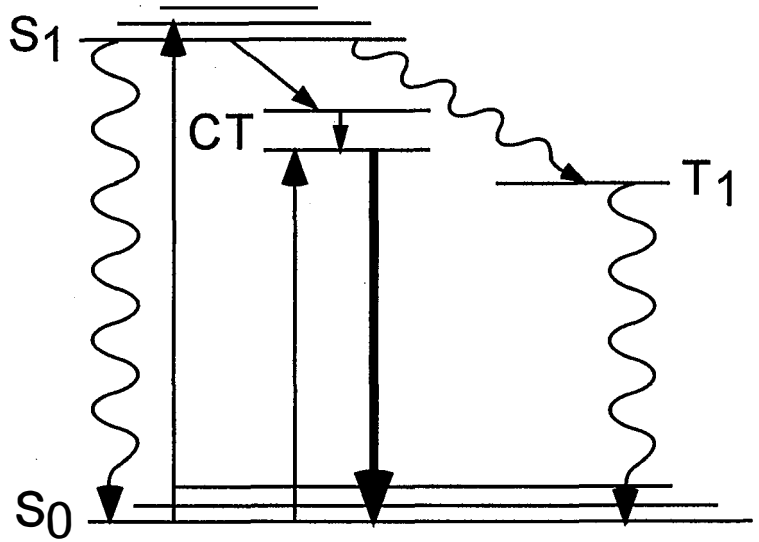

Fig. 9

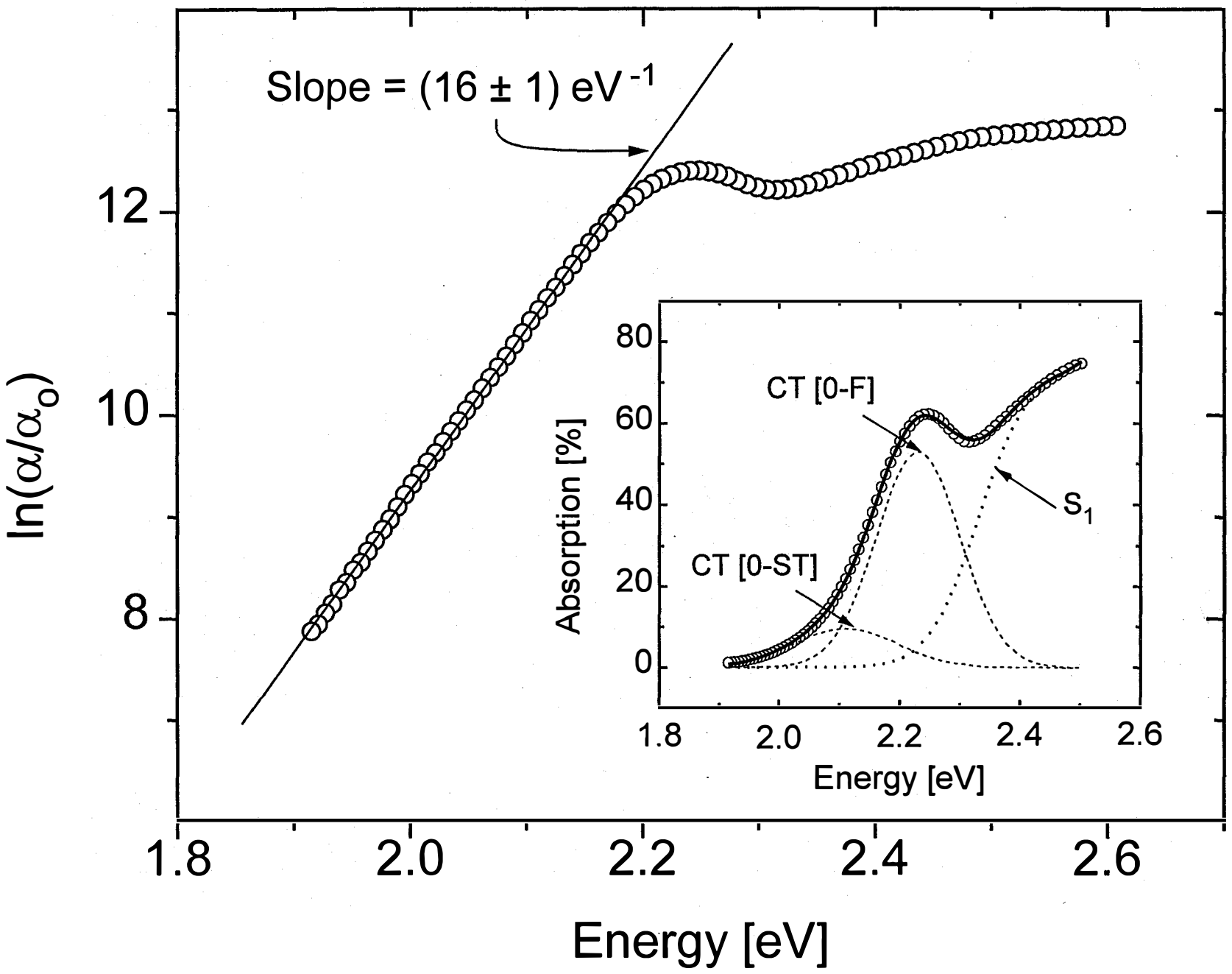
Slope = (16 ± 1) eV -1
12
10
8
ln(α/α0)
1.8
2.0
2.2
2.4
2.6
Energy [eV]
80
60
40
20
0
Absorption [%]
CT [0-F]
S1
CT [0-ST]
1.8
2.0
2.2
2.4
2.6
Energy [eV]

Study of Localized and Extended Excitons in 3,4,9,10 - Perylenetetracarboxylic Dianhydride (PTCDA) II. Photocurrent Response at Low Electric Fields

V. Bulović and S.R. Forrest
Advanced Technology Center for Photonics and Optoelectronic Materials
Department of Electrical Engineering and the Princeton Materials Institute
Princeton University, Princeton, NJ 08544

Abstract

We study excitons in crystalline thin films of the archetype organic molecular compound 3,4,9,10-perylenetetracarboxylic dianhydride (PTCDA) by measuring the photocurrent response under small electric fields ($< 10^4$ V/cm). Photocurrent data reveal the existence of a response tail at energies from E = 1.99 to 2.10 eV above the PTCDA highest occupied molecular orbital, corresponding to a previously identified (Paper I) self-trapped exciton located at E = (2.11 ± 0.04) eV. The diffusion length of this self-trapped state is L_D = (225 ± 15) nm, compared to L_D = (88 ± 6) nm for excitons generated between E = 3.27 eV and 2.36 eV. Fits to absorption data also indicate strong mixing between this self-trapped state and the E = 2.23 eV charge transfer exciton. Exciton diffusion lengths are extracted using a simple model of photocurrent generation in low electric fields, which includes the effects of exciton diffusion, dissociation at the organic/electrode interfaces, and subsequent carrier transport. The data reconfirm that PTCDA is preferentially hole conducting material which is lightly "p-type" at equilibrium. This paper is the second in a two part series investigating excitons in PTCDA thin films.

Study of Localized and Extended Excitons in
3,4,9,10 - Perylenetetracarboxylic Dianhydride (PTCDA)
II. Photocurrent Response at Low Electric Fields

V. Bulović and S.R. Forrest
Advanced Technology Center for Photonics and Optoelectronic Materials
Department of Electrical Engineering and the Princeton Materials Institute
Princeton University, Princeton, NJ 08544

I. Introduction

Excitons play a fundamental role in optical absorption and charge generation in organic molecular crystals (OMCs). Due to the weak van der Waals intermolecular bonding of many OMCs, excitons in these materials are typically either Frenkel or charge-transfer (CT) like, where the Frenkel exciton corresponds to an excited state of a single molecule, whereas the CT state is a correlated system of an electron located on a molecule adjacent to the hole site. Of the two states, the Frenkel exciton is more tightly bound, has a smaller radius and in some cases has a longer diffusion length.[1]

In this work we study exciton transport in the archetype molecular compound: 3,4,9,10-perylenetetracarboxylic dianhydride[2] (PTCDA). PTCDA has recently been the subject of numerous investigations due to its promising optoelectronic properties following the demonstration in several laboratories worldwide of the growth of highly ordered crystalline PTCDA thin films.[3,4] Numerous studies of fundamental properties of excitons in PTCDA and in PTCDA-based multilayers through the measurement of absorption,[5] electroabsorption,[6,7] photoluminescence,[6] and photoconduction,[8,9] as well as in theoretical studies,[10] indicates the importance of PTCDA in the understanding of fundamental optical processes in OMCs. The potential of PTCDA and other perylene derivatives as a technological material is also evident from many publications for its use

in photoconductors,[11] organic photovoltaic cells,[12,13,14] photoelectrochemical cells,[15] optical waveguides[16] and modulators.[17]

Previous studies[18] (referred to as Paper I) of the optical absorption spectrum of PTCDA have identified both Frenkel excitons and extended CT states. Specifically, in Paper I we identified a Frenkel singlet S_1 state which is present in both colloidal solution and thin film absorption spectra, suggesting that it is associated with the PTCDA monomer. In that same study we also confirmed the conclusions of previous multiple-quantum-well absorption[5,7] and electroabsorption studies[6] which identified the prominent lowest energy absorption peak at $E_{CT} = 2.23$ eV (Fig. 1) to be principally a free CT exciton with a radius of ~12Å. It has been shown[5,7] that such large-radius excitonic states exhibit quantum confinement in ultrathin layers whose thickness approaches that of the excitonic "Bohr" radius.

In this study (Paper II), we extend this past work on excitons in PTCDA thin films by measuring the photocurrent response at very low electric fields (typically < 1 V/μm). We clearly resolve an excitonic transition at $E < 2.10$ eV, which in combination with findings in Paper I is identified as the tail of a self-trapped exciton that peaks $E_{CT}^{ST} = (2.11 \pm 0.04)$ eV. We note that previous analysis[8] tentatively assigned this low energy absorption feature to a tightly bound Frenkel exciton. However, in Paper I we have shown that this is more likely a self-trapped CT state. The absorption line of the self-trapped state is characterized by a weak oscillator strength and a broad energy width which overlaps with the free CT exciton at $E_{CT}^{F} = 2.23$ eV. This overlap accounts for the apparent "absence" of the self-trapped state in previous studies of the PTCDA absorption spectrum.

The study of the photocurrent response is of particular importance in highly-ordered organic thin films such as vacuum deposited PTCDA. Dissociation of excitons leading to photocurrent generation is understood to occur at defect sites such as a crystal terrace, a kink, a point defect, an impurity site[19] or an interface.[20] Hence, both the crystal structure and material purity are expected to strongly influence the photogeneration process. Highly ordered PTCDA films, therefore, provide a unique environment for investigations of the fundamental processes underlying photocurrent response in OMCs.

The paper is organized as follows: In Sec. II we discuss sample preparation, film growth, and the experimental measurement setup. Measurement results are presented in Sec. III, including the wavelength-dependent photocurrent and photovoltage response, as well as the absorption spectra of the thin film samples. Also, the voltage and sample-thickness dependence of the photocurrent response is measured. In Sec. IV, the role played by excitons in the photoresponse of OMCs is discussed. Section V presents analysis and discussion of the data in Sec. II. From the photocurrent and absorption spectra, exciton diffusion lengths are inferred. A simple model of voltage dependent photocurrent response from Sec. IV is then compared to the experimental data. Time-of-flight measurements are used in support of this simple model. In Sec. VI, the evidence for the existence of self-trapped CT excitons as well as their technological implications are discussed. Finally, conclusions are presented in Sec. VII.

II. Experimental

Crystalline organic thin films of PTCDA were grown on 10 x 20 mm^2, 15 Ω/□ ITO-coated glass slides which are ~ 94% transparent across the visible spectrum. Prior to growth, the slides were cleaned by three rinsing cycles in boiling 1, 1, 1 - trichloroethane, followed by three cycles in acetone, and a final rinse in boiling methanol. The slides were dried in ultrahigh purity nitrogen between each step. A 5 x 10 mm^2 contact edge strip on the ITO surface was masked prior to organic film deposition. The samples were then loaded into a vacuum chamber with a base pressure of 5 x 10^{-7} Torr. Film growth was preceded by cooling the substrates[3] to less than 90 K, after which 1000 Å to 1 μm thick, pre-purified[21] PTCDA was deposited by thermal evaporation from a baffled Mo crucible at a rate of 3-5 Å/s. Using grazing incidence x-ray[22] and in-situ reflection high energy electron diffraction,[3] we have previously shown that under these growth conditions ordered thin films consisting of extended stacks of planar PTCDA molecules may be obtained over large surface areas on a variety of substrates, such as glass, graphite, and gold. On top of the organic layer, an array of 1mm^2, 4000 Å thick In electrodes was deposited by thermal evaporation through a shadow mask. A schematic cross-section of the test device is shown in the inset of Fig. 1.

Device photoresponse was measured at room temperature and atmosphere by illumination with a 1000 W tungsten-halogen lamp in conjunction with a 1.2 nm linewidth resolution monochromator. The photon flux varied between 5×10^{13} $cm^{-2}s^{-1}$ and 5×10^{15} $cm^{-2}s^{-1}$ depending on the wavelength of the light incident through the transparent ITO electrode. Linear photoresponse was observed at all illumination conditions used. The light was chopped at 165 Hz, and detected using a current amplifier at the input of a lock-in amplifier. For photovoltage measurements made at zero bias, the sample probes were connected directly to the 100 MΩ input of the lock-in.

Time-of-flight measurements were performed by optical excitation through the ITO electrode with a pulsed nitrogen laser in conjunction with a dye laser ($\lambda = 480$ nm). Excitation pulses at a rate of 1 Hz, and ~1 ns duration were incident through 100 m of low dispersion, multimode fiber to reduce laser-generated electrical noise. Bias was applied to the film using a millisecond pulse which was introduced several dielectric relaxation time constants (70 ns) prior to the laser pulse. The transient photocurrent was recorded using a digital oscilloscope.

III. Results of Photocurrent, Photovoltage, and Absorption Measurements

Typical absorption, zero voltage photocurrent, and photovoltage response spectra of a 5000Å thick PTCDA film are shown in Fig. 1. It is evident that all three curves follow the same trend.

Figure 2 shows the dependence of the photocurrent spectral response on the polarity and amplitude of the applied electric field. At very small fields (±0.01 V/μm), photoconduction peaks at the absorption edges (3.2 eV and 2.1 eV) appear. Further increase in the applied field (> 0.1 V/μm) results in significant differences between the spectra obtained at positive and negative voltages (as referenced to the In electrode). Positive fields > 0.1 V/μm (Fig. 2a) distort the spectral response by suppressing the photocurrent in the highly absorptive region (2.9 - 2.2 eV), and enhancing the response at the absorption edges. Increasing the field to > 0.4 V/μm results in a renewed increase in the photoresponse at wavelengths between 2.9 eV and 2.2 eV. On the other hand, for

negative bias (Fig. 2b), a uniform increase in yield at all wavelengths preserves the shape of the spectral response, until at -0.4 V/μm, a flattening in the response is observed.

The photocurrent response of positively biased devices with 3000 Å and 1μm thick PTCDA films is shown in Figures 3a and 3b respectively. The 3000 Å film exhibits an increase in the photocurrent with increasing applied bias, while the 1μm thick film has a similar behavior to that described for the 5000 Å device. It is evident that at 0V, the integrated photocurrent yield increases as the PTCDA film thickness decreases.

IV. Theory of Photocurrent Generation via Excitons

The absorption in the visible spectral region in organic molecular crystals is generally attributed to the creation of excitons.[1] In contrast, band-to-band transitions in OMCs occur at higher energies and typically result in narrow[23] (~ kT) absorption lines. The photogenerated exciton diffuses through the sample, until it encounters a crystal defect site or other structural inhomogeneity, such as the electrode/thin-film interface. At this site or in the bulk, the exciton can either dissociate into an electron and hole, or it can undergo geminate recombination, depending on the temperature and the local electric field. The electric field separates the electron and hole, contributing to the photocurrent. Hence, the total photocurrent yield (η) can be expressed as a product of efficiencies corresponding to the several processes leading to charge generation and collection, *viz.*:

$$\eta = \eta_g \, \eta_d \, \eta_c \qquad (1)$$

Here, η_g is the quantum efficiency for exciton generation, η_d is the efficiency of exciton dissociation resulting in the generation of carriers, and η_c is the carrier collection efficiency in the external circuit. Since it is evident that this photogeneration process is affected by the local electric fields, as well as the initial exciton density distribution within the thin PTCDA films, we now address these two issues.

The exciton spatial concentration dependence on the absorption coefficient can be solved in steady-state assuming boundary conditions of vanishing exciton density at the organic/electrode interfaces,[24] where the excitons readily dissociate or recombine. The rate of exciton generation in the volume between z and z + dz is $\alpha\phi\eta_g \exp(-\alpha z)$, which in steady-state equals the sum of the rates of exciton recombination ($-n(z)/\tau$) and diffusion

($-D\,d^2n/dx^2$). Here, α is the absorption coefficient at energy E, ϕ is the incident photon flux, τ is the exciton lifetime, and D is the exciton diffusion constant. The exciton density distribution as a function of distance, z, from the transparent ITO electrode is then:[24]

$$n(E,z) = \frac{\alpha\phi\eta_g}{D}\frac{1}{\left(\frac{1}{L_D}\right)^2 - \alpha^2}\left[\frac{\exp\left(\frac{L}{L_D}\right) - \exp(-\alpha L)}{\exp\left(-\frac{L}{L_D}\right) - \exp\left(\frac{L}{L_D}\right)}\exp\left(-\frac{L}{L_D}\right)\right.$$
$$\left. - \frac{\exp\left(-\frac{L}{L_D}\right) - \exp(-\alpha L)}{\exp\left(-\frac{L}{L_D}\right) - \exp\left(\frac{L}{L_D}\right)}\exp\left(\frac{z}{L_D}\right) + \exp(-\alpha z)\right] \quad (2)$$

where L_D is the exciton diffusion length, and L is the organic film thickness.

Since the organic/electrode interface provides a site for exciton dissociation, the photocurrent yield (η_d) is directly proportional to the exciton diffusion current (J_{diff}) near the electrodes at z = 0 or L. Assuming that η_g and η_d are independent of applied voltage, then:

$$\eta(E,z,V) = A\frac{\eta_c(V)J_{diff}(E,z)}{\phi}. \quad (3)$$

with

$$J_{diff}(E,z) = -D\frac{dn(E,z)}{dz} \quad (4)$$

Here A, assumed independent of E, is the fraction of J_{diff} that contributes to carrier generation. Using $L_D < L$ in Eq. (2), the photocurrent yield due to generation at the ITO electrode (at z = 0) can be shown to be: $\eta_{NEAR} \propto \eta_c(V)\,[\alpha / (\alpha+1/L_D)]$. A plot of $1/\eta_{NEAR}$ vs. $1/\alpha$ should, therefore, be a straight line which intersects the abscissa at $-L_D$. Similarly, for generation at the In electrode (z = L), the photocurrent yield is $\eta_{FAR} \propto \eta_c(V)\,\alpha \exp(-\alpha L) / (1/L_D-\alpha)$. In this case, $1 / [\eta_{FAR} \exp(\alpha L)]$ vs. $1/\alpha$ is a straight line which intersects the abscissa at $+L_D$. In general, $\eta = \eta_{NEAR} + \eta_{FAR}$ since the electric field can be present near both electrode/organic contacts, rendering them both photoactive. However, by applying external bias, the field within the PTCDA film can be

tailored so that the energy band bending is significant only near one of the two electrodes. allowing for the separate measurement of the photocurrent yields at either the near or far electrode. By this means, we can unambiguously determine the exciton diffusion length using the above analysis.

The 0V electric field distribution within the PTCDA thin films can be inferred from the photoresponse. From the above discussion, photocurrent is generated only if the electric field is present in regions where exciton dissociation occurs. This electric field can be due either to the applied electric field, to the field build-up within the bulk due to charge trapping, or to the built-in field at the organic/electrode interfaces. The magnitude of the built-in fields at the interfaces has not previously been measured. However, a built-in voltage of only 0.1V at each interface would be sufficient to completely deplete a 5000Å thick film with a free carrier concentration of 5×10^{14} cm^{-3} -- a value typical of PTCDA films grown under conditions similar to those used here.[25] Previous studies have shown that both ITO/PTCDA and In/PTCDA contacts are nearly ohmic,[26,27] suggesting that built-in voltages of this magnitude are reasonable. Assuming that the electric field due to bulk traps is smaller than the built-in field of the depleted film, and noting the nearly identical shapes of the photocurrent and photovoltage spectra (Fig. 1) which indicate that electric fields due to photogenerated carriers are much smaller than the built-in field, we conclude that it is likely that the 0V photocurrent response is determined primarily by the contact built-in potentials. The dominance of the photocurrent peaks at 2.6 eV and 2.25 eV in Fig. 1 implies that this built-in field separates carriers at the ITO/PTCDA interface, where most of the incident light is absorbed. Conversely, absorption tails 3.2 eV and 2.1 eV correspond to a lower α, implying a more uniform exciton distribution throughout PTCDA thin film. Excitons generated at these wavelengths therefore dissociate at both contacts. If the built-in field at the In/PTCDA interface is directed in the opposite direction to that of the ITO/PTCDA interface, then the carriers generated at the two interfaces would flow in the opposite directions and could cancel, substantially reducing the 0V photocurrent signal in the absorption wings.

To confirm that the photocurrent in PTCDA is generated at both interfaces depending on excitation wavelength, we compare the 0V photocurrent response of the

5000Å thick PTCDA film (Fig 2b) to the photocurrent yields of 3000 Å (Fig. 3a), and 1 μm (Fig. 3b) thick samples. The electric field near the organic/electrode interfaces should be similar for all three films as it is due to the built-in electrode potentials. However, the exciton distributions within the films should differ: for thicker samples, the exciton density next to the In (far) electrode will be smaller compared to that for the thinner samples. This difference in exciton distribution should result in a reduction in η_{FAR} for thicker samples. If for the 5000Å sample, η_{NEAR} and η_{FAR} are nearly equal and cancel, resulting in negligible photocurrent yield at E = 2.1 eV for 0V applied bias (Fig. 2b), then η_{NEAR} and η_{FAR} cannot be equal in a sample with a thicker or a thinner PTCDA film. Consequently, the E = 2.1 eV signal at 0V applied bias is clearly enhanced for both the 3000 Å (Fig. 3a), and 1 μm (Fig. 3b) thick samples. The measured photocurrent dependence with sample thickness is therefore consistent with the model of photocurrent generation occurring primarily at the interfaces, with carrier collection enhanced only by built-in fields at 0V.

We note that our data show an increase in the photocurrent yield for thinner samples. This is also expected when the photocurrent results from exciton dissociation at the interfaces. In thinner (3000Å) films, excitons have a higher probability of diffusing to an interface and contributing to the photocurrent. In thicker samples (1 μm), excitons generated deep in the film bulk recombine before reaching an interface, consequently decreasing the photocurrent yield.[41]

Electroluminescence[28] as well as time of flight studies[25] have previously identified PTCDA as a hole-transporting semiconductor with an effective bandgap[25] of 2.2 eV. We, therefore, propose the PTCDA photoconductor equilibrium band diagram shown in Fig. 4a. The band diagrams inferred for positive and negative applied bias are shown in Figs. 4b and 4c, respectively. The low applied electric fields used in this study (≤ 1 V/μm) are not sufficient to ionize excitons[1] or to induce space-charge effects,[29] but rather only serve to provide a field gradient for electron and hole drift across the thin film. The above discussion also assumes that carrier generation via exciton dissociation at the organic/electrode interfaces is significantly larger than that due to dissociation in

the bulk. This is justified for exciton diffusion lengths comparable to the PTCDA film thickness, and for electric fields which peak at the electrodes, as is the case in this study.

Finally, to determine the voltage dependence of the photocurrent response in Eq. (3), we note that $\eta_c(V)$ is a function of the carrier transit time through the film, as well as the electric-field-dependent efficiency of exciton dissociation at electrode/organic interfaces. The relative importance of the two processes can be ascertained by first examining the electric-field-dependent exciton dissociation efficiency: A charge pair bound by Coulomb forces dissociates more readily when an external electric field (F) is present.[30] The electric field dependent dissociation probability P(F) is increased from the zero F-field case, P(0), by the ratio[31]:

$$\frac{P(F)}{P(0)} = 1 + \frac{1}{2!}\left(\frac{\alpha^2}{4}\right) + \frac{1}{2!3!}\left(\frac{\alpha^2}{4}\right)^2\left(1 - \frac{2r_o}{r_c}\right) + \frac{1}{3!4!}\left(\frac{\alpha^2}{4}\right)^3\left(1 + 3!\frac{r_o^2}{r_c^2} - 3!\frac{r_o}{r_c}\right) \quad (5)$$

Here $\alpha^2 = \frac{q^3 F}{\pi\varepsilon_s\varepsilon_o(kT)^2}$, $r_c = \frac{q^2}{4\pi\varepsilon_s\varepsilon_o kT}$, where ε_s = 1.9 is the dielectric constant for PTCDA film in the direction normal to the substrate plane,[32] and r_o is the exciton radius. The maximum value of the exciton dissociation enhancement ratio (Eq. 5) is obtained when the initial field is assumed to be zero (i.e. no built-in fields), and $r_o = 0$. Under these extreme assumptions, for the largest electric field used in our experiment ($F = 10^4$ V/cm), we calculate P(F) / P(0) = 1.7. In contrast, the observed photocurrent enhancement ratio for 2.60 eV signal. for example, is as high as 13 (see Sec. V), indicating that field-dependent exciton dissociation is not the dominant process leading to the observed field dependence of the photocurrent in PTCDA.

On the other hand, field dependence of the carrier transit time can also influence $\eta_c(V)$. Since exciton dissociation results in the generation of a free electron and hole, one of these charge carriers is immediately collected at the adjacent electrode while the other carrier is swept across the thin film with probability: $\eta_c(V) = \exp(-t / \tau_{rec})$ of reaching the opposite electrode. Here, t is the carrier transit time, and τ_{rec} is the carrier recombination

time. Competing with carrier collection is recombination of the mobile charge with the background fixed charge in the PTCDA film.[33] For mobility-limited transport, t is dependent on the applied voltage V, via $t = L^2 / \mu V$, where μ is the carrier mobility. No significant change in μ is observed for $F < 10^4$ V/cm. In this case the voltage-dependent photocurrent yield is therefore (using Eq. 3):

$$\eta(E,z,V) = A\frac{J_{diff}(E,z)}{\phi}\exp(-t/\tau_{rec}) = \eta_o(E,z)\ \exp(-L^2/V\mu_h\tau_{rec}) \qquad (6)$$

In addition to this field-dependent photocurrent, we also expect a small field-independent diffusion current contribution (η_{diff}) from pile-up of carriers photogenerated at the contacts. We expect that contributions of η_{diff} are significant only for very small applied external electric fields, where drift currents (c.f. Eq. (6)) are minimal.

V. Data Analysis

Figure 5a is a plot of $1/[\eta_{FAR}\exp(\alpha L)]$ vs. $1/\alpha$ at positive voltages for the energy range between E = 2.10 and 1.99 eV. All of the linear fits to the data intersect the $1/\alpha$ axis at $L_D = (225 \pm 15)$ nm, which corresponds to the diffusion length of excitons generated at E < 2.10 eV. A straight line fit to the data indicates that, at positive voltages, photocurrent originates primarily from the dissociation of these excitons at the In (far) electrode (see Fig. 4b). This is consistent with preferential hole conduction for PTCDA,[25] where positive bias flattens the energy bands near the ITO/PTCDA interface, and increases the slope of the bands near the In/PTCDA electrode, requiring photogenerated holes to traverse the film prior to collection. As a test of our assumption the inset of Fig. 5a shows the same data plotted versus $1/\eta_{NEAR}$. Here, a linear fit was not obtained, indicating that the principal site of exciton dissociation is indeed at the In (far) electrode.

Excitons in the high absorbance region (E = 2.9 to 2.2 eV) are expected to be generated closer to the ITO electrode than those generated in the absorption tails at 3.2 eV and 2.1 eV. Under negative bias, the bands near the In/PTCDA electrode flatten, and those near the ITO/PTCDA electrode increase in slope (Fig. 4c). In Fig. 5b,

therefore, we plot $1/\eta_{NEAR}$ vs. $1/\alpha$ for the photocurrent generated at $V < 0$ and energies between $E = 2.60$ and 2.36 eV. Linear fits to the data intersect the $1/\alpha$ axis, corresponding to a diffusion length of (88 ± 6) nm. This value is in good agreement with previous measurements for the diffusion length of these "short wavelength" PTCDA excitons.[8]

The photocurrent signal at $E > 2.95$ eV exhibits the same voltage behavior as that at $E < 2.10$ eV since the film is also transparent at these short wavelengths (c.f. Fig. 1). In Fig. 5c, therefore, we plot $1/[\eta_{FAR}\exp(\alpha L)]$ vs. $1/\alpha$ for the energy range between $E = 3.27$ and 2.95 eV at positive voltages. Linear fits to the data yield a diffusion length of (79 ± 7) nm, in excellent agreement with the value obtained for the mid-wavelength data in Fig. 5b. This indicates that the 3.2 eV signal is of the same origin as that of the high absorbance region. Due to the smaller absorption coefficient, the 3.2 eV signal is enhanced when bias is applied, also similar to the situation at the long wavelength absorption edge. All three of the fits in Fig. 5 show that the diffusion length is voltage independent, which is consistent with our interpretation that the signal is due to the photogeneration of neutral excitons.

Using the diffusion lengths of $L_D = 88$ nm for excitons generated at $E = 2.60$ eV, and $L_D = 225$ nm for generation between $E = 2.23$ and 2.10 eV, we calculate the exciton density in Fig. 6 using Eq. (2).[34] It is evident that at $E = 2.60$ eV and 2.23 eV, excitons are predominantly concentrated near the ITO electrode, while at 2.10 eV the excitons are generated closer to the In electrode. This is again consistent with the foregoing analysis.

The voltage dependence of the photocurrent response of Fig. 2 can be interpreted through analysis of the exciton diffusion current (J_{diff}), which is proportional to the gradient of the exciton density, n, via Eq. 4. Referring to Fig. 6, we observe that $J_{diff}(2.60eV, L) \approx 0$ since the exciton density at the In/PTCDA interface (at $z = L$) is relatively independent of distance. Further, since the photocurrent is proportional to J_{diff}, from Eq. (2), this suggests that at $E = 2.60$ eV, exciton dissociation at the In electrode does not contribute significantly to the current. In contrast, exciton dissociation near $E = 2.10$ eV where the sample is relatively transparent, is significant at both

interfaces. As discussed previously, the photocurrent contributions at the two interfaces nearly cancel for the 5000 Å thick film at 0V (since $J_{diff}(2.10eV,0) \approx -J_{diff}(2.10eV,L)$), leaving only contributions from the E = 2.60 eV and 2.23 eV signals. Biasing the sample changes the ratio of potential drops at the two electrode/PTCDA interfaces, resulting in an increase in the E = 2.10 eV photocurrent response at both positive and negative bias. At negative bias, the E = 2.60 eV and 2.23 eV photocurrent peak intensities also increase (Fig. 2b) as the slope of the PTCDA bands near the ITO/PTCDA interface increases (Fig. 4c), whereas for small positive bias (corresponding to fields < 0.4 V/μm) these two peaks initially decrease (Fig 2a) as the bands near the ITO/PTCDA electrode flatten (Fig. 4b). In this case, the internal drift field is insufficiently large to separate the electron and hole, leading to recombination prior to carrier collection. For higher fields (> 0.4 V/μm), the response again increases as the slope of the bands changes sign.

The above treatment assumes that PTCDA is a p-type semiconductor in equilibrium, as depicted in Fig. 4. A similar analysis assuming an n-type semiconductor does not reproduce the observed voltage dependencies: Positive bias applied to the n-type film flattens the PTCDA bands near In/PTCDA interface and increases the slope adjacent to the ITO/PTCDA electrode. This implies that for n-type material, the photocurrent yield at E = 2.60 eV (where light is primarily absorbed at the ITO electrode) should be dominant at positive bias, when, in fact the data in Fig. 2a show that the signal at longer wavelengths (E = 2.10 eV) dominates at +1.0 V/μm. Similarly, for negative bias, the bands flatten at the ITO/PTCDA interface and increase in slope next to the In/PTCDA electrode, implying that the photocurrent generated at E = 2.10 eV will dominate, when in fact photocurrent at E = 2.60 eV is observed to be the largest under these bias conditions. From the foregoing, we conclude that PTCDA behaves as a lightly p-type, preferentially hole conducting material. At present, we do not know the source of the excess hole concentration in as-grown PTCDA. This may be due to doping from impurities, diffusion of impurities or metal atoms[35] from the In or ITO contacts, or from diffusion of atmospheric contaminants into the film after exposure to air.

The voltage dependence of the photocurrent for a 5000 Å thick PTCDA film at E = 2.60 eV, 2.23 eV, 2.10 eV is shown in Fig. 7. The dashed lines correspond to the

photocurrent yield, η, calculated using Eq. (6) and the exciton density distribution shown in Fig. 6. In calculating η, we assume a built-in potential of $V_{bi} = 0.1$ V at each interface, consistent with the discussion in Sec. IV. The voltage, V, in Eq. (6) is thus replaced by $V + V_{bi}$. To fit the data near V = 0, we assume very small field independent photocurrent yields of $\eta_{diff} = 0.04$ %, 0.03 %, and 0.01 %, at E = 2.60 eV, 2.23 eV, 2.10 eV, respectively. As noted previously, the observation of these diffusion currents (as seen by the small offset current near V = 0) is further indication of the high stacking order leading to efficient carrier collection in these films. All the fits for $\eta(V)$ at different wavelengths shown in Fig. 7 consistently result in $\mu_h\tau_{rec} = 1 \times 10^{-8}$ cm^2/V, where μ_h is the hole mobility.

To check the value of $\mu_h\tau_{rec}$ obtained from the fits of Fig. 7, we have independently measured μ_h by the time-of-flight (TOF) method. Here, a 1μm thick PTCDA film was excited by a 1ns pulse at E = 2.59 eV, producing excitons near to the ITO electrode. The application of negative bias causes photogenerated holes to traverse the sample, and induces electron injection from the In electrode. Since PTCDA is preferentially hole conducting[25,28] and lightly p-type, the TOF signal is primarily due to hole transport. This is immediately apparent by measuring the TOF signal under bias opposite to the above. In this case, only an extremely small photocurrent is detected suggesting the relatively poor conductivity of electrons in PTCDA.

Since the electric field is uniform throughout the sample under the very low injection conditions used, we let $\mu_h = L^2 / (\tau_h V)$. Here, τ_h is the hole transit time across the film. The inset of Fig. 7 shows τ_h as a function of the inverse electric field. Using $\tau_h = (11 \pm 2)$ ns at V/L = 30 V/μm, we find $\mu_h = (0.03 \pm 0.01)$ cm^2/Vs, which is in the range of values obtained from previous TOF measurements.[25] Note that the τ_h value used to determine μ_h was measured at fields < 35 V/μm. At higher fields, the circuit is RC time (τ_{RC}) limited, as sample resistance R = (300 ± 50) Ω and capacitance C = (20 ± 5) pF yield $\tau_{RC} = (6 \pm 2)$ ns.

Using $\mu_h\tau_{rec} = 1 \times 10^{-8}$ cm^2/V from the fits to the data in Fig. 7, along with $\mu_h = 0.03$ cm^2/Vs, we find $\tau_{rec} = 0.3$ μs. This value is more than an order of magnitude smaller than measured in previous optical modulation experiments[17], which found

$\tau_{rec} = 17 \pm 1$ μs. This discrepancy could arise from the difference in sample structures used for the two studies. In our measurements, the presence of electrodes and built-in fields, as well as the injection of carriers from the external circuit, should result in an enhanced recombination rate, and thus a shorter τ_{rec} than in the waveguide structures studied in Ref. 17. Also, the hole mobility in our samples is about 30 times smaller than that of the most conductive PTCDA films,[25] indicating that τ_{rec} should be reduced as well. Finally, the measurement of μ_h was done at electric fields one order of magnitude higher than those used in the photoconduction experiments. Carrier mobility in OMCs typically increases with the electric field,[36] indicating that the value of μ_h is likely an overestimate, resulting in an underestimate for τ_{rec}. We therefore conclude that the simple photogeneration model based on exciton dissociation at the organic/electrode interface and subsequent carrier transport is in reasonable agreement with the measured photocurrent data.

VI. Discussion

The dependence of L_D on wavelength indicates that at $E < 2.10$ eV, the photocurrent response is due to the generation of an exciton unlike those generated at higher energies. It was previously proposed that the lower energy and longer diffusion length of this exciton were characteristic of a Frenkel state. That is, Frenkel excitons have a smaller radius than CT excitons, and thus should exhibit longer diffusion lengths.[37] However, in Paper I we found that self-trapping of the free CT state at $E_{CT}^{F} = 2.23$ eV gives rise to this additional broad feature centered at $E_{CT}^{ST} = 2.11$ eV. Strong exciton-phonon coupling, characteristic of numerous organic crystals such as pyrene and perylene, leads to the formation of a self-trapped state which is lower in energy than the corresponding free exciton. Such strong exciton-phonon coupling has also been observed[7] in PTCDA, indicating that self-trapping is very likely for the free CT state.

To separate the contributions of the free state from the corresponding self-trapped exciton, we have quantitatively fit the low energy absorption spectrum of PTCDA to a pair of Gaussian curves, one corresponding to each of these two species (see Fig. 8). A

sample thickness of 400 Å was chosen to accentuate the absorption characteristics in the energy range of interest. However, any sample thickness yields a fit similar to that shown in Fig. 8. For the free CT state, we use the Gaussian peak energy of $E_{CT}^{F} = 2.23$ eV, and half-width of $\sigma_{CT}^{F} = 140$ meV independently obtained from the electroabsorption data of Shen *et al.*,[6] Haskal *et al.*,[7] and from spectroscopic studies presented in Paper I. The self-trapped state peak energy (E_{CT}^{ST}) and half-width (σ_{CT}^{ST}) are then chosen to obtain the best fit to the measured long wavelength absorption spectrum of PTCDA. (Absorption features above 2.35 eV correspond to the Frenkel manifold.[18]) From Fig. 8 we see that for $E_{CT}^{ST} = 2.11$ eV and $\sigma_{CT}^{ST} = 170$ meV, we obtain an excellent fit (solid line) to the observed absorption spectrum (open circles). Due to its large half-width, this low energy peak dominates at $E < 2.10$ eV. The energy difference, or trapping barrier, between the two states is $\Delta E_{ST} = (0.12 \pm 0.07)$ eV. It is in good agreement with the value obtained using a simple analysis of the Urbach absorption tail,[38] yielding $\Delta E_{ST} = (0.04 \pm 0.02)$ eV. We also note that the σ_{CT}^{ST} is broader than σ_{CT}^{F}, and the absorption oscillator strength is lower for the $E_{CT}^{ST} = 2.11$ eV peak. Both of these characteristics are expected for a self-trapped state.[39]

In comparing these data with the spectroscopic assignments in Paper I, we conclude that for absorption transitions directly into S_1 band, we generate excitons with diffusion length of $L_D = (88 \pm 6)$ nm. Absorption at lower energy occurs directly into CT^F or CT^{ST} -- two states which are in thermal equilibrium due to the very small self-trapping energy of $\Delta E_{ST} = (0.12 \pm 0.07)$ eV. Once in CT^{ST}, this extended exciton has a diffusion length of $L_D = (225 \pm 15)$ nm.

Exciton fluorescence spectra[18] for PTCDA also indicate that S_1 and CT are in thermal equilibrium which leads to an apparent contradiction -- if this were the case, why do we observe different exciton diffusion lengths for these two states? Also, as noted in Ref. 18, S_1 has two routes for decay corresponding to $S_1 \rightarrow CT$ and $S_1 \rightarrow T_1$, where T_1 is the first triplet manifold of the excited PTCDA molecule. Indeed, the low radiative efficiency of PTCDA thin films, and short radiative lifetimes of PTCDA in solution indicates that this later transition is favored. Hence, $L_D = (88 \pm 6)$ nm in fact corresponds to the diffusion constant of the *triplet* state rather than S_1. Its relatively short diffusion

length results from numerous non-radiative recombination pathways available to excitons in OMCs.

Longer exciton diffusion lengths, such as those observed for the CT state, result in a higher probability for the exciton encountering a dissociation site before spontaneously recombining. The technological significance of this property is apparent if the organic materials are to be used in photovoltaic cells,[12,13,40] in xerographic photoconductors,[11] or chemical sensors.[41] Specifically, in photovoltaic cells, excitons with a long L_D such as the weakly-self-trapped CT exciton of PTCDA, can result in a higher quantum yield in an optimized device in comparison to excitons with a smaller L_D. However, the advantage of the long diffusion can be offset by the lower absorption constant at the longest wavelengths. The quantum yield can further be increased by an electric field, as apparent from of our measurement of PTCDA films where the yield increased from 0.01% to 1% under external bias. Therefore, choosing contacts with a larger built-in voltage should result in a significant increase in quantum efficiency.

The investigations of Tang,[12] Popović *et al.*[20] and Arbour *et al.*[41] all speculate that organic/organic interfaces provide exciton dissociation sites. Similarly, Hiramoto *et al.*[42] found that the introduction of a thin metal layer between organic layers increases the photocurrent by a factor of two. Combining these conclusions with our results indicates that the introduction of interfaces in the high absorbance region of the organic thin film is an effective means for further enhancing the photocurrent yield of organic photovoltaic cells.

VII. Summary and Conclusions

We have investigated exciton transport in the archetype OMC, PTCDA, via analysis of the thin film photocurrent spectrum. The Frenkel and charge-transfer exciton state transport properties were separately resolved and analyzed. The CT state was found to have a self-trapping energy of $\Delta E_{ST} = (0.12 \pm 0.07)$ eV, consistent with previous spectroscopic results. Through the analysis of its photocurrent response, a CT diffusion length of $L_D = (225 \pm 15)$ nm was measured. This is significantly longer that

$L_D = (88 \pm 6)$ nm measured for the higher energy, triplet T_1 states accessed through a rapid $S_1 \rightarrow T_1$ transition, which are proposed using these results along with spectroscopic studies of Paper I.

The presence of both Frenkel and large radius CT excitons in PTCDA identifies this material as a transitional molecular crystal, sharing many properties of both insulators and semiconductors. This "dual" character of PTCDA is attributed to the high degree of overlap of the π-orbital system resulting from unusually close intermolecular stacking. As such, crystalline PTCDA provides a unique *"test-bed"* environment to study fundamental properties of transitional solids, as well as the evolution from a disordered to an ordered organic material.

Linking exciton diffusion and carrier transport, we also obtained a quantitative description of the voltage dependent photocurrent at very small applied electric fields (10^2 V/cm to 10^4 V/cm). Our model gives a clear qualitative picture of photocurrent generation in OMCs that is predominantly dependent on the photogenerated-carrier transit time, rather than on the field-dependent Onsager geminate exciton recombination, or field-dependent changes in carrier mobility. This work, therefore, extends previous studies which primarily focused on photogeneration in OMCs under higher electric fields.

Our understanding of exciton processes in PTCDA is based on previous investigations of absorption, electroabsorption and photoluminescence of single and multilayer structures, as well as on absorption and luminescence studies of PTCDA solutions, presented in Paper I. The present study adds to our understanding of excitons by further quantifying properties of distinct absorption features, and elaborating on the relationship between exitonic states and photogeneration in this archetype OMC. However, a number of fundamental issues remain unresolved: We do not yet have a detailed understanding of the process of dissociation of excitons at interfaces that leads to the generation of free carriers. Similarly, the energy of the extended conduction state ("conduction band") energy of PTCDA is as yet undetermined, although it is probably buried in the strong absorption features of the exciton spectrum. These issues must be clarified if we are to fully understand this important organic molecular system.

Acknowledgments

The authors thank J. McHale for assistance in the growth of the thin films, and S. Sherman for help with the time-of-flight measurements. We also thank Z. Shen, P.E. Burrows, D.Z. Garbuzov, E.I. Haskal and Prof. N. Karl for helpful discussions. We gratefully acknowledge AFOSR, NREL and the NSF MRSEC program for their generous support of this research.

Figure Captions

Figure 1 Short circuit photocurrent and open circuit photovoltage spectra of a 5000 Å thick PTCDA film sandwiched between ITO and In electrodes. The PTCDA absorption coefficient (α) spectrum is also shown for comparison. *Inset:* Schematic cross-section of the sample under investigation.

Figure 2 Short circuit photocurrent response of a 5000 Å thick PTCDA film at (a) positive and (b) negative applied electric fields. Field polarity is referenced to the In electrode.

Figure 3 Short circuit photocurrent response of (a) 3000 Å and (b) 1μm thick PTCDA films at 0V and positive applied electric fields.

Figure 4 Proposed band structure for a PTCDA film at (a) zero, (b) positive, and (c) negative bias.

Figure 5 Inverse quantum yield ($1/\eta$) at different applied fields versus inverse absorption coefficient ($1/\alpha$). Diffusion lengths of (a) $L_D = 225 \pm 15$ nm for E = 2.10 to 1.99 eV region, (b) $L_D = 88 \pm 6$ nm for absorption between E = 2.60 and 2.36 eV and (c) $L_D = 79 \pm 7$ nm for the E =3.2 eV absorption peak were determined from linear least squares fits to the data. The inset shows the same data as that of Fig. 5a except plotted vs. $1/\eta$.

Figure 6 Calculated exciton concentration profiles. Diffusion lengths (L_D) of 88 nm, 225 nm, and 225 nm and absorption coefficients (α) of 3.0×10^5 cm^{-1}, 2.2×10^5 cm^{-1}, and 5.0×10^4 cm^{-1} have been used for E = 2.60 eV, 2.23 eV, and 2.10 eV, respectively. The sample thickness was taken as L = 5000 Å.

Figure 7 Short circuit photocurrent response at E = 2.60 eV, 2.23 eV, and 2.10 eV as a function of applied voltage. Data at E = 2.60 eV and 2.10 eV have been offset along the vertical axis by -2×10^{-3} and 2×10^{-3}, respectively, for clarity. The dashed lines represent numerical fits that are based on the exciton diffusion and carrier transport analysis discussed in the text. *Inset:* Hole time of flight as a function of inverse electric field.

Figure 8 Least squares fit of the sum of two Gaussians to the absorption spectrum of a 400 Å thick PTCDA sample. The small contribution from higher energy excitons is accounted for by a decaying tail of a third Gaussian. The two Gaussians peaks (dashed lines) are at $E_{CT}^{F} = 2.23$ eV and $E_{CT}^{ST} = 2.11$ eV, and have full-widths-at-half-maximum of $\sigma_{CT}^{F} = 140$ meV and $\sigma_{CT}^{ST} = 170$ meV, respectively. The total measured (open dots) and calculated (solid line) absorption spectra at long wavelengths are also shown.

References

[1] M. Pope and C.E. Swenberg, Electronic Processes in Organic Crystals, *Oxford University Press, New York (1982).*

[2] Aldrich Chemical Company, Milwaukee, WI.

[3] S.R. Forrest, P.E. Burrows, E.I. Haskal and F.F. So, *Phys. Rev. B* ***49****, 11309 (1994).*

[4] E.I. Haskal, F.F. So, P.E. Burrows and S.R. Forrest, *Appl. Phys. Lett.* ***60****, 3223 (1992).*

[5] F.F. So and S.R. Forrest, *Phys. Rev. Lett.,* ***66****, 2649 (1991).*

[6] Z. Shen and S.R. Forrest, *Chem. Phys. Lett.,* ***236****, 129 (1995).*

[7] E.I. Haskal, Z. Shen, P.E. Burrows and S.R. Forrest, *Phys. Rev. B* ***51****, 4449 (1995).*

[8] V. Bulović and S.R. Forrest, *Chem. Phys. Lett.,* ***238****, 88 (1995).*

[9] N. Karl, A. Bauer, J. Holzäpfel, J. Marktanner, M. Möbus and F. Stölzle, *Mol. Cryst. Liq. Cryst.,* ***252****, 243 (1994).*

[10] V.M. Agranovich, R.D. Atanasov and G.F. Bassani, *Chem. Phys. Lett.* ***199****, 621 (1992).*

[11] K.-Y. Law, *Chem. Reviews* ***93****, 449 (1993).*

[12] C.W. Tang, *Appl. Phys. Lett.* ***48****, 183 (1986).*

[13] M. Hiramoto, Y. Kishigami and M. Yokoyama, *Chem. Lett., 119 (1990).*

[14] G. Tamizhmani, J.-P. Dodelet, R. Côté and D. Gravel, *Chem. Mater.,* ***3****, 1046 (1991).*

[15] J. Danziger, J.-P. Dodelet, P.Lee, K.W. Nebesny,and N.R. Armstrong, *Chem. Mater. 3, 821 (1991).*

[16] R. Taylor, Z. Shen and S.R. Forrest, *Topical Meeting on Organic Thin Films for Photonics Applications,* Paper MB-5, Portland, Oregon (September 11-14, 1995).

[17] D.Y. Zang and S.R. Forrest, *Appl. Phys. Lett.,* ***60****, 189 (1992).*

[18] V. Bulović, P.E. Burrows, S.R. Forrest, J.A. Cronin and M.E. Thompson, *Chem. Phys., Paper I, preceeding this paper.*

[19] Z.D. Popović, *J. Chem. Phys.* ***77****, 498 (1982).*

[20] Z.D. Popović, A.-M. Hor, R.O Loutfy, *Chem. Phys.* ***127****. 451 (1988).*

[21] PTCDA was purified by three successive ~5 day cycles of thermal gradient sublimation, with a typical sublimation temperature of 400°C.

[22] P. Fenter, P.E. Burrows, P. Eisenberger and S.R. Forrest, *J. Cryst. Growth, **152**, 65 (1995).*

[23] F. Gutmann and L.E. Lyons, Organic Semiconductors, Ch. 4, *Robert E. Krieger Publishing Co., Malabar, Florida (1981).*

[24] A.K. Ghosh and T. Feng, *J. Appl. Phys. **49**, 5982 (1978).*

[25] S.R. Forrest, M.L. Kaplan and P.H. Schmidt, *J. Appl. Phys. **55**, 1492 (1984).*

[26] S.R. Forrest, M.L. Kaplan and P.H. Schmidt, *J. Appl. Phys. **56**, 543 (1984).*

[27] F.F. So and S.R. Forrest, *IEEE Trans. Electron Devices **36**, 66 (1989).*

[28] P.E. Burrows and S.R. Forrest, *Appl. Phys. Lett. **61**, 2285 (1993).*

[29] S.R. Forrest and F.F. So, *J. Appl. Phys. **64**, 399 (1988).*

[30] L. Onsager, *Phys. Rev. **54**, 554 (1938); J. Chem. Phys. **2**, 599 (1934).*

[31] D.M. Pai, *J. Appl. Phys. **46**, 5122 (1975).*

[32] D.Y. Zang, F.F. So and S.R. Forrest, *Appl. Phys. Lett., **59**, 823 (1991).*

[33] For this model to be valid, recombination of free carriers swept through the film with the fixed charge in the depleted film must not result in significant film charging. This is evident when we consider that for our experiments, there are 5×10^{12} carriers photogenerated per second, with a transit time through the film of $t \sim 0.1$ ms (see Fig. 7). This implies that in steady state, 5×10^5 photogenerated carriers are contained within the depleted 5000 Å thick PTCDA film. With a fixed charge density of 5×10^{14} cm^{-3}, the film bulk contains a a total of 2.5×10^9 carrier recombination centers. The ratio of the number of photogenerated carriers to the number of available recombination centers is therefore 2×10^{-4}, which is sufficiently small to avoid film charging over the time scale of the experiment, even assuming the worst case condition of an infinite recombination lifetime (i.e. $t_{rec} >> t$).

[34] Note that the diffusion length of the exciton whose peak is at $E_{CT} = 2.23$ eV can not be directly measured. However, in Paper I we showed that this CT state is strongly mixed and in thermal equilibrium with the $E_{CT}^{ST} = 2.11$ eV self trapped state, which suggests that it has the same diffusion length.

[35] Y. Hirose, A. Kahn, V. Aristov and P. Soukiassian, *Appl. Phys. Lett.* ***68****, 217 (1996).*

[36] L.B. Schein, A. Peled and D. Glatz, *J. Appl. Phys.* ***66****, 686 (1989).*

[37] J.D. Wright, Molecular Crystals, 2nd Ed., *Cambridge University Press (1995).*

[38] K.S. Song and R.T. Williams, Self-Trapped Excitons, *Springer-Verlag, Berlin (1993).*

[39] E.I. Rashba, "Self-Trapping of Excitons," in Excitons, Ed. E.I. Rashba and M.D. Sturge, *North Holland Publishing Co., Amsterdam (1982).*

[40] D. Wöhrle and D. Meissner, *Adv. Mater.* ***3****, 129 (1991).*

[41] C. Arbour, N.R. Armstrong, R. Brina, G. Collins, J. Danziger, J.-P. Dodelet, P. Lee, K.W. Nebesny, J. Pankow and S. Waite, *Mol. Cryst. Liq. Cryst.,* ***183****, 307 (1990).*

[42] M. Hiramoto, M. Suezaki and M. Yokoyama, *Chem. Lett. 327 (1990).*

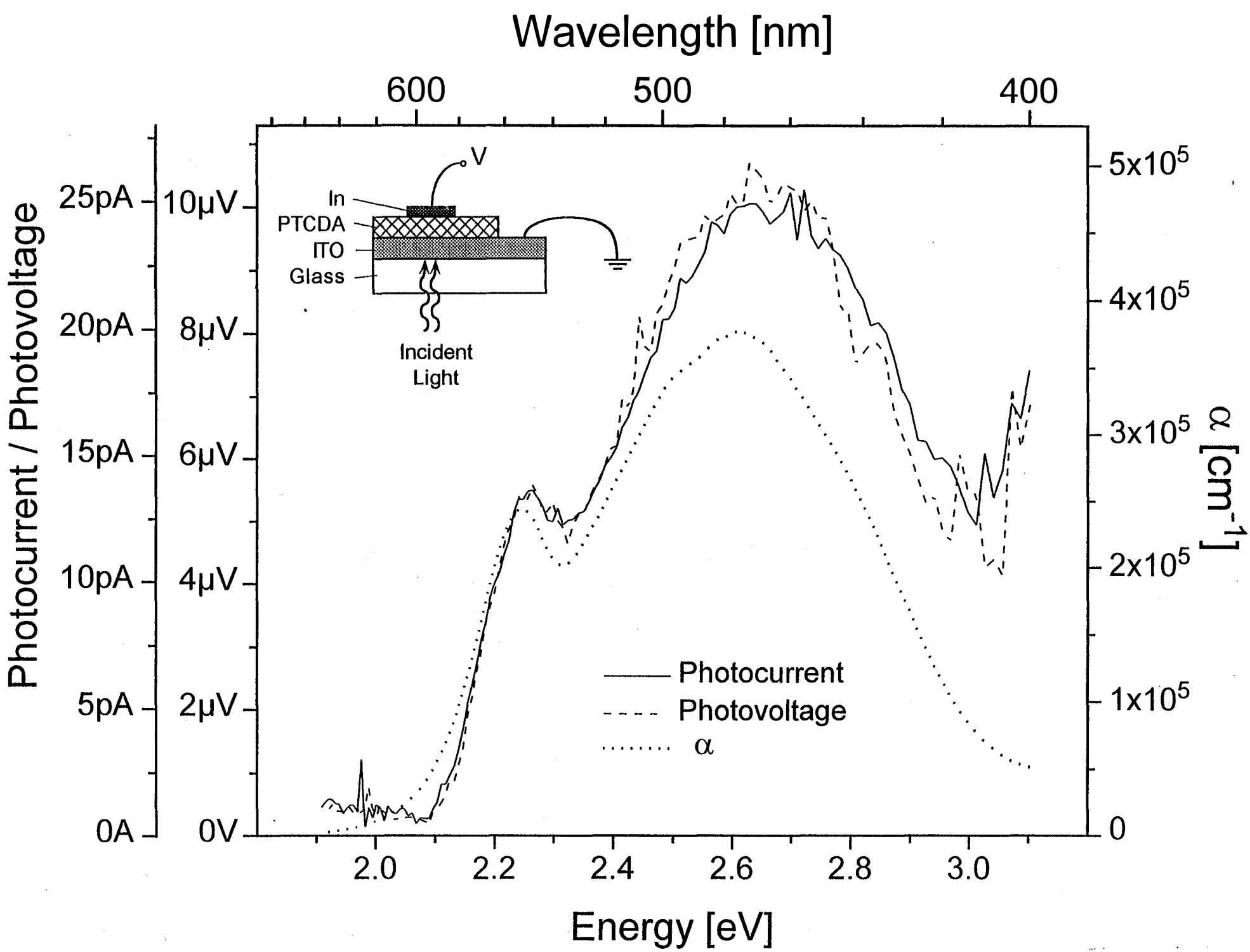
Wavelength [nm]
600
500
400
Photocurrent / Photovoltage
25pA
20pA
15pA
10pA
5pA
0A
10μV
8μV
6μV
4μV
2μV
0V
α [cm-1]
5x10^5
4x10^5
3x10^5
2x10^5
1x10^5
0
V
In
PTCDA
ITO
Glass
Incident
Light
Photocurrent
Photovoltage
α
2.0
2.2
2.4
2.6
2.8
3.0
Energy [eV]

Fig. 1

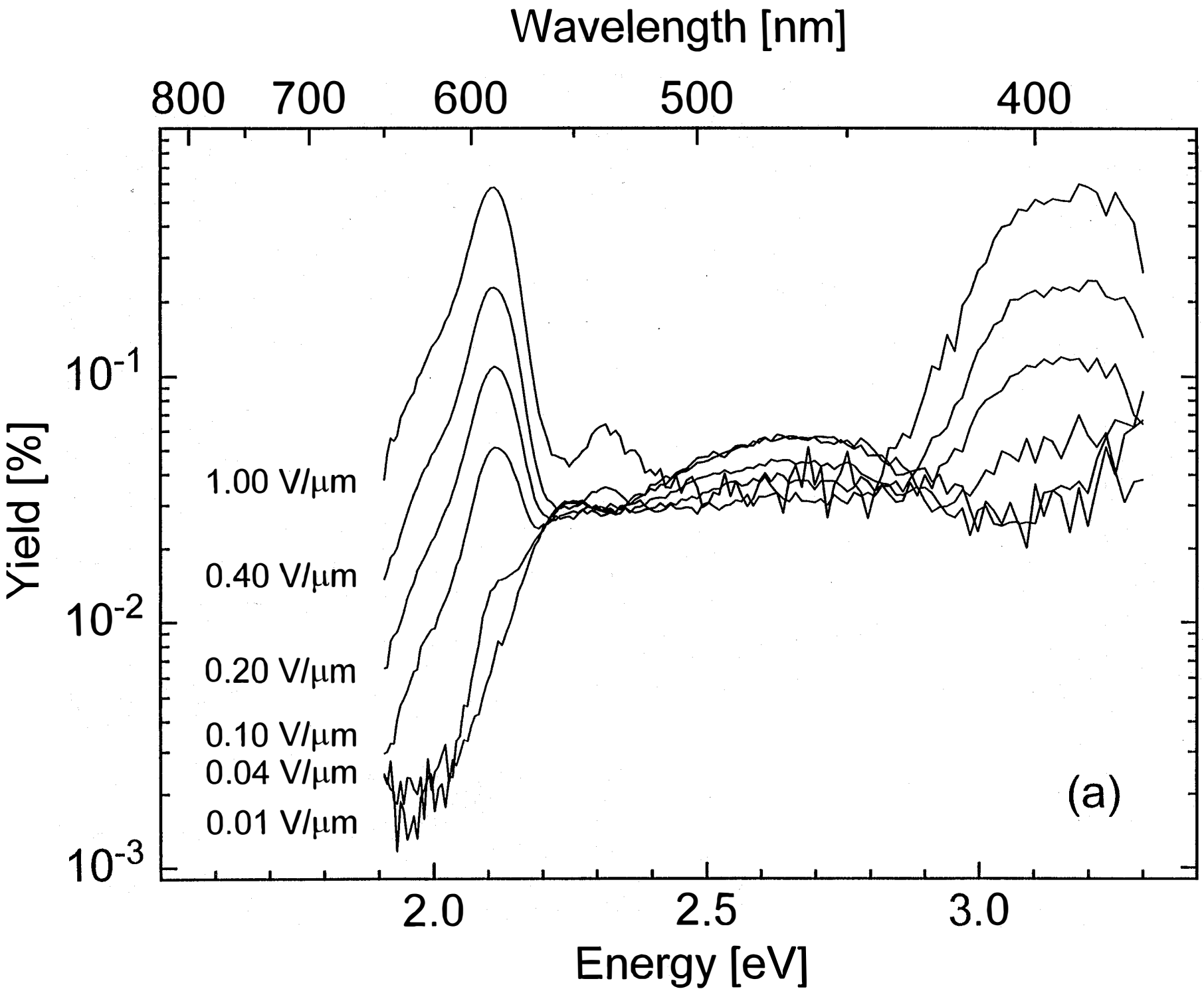
Wavelength [nm]
800
700
600
500
400
Yield [%]
10^{-1}
10^{-2}
10^{-3}
1.00 V/μm
0.40 V/μm
0.20 V/μm
0.10 V/μm
0.04 V/μm
0.01 V/μm
(a)
2.0
2.5
3.0
Energy [eV]

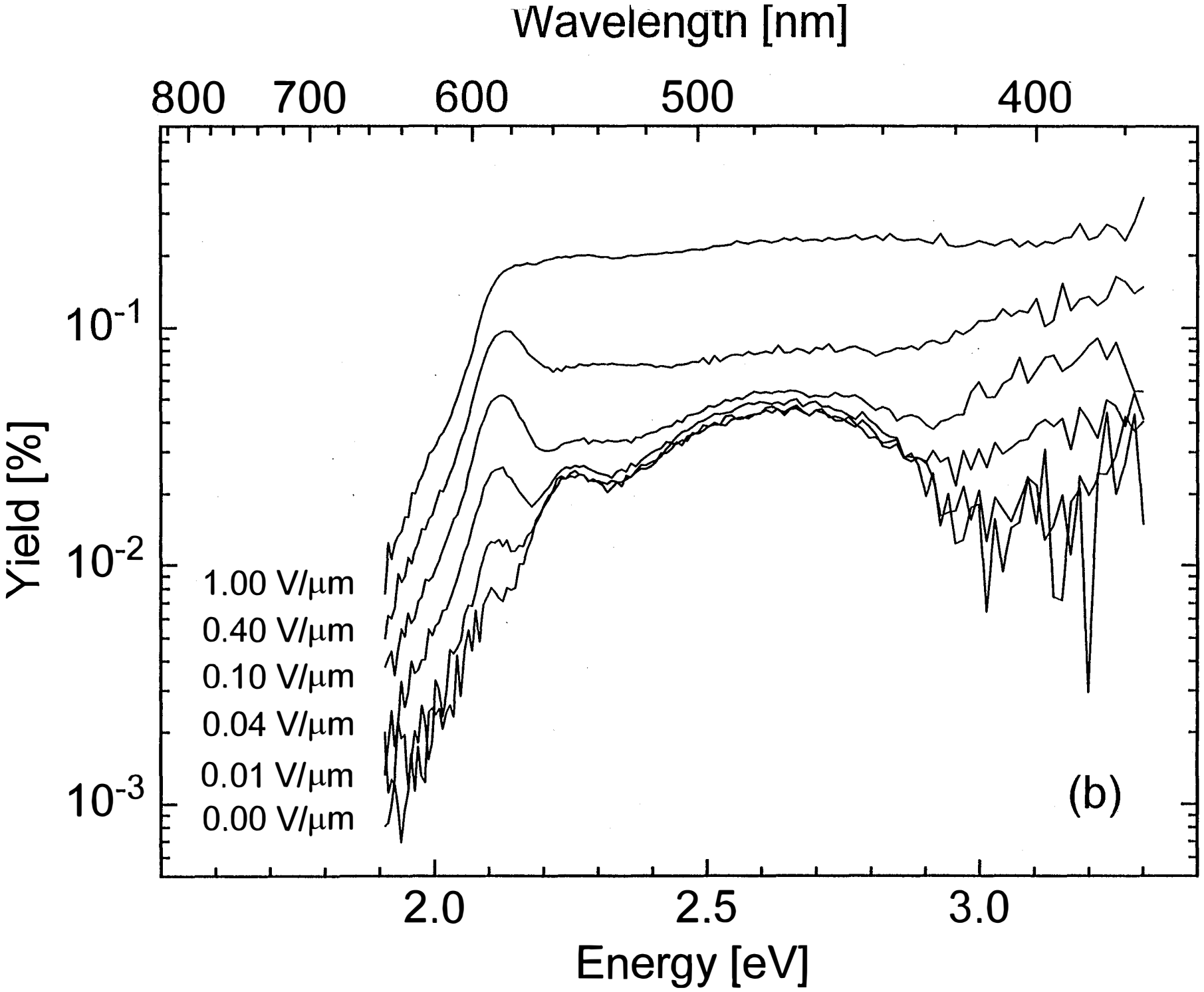
Wavelength [nm]
800
700
600
500
400
Yield [%]
10^{-1}
10^{-2}
10^{-3}
1.00 V/μm
0.40 V/μm
0.10 V/μm
0.04 V/μm
0.01 V/μm
0.00 V/μm
(b)
2.0
2.5
3.0
Energy [eV]

Fig. 2b

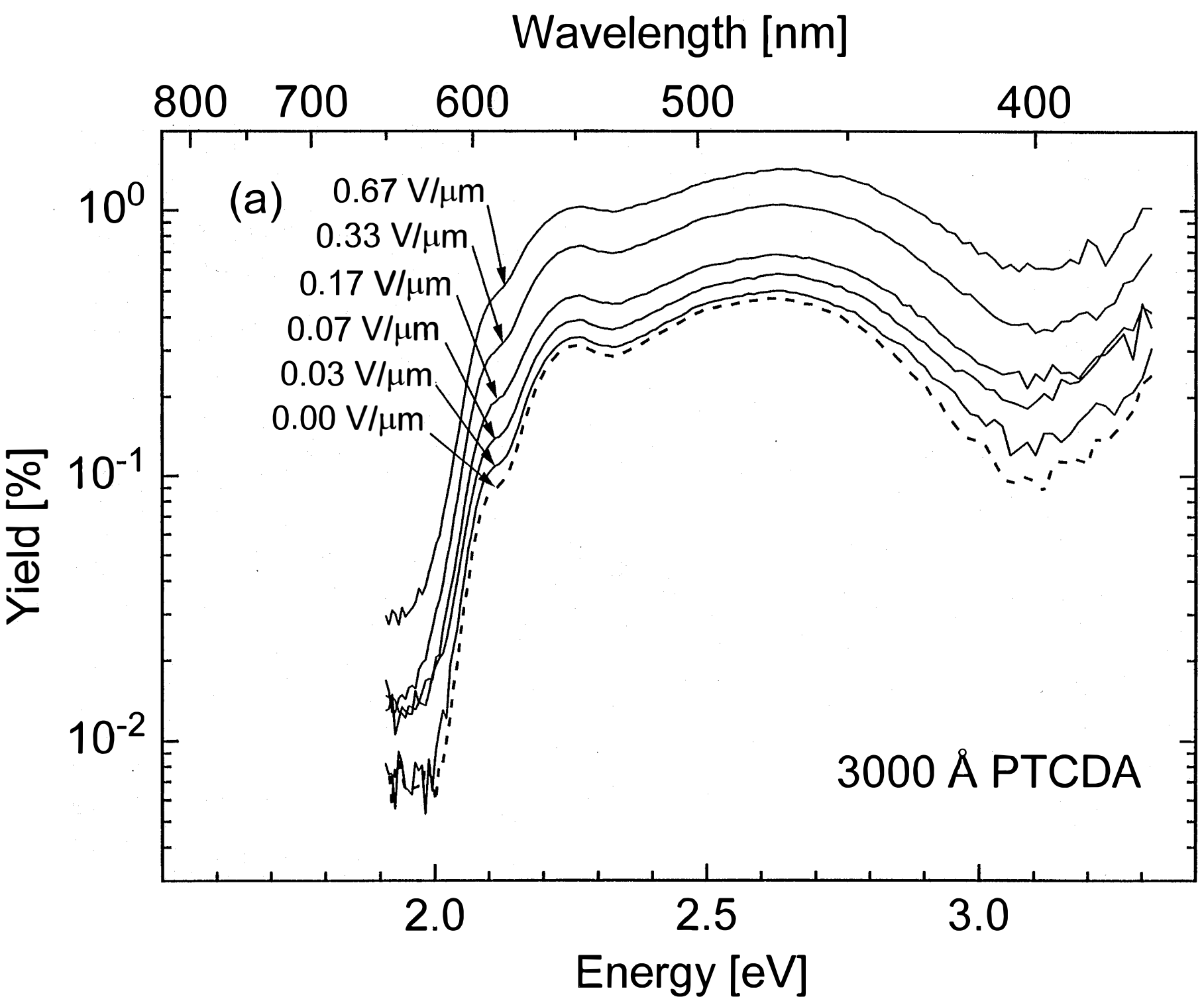
Wavelength [nm]
800
700
600
500
400
(a)
0.67 V/μm
0.33 V/μm
0.17 V/μm
0.07 V/μm
0.03 V/μm
0.00 V/μm
10^0
10^{-1}
10^{-2}
Yield [%]
3000 Å PTCDA
2.0
2.5
3.0
Energy [eV]

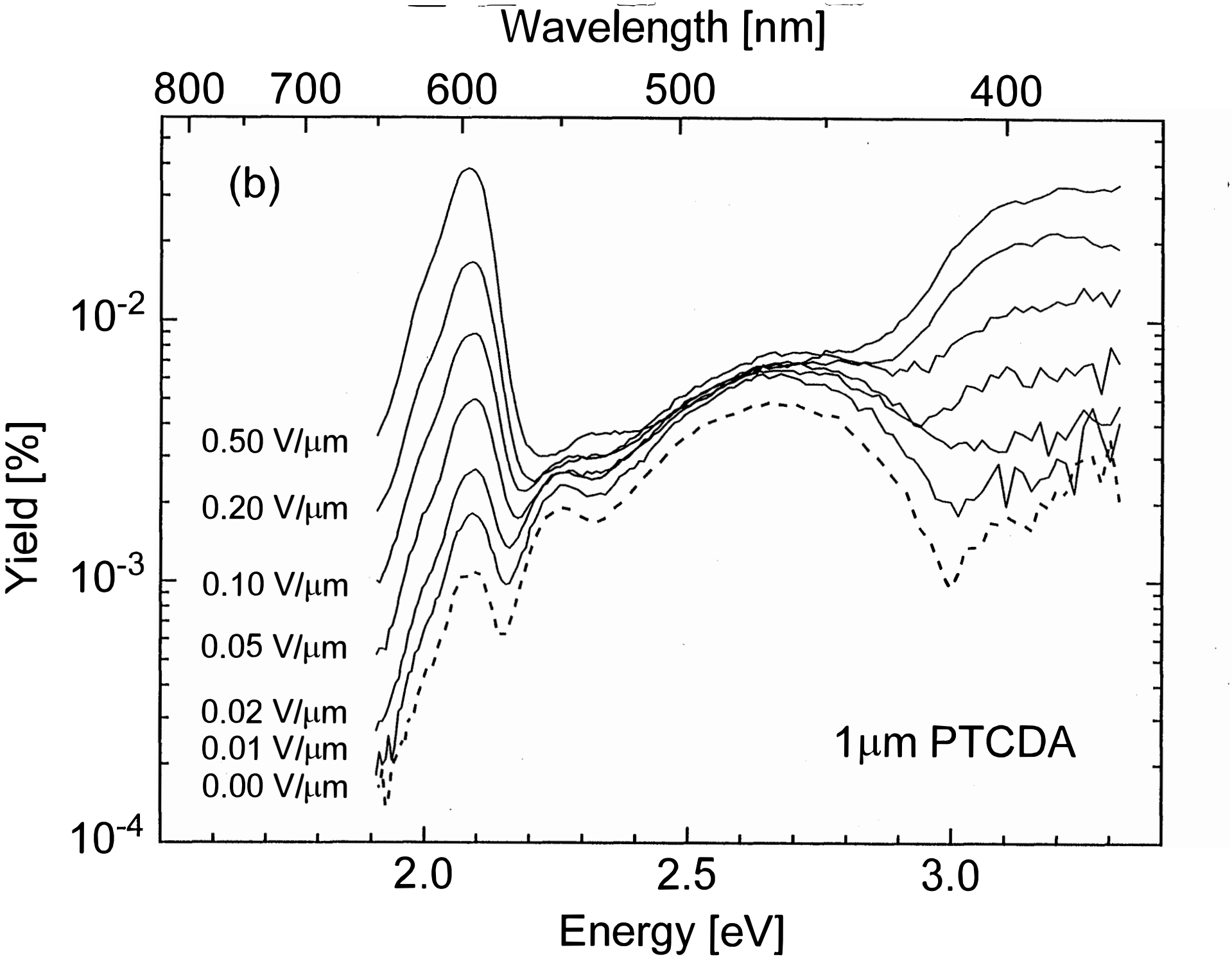
Wavelength [nm]
800
700
600
500
400
(b)
10^{-2}
10^{-3}
10^{-4}
Yield [%]
0.50 V/μm
0.20 V/μm
0.10 V/μm
0.05 V/μm
0.02 V/μm
0.01 V/μm
0.00 V/μm
1μm PTCDA
2.0
2.5
3.0
Energy [eV]

Fig. 2b

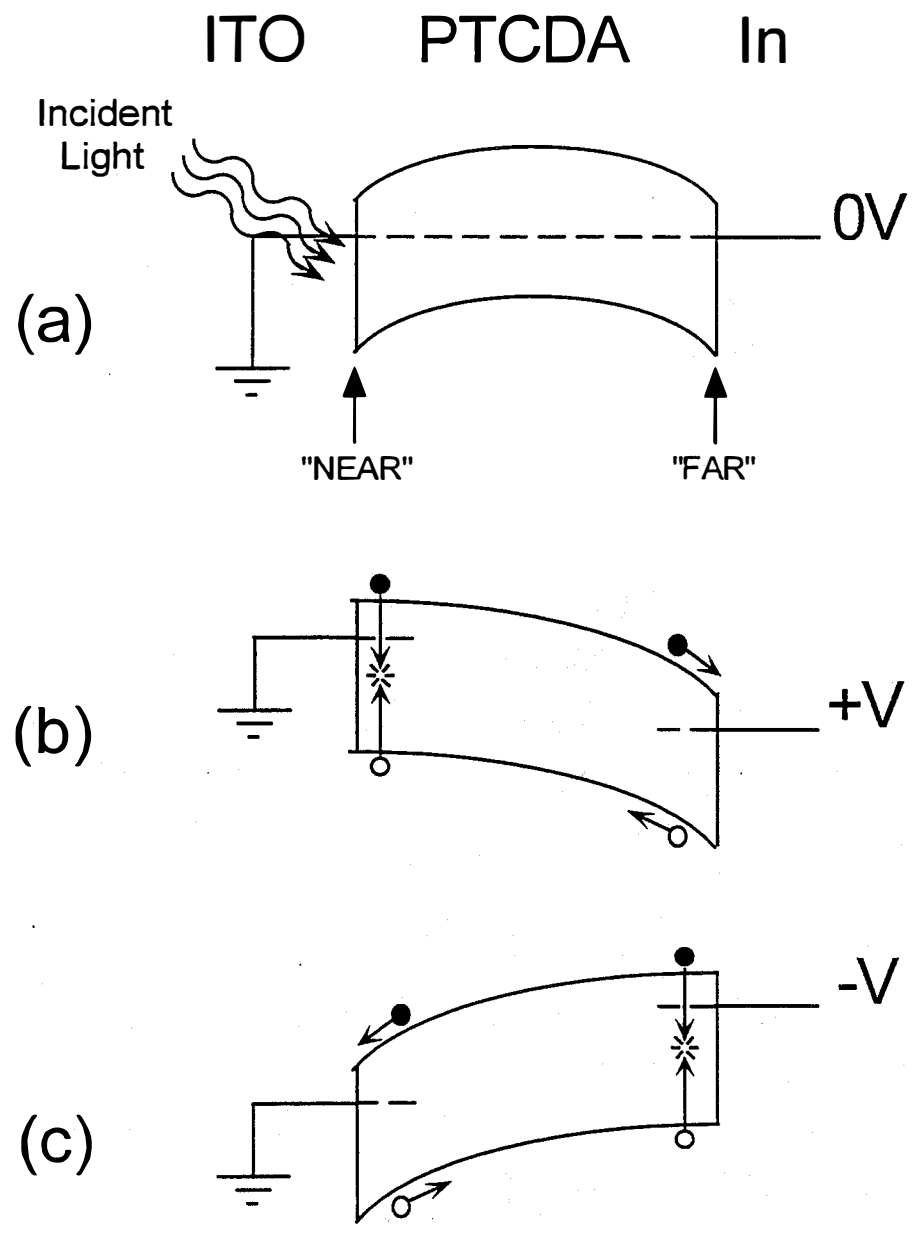
ITO
PTCDA
In
Incident
Light
0V
(a)
"NEAR"
"FAR"
(b)
+V
(c)
-V

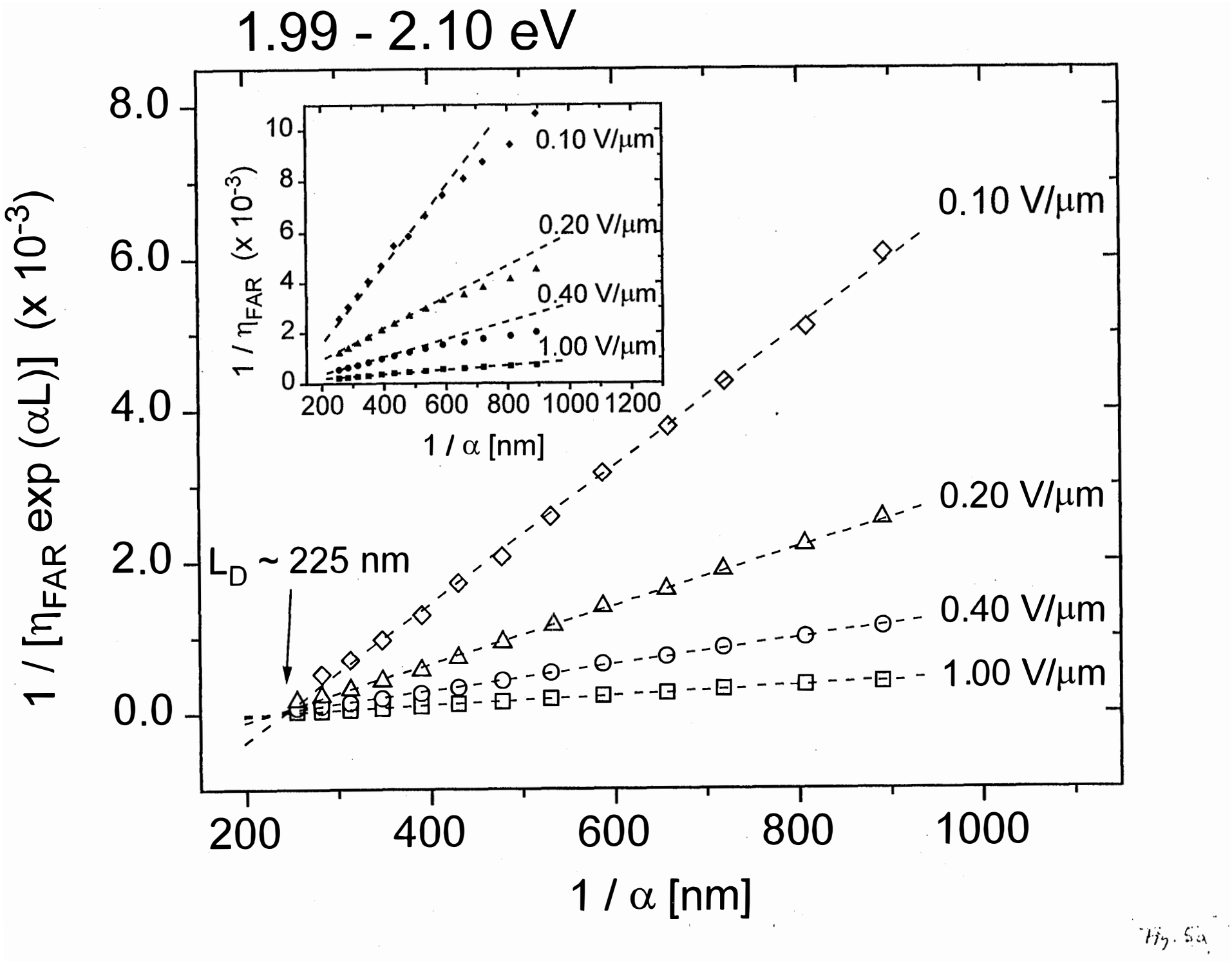
1.99 - 2.10 eV
1 / [η_FAR exp (αL)] (x 10^-3)
1 / α [nm]
L_D ~ 225 nm
0.10 V/μm
0.20 V/μm
0.40 V/μm
1.00 V/μm
1 / η_FAR (x 10^-3)
1 / α [nm]

Fig. 5a

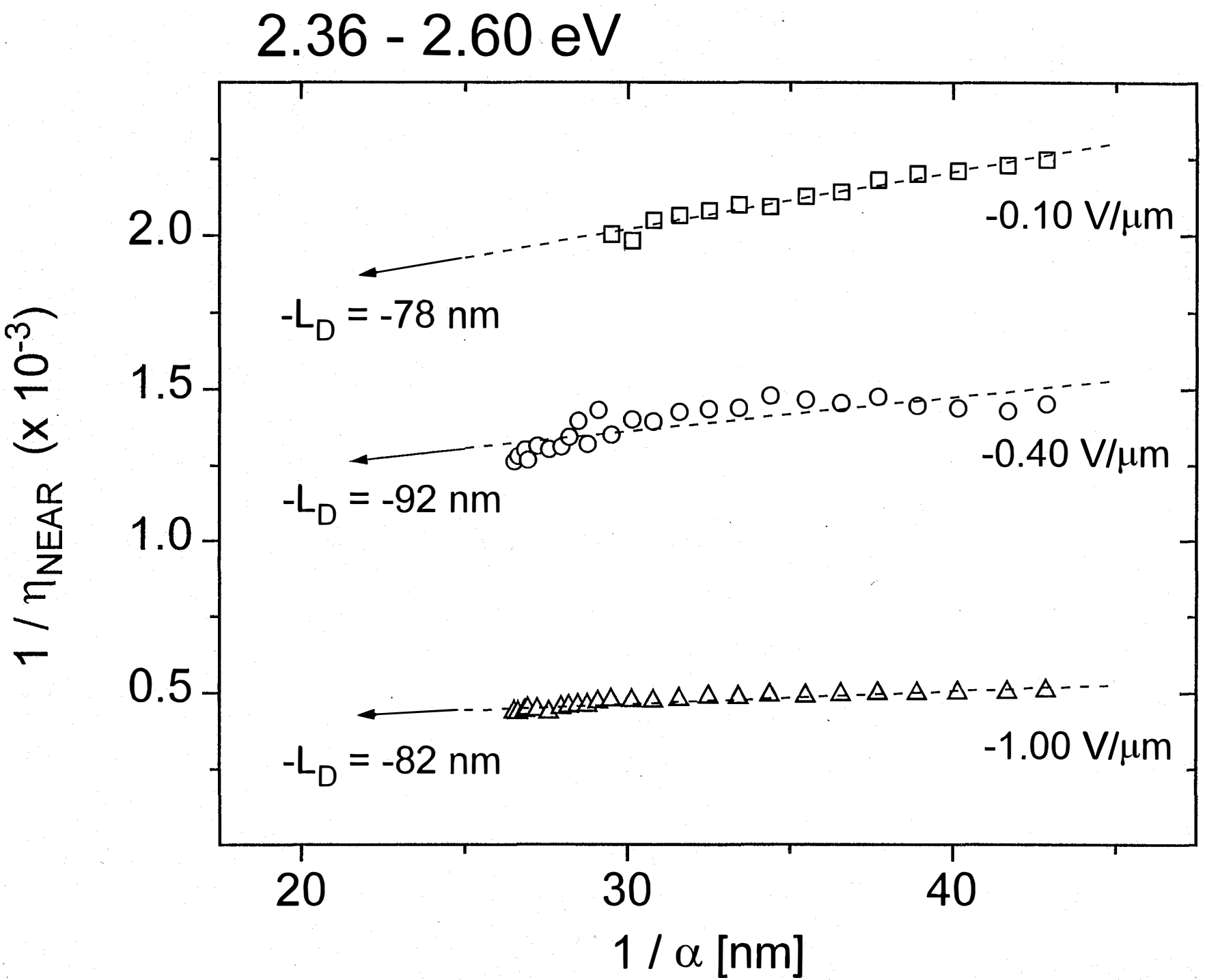
2.36 - 2.60 eV
2.0
1.5
1.0
0.5
1 / η_{NEAR} (x 10^{-3})
-0.10 V/μm
-L_D = -78 nm
-0.40 V/μm
-L_D = -92 nm
-1.00 V/μm
-L_D = -82 nm
20
30
40
1 / α [nm]

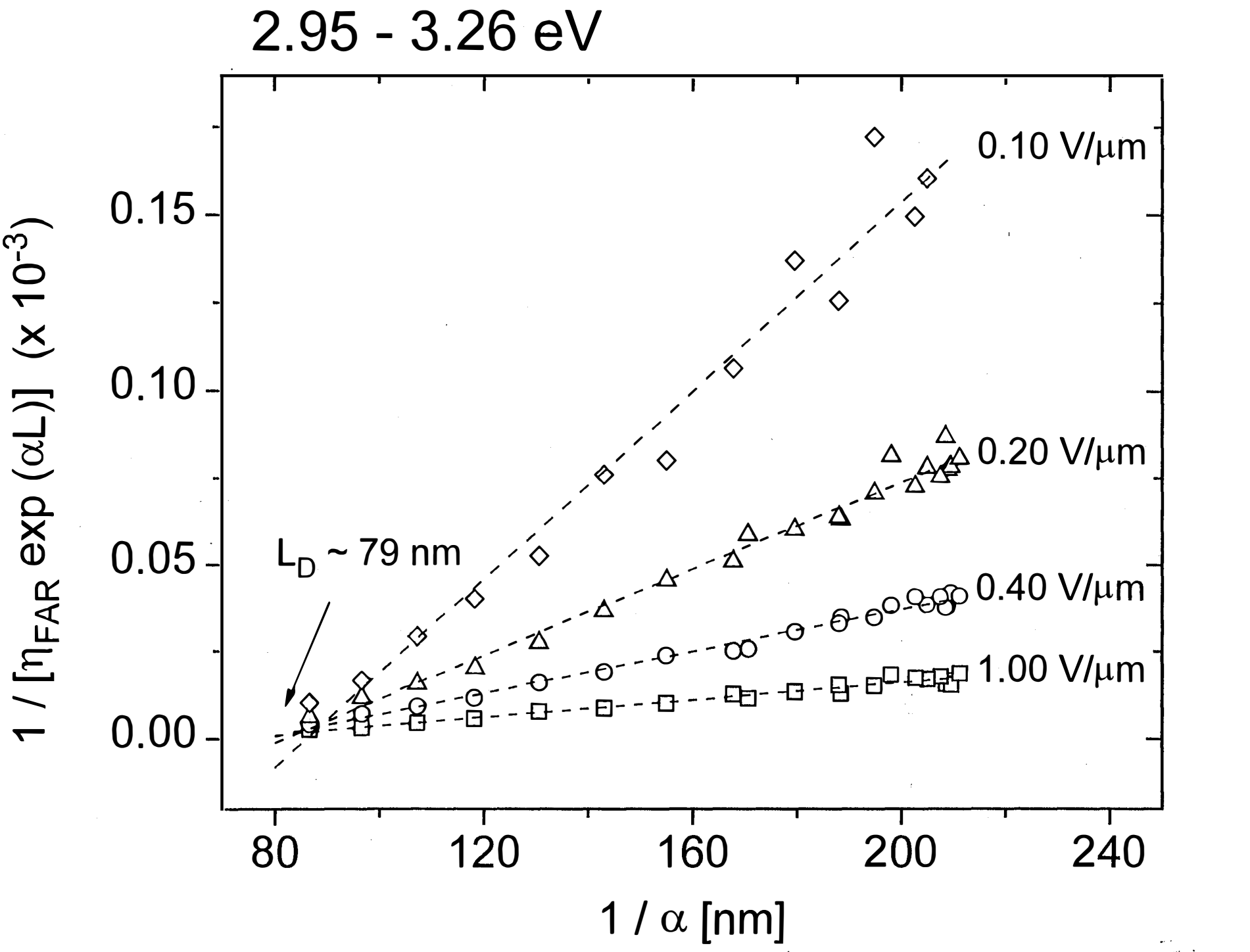
2.95 - 3.26 eV
0.10 V/μm
0.20 V/μm
0.40 V/μm
1.00 V/μm
L_D ~ 79 nm
0.15
0.10
0.05
0.00
80
120
160
200
240
1 / α [nm]
1 / [η_{FAR} exp (αL)] (x 10^{-3})

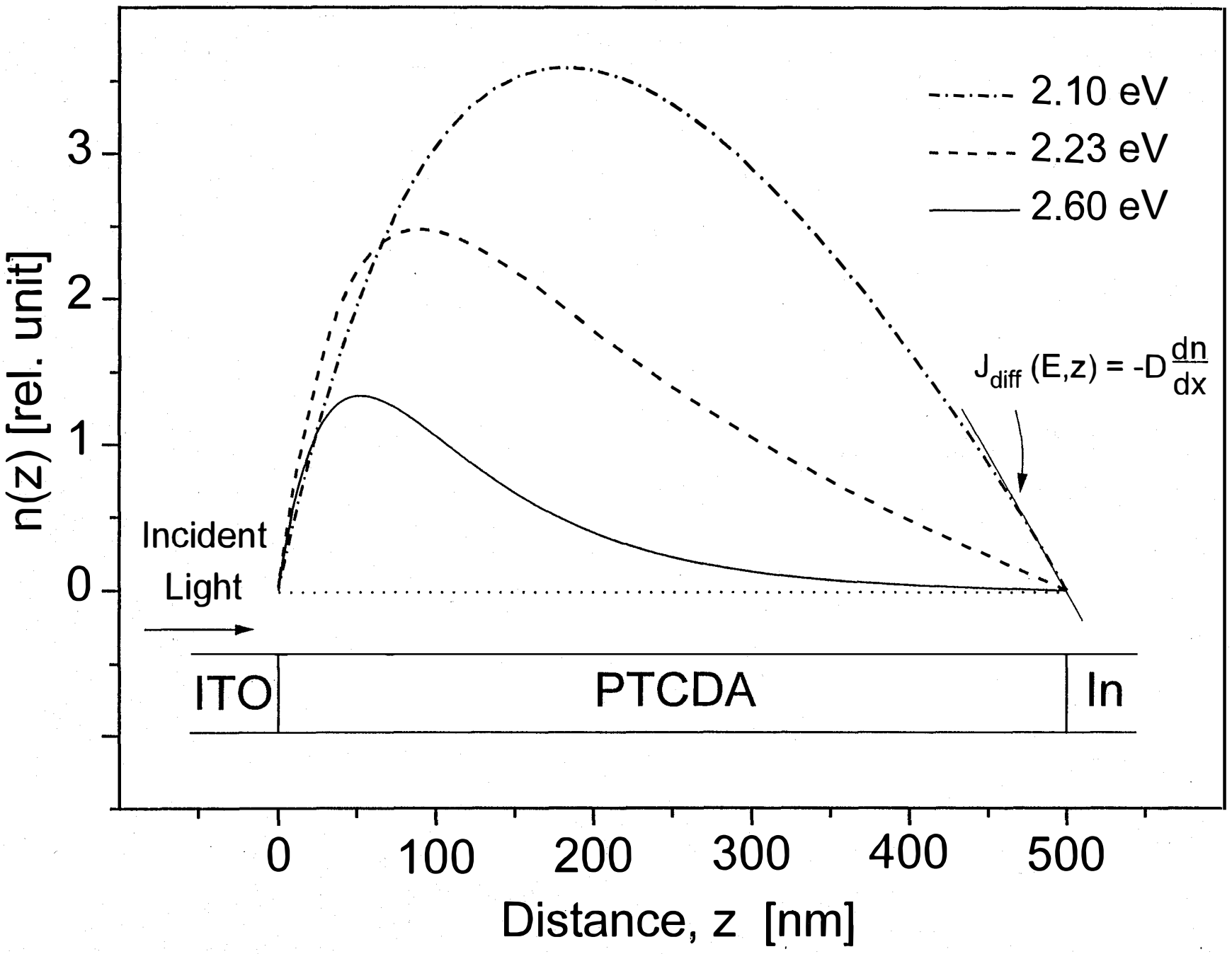
2.10 eV
2.23 eV
2.60 eV
$J_{diff}(E,z) = -D\frac{dn}{dx}$
Incident Light
ITO
PTCDA
In
n(z) [rel. unit]
0
1
2
3
0
100
200
300
400
500
Distance, z [nm]

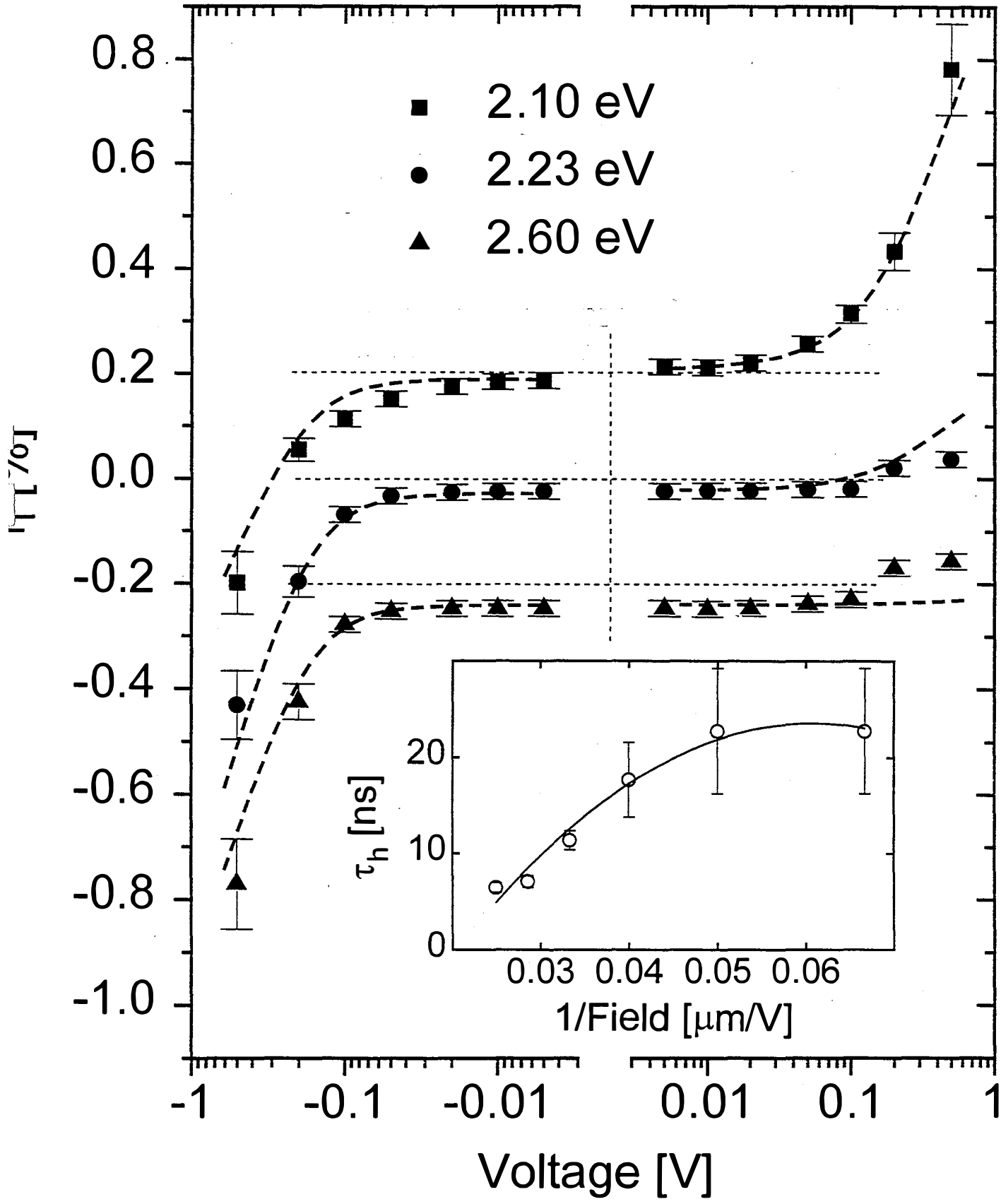
2.10 eV
2.23 eV
2.60 eV
0.8
0.6
0.4
0.2
0.0
-0.2
-0.4
-0.6
-0.8
-1.0
-1
-0.1
-0.01
0.01
0.1
1
Voltage [V]
τ_h [ns]
20
10
0
0.03
0.04
0.05
0.06
1/Field [μm/V]

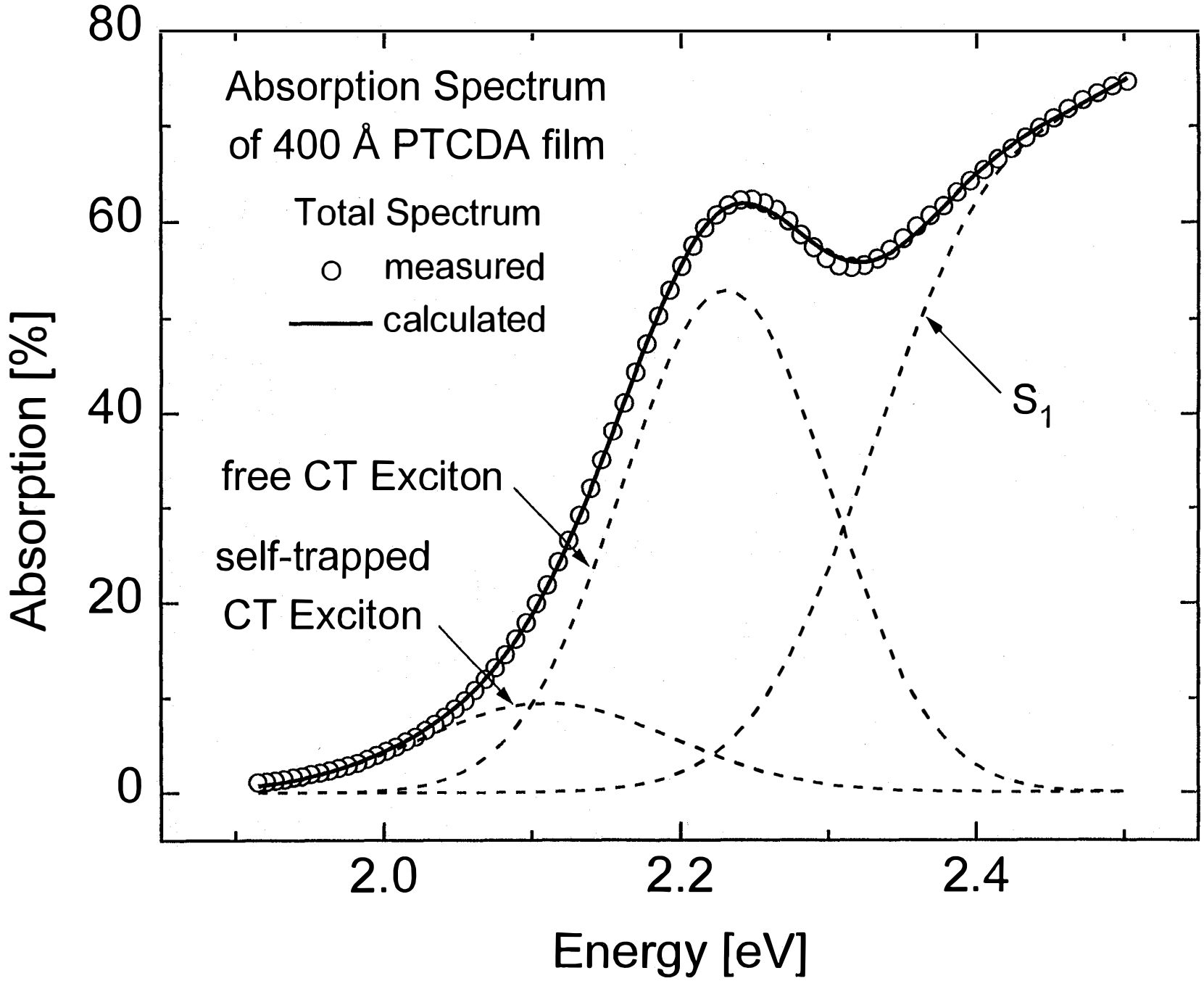
Absorption Spectrum
of 400 Å PTCDA film
Total Spectrum
measured
calculated
free CT Exciton
self-trapped
CT Exciton
S1
Absorption [%]
Energy [eV]
80
60
40
20
0
2.0
2.2
2.4

REPORT DOCUMENTATION PAGE

Form Approved
OMB NO. 0704-0188

1. AGENCY USE ONLY (Leave blank)	2. REPORT DATE	3. REPORT TYPE AND DATES COVERED
	March 1997	Final Report

4. TITLE AND SUBTITLE

Very High Efficiency Photovoltaic Cells Based on Fully Organic Multiple Quantum Wells; Final Report

5. FUNDING NUMBERS

C: XAI-3-11167-03
TA: PV701701

6. AUTHOR(S)

S.R. Forrest

7. PERFORMING ORGANIZATION NAME(S) AND ADDRESS(ES)

Center for Photonics and Optoelectronic Materials
Department of Electrical Engineering
Princeton University
Princeton, NJ 08544

8. PERFORMING ORGANIZATION REPORT NUMBER

9. SPONSORING/MONITORING AGENCY NAME(S) AND ADDRESS(ES)

National Renewable Energy Laboratory
1617 Cole Blvd.
Golden, CO 80401-3393

10. SPONSORING/MONITORING AGENCY REPORT NUMBER

SR-520-21882

DE97000063

11. SUPPLEMENTARY NOTES

NREL Technical Monitor: R. McConnell

12a. DISTRIBUTION/AVAILABILITY STATEMENT

12b. DISTRIBUTION CODE

UC-1260

13. ABSTRACT *(Maximum 200 words)*

The principal project objective is to demonstrate relatively high solar conversion efficiency using extremely low-cost, thin-film technology based on crystalline organic multiple quantum well (MQW) photovoltaic cells. We base our work on recent observations both in our laboratory and elsewhere that have indicated the quantum efficiency of organic photoconductors based on vacuum-deposited thin films can be increased by at least two orders of magnitude (to at least 10%) if the organic films are grown in a highly ordered manner, and if organic multiple quantum wells are used in the absorption region. Thus, we are investigating the physical origin of this phenomenon, and we are growing thin-film MQW cells that demonstrate relatively high quantum efficiencies to determine the practicality of crystalline organic thin-film cells for solar power applications. The investigations are based on a unique, ultrahigh-vacuum organic molecular beam deposition system in our laboratory.

14. SUBJECT TERMS

photovoltaics ; high efficiency photovoltaic cells ; fully organic multiple quantum wells

15. NUMBER OF PAGES
95

16. PRICE CODE

17. SECURITY CLASSIFICATION OF REPORT	18. SECURITY CLASSIFICATION OF THIS PAGE	19. SECURITY CLASSIFICATION OF ABSTRACT	20. LIMITATION OF ABSTRACT
Unclassified	Unclassified	Unclassified	UL